Towards a composite exhaust system

Investigation of the flow, thermal and wear resistance of an insulating, ceramic fibrous liner of combustion engine exhaust ducts and their influence on the design space

Reurings, C.

DOI
10.4233/uuid:c7c9260b-96af-4faa-9bf8-00d115200ac9

Publication date
2022

Document Version
Final published version

Citation (APA)
Reurings, C. (2022). *Towards a composite exhaust system: Investigation of the flow, thermal and wear resistance of an insulating, ceramic fibrous liner of combustion engine exhaust ducts and their influence on the design space* . [Dissertation (TU Delft), Delft University of Technology].
https://doi.org/10.4233/uuid:c7c9260b-96af-4faa-9bf8-00d115200ac9

Important note
To cite this publication, please use the final published version (if applicable).
Please check the document version above.

Towards a composite exhaust system

Investigation of the flow, thermal and wear resistance of an insulating, ceramic fibrous liner of combustion engine exhaust ducts and their influence on the design space

Towards a composite exhaust system

Investigation of the flow, thermal and wear resistance of an insulating, ceramic fibrous liner of combustion engine exhaust ducts and their influence on the design space

Proefschrift

ter verkrijging van de graad van doctor
aan de Technische Universiteit Delft,
op gezag van de Rector Magnificus prof. dr. ir. T.H.J.J. van der Hagen,
voorzitter van het College voor Promoties,
in het openbaar te verdedigen op vrijdag 7 oktober 2022 om 10.00 uur

door

Cornelis REURINGS

Ingenieur Luchtvaart- & Ruimtevaarttechniek,
Technische Universiteit Delft,
geboren te Amsterdam.

Dit proefschrift is goedgekeurd door de promotoren.

Samenstelling promotiecommissie:

Rector Magnificus,	voorzitter
Prof. dr. ir. R. Benedictus,	Technische Universiteit Delft, promotor
Dr. ir. S. Koussios,	Technische Universiteit Delft, copromotor
Onafhankelijke leden:	
Prof. dr. K. Suga	Osaka Prefecture University, Japan
Prof. dr. K.M.B. Jansen	Technische Universiteit Delft
Dr. ir. W.-P. Breugem	Technische Universiteit Delft
Dr. ir. K.C.L. Vergote	BOSAL Emission Control Systems n.v., België
Prof. dr. ir. C. Kassapoglou,	Technische Universiteit Delft, reservelid
Overige leden:	
Dr. ir. O.K. Bergsma,	Technische Universiteit Delft

Keywords: combustion engine exhaust, ceramic fibrous insulation, friction, heat transfer, wear, design

Printed by: Ipskamp Printing

Front & Back: C. Reurings (photo at the top of the backside: iStock)

An electronic version of this dissertation is available at
http://repository.tudelft.nl/.

Aan mijn ouders, Joost en Tineke.
Aan mijn zus, Lisanne.
Aan Juliette.

Contents

Summary

The current concerns regarding global warming and climate change in Europe and other parts of the world also influence developments in the automotive sector. Not only are alternative energy and power sources making their advent, but greenhouse gas emission reduction has also become a major factor in the development of vehicles with combustion engines. As passenger vehicles with such engines will be sold for probably a few more decades, additional options for emission reduction are still welcome. Mass reduction results directly in less greenhouse gas emission per driven kilometer, both in practice as in the official carbon dioxide (CO_2) emission determination procedures.

This thesis is part of a project that tries to develop an additional option for passenger vehicle mass reduction, more specifically by replacing steel in the exhaust system with fibre-reinforced plastic. The principle behind this solution is that fibre-reinforced plastic has better mechanical properties per kilogram of material than steel. Yet, no plastic could endure direct exposure to exhaust gas flows because of the maximum gas temperature of 800 - 1000 °C.

The addition of thermal protection between the gas and fibre-reinforced plastic ducts is therefore a necessary increase in solution complexity. Based on earlier work by others, the thermal protection comprises three layers: firstly, ceramic fibrous insulation, secondly, a woven fabric lining the insulation surface and thirdly, a steel mesh for mechanical support. The additional complexity stems not only from the increased number of materials and components, but also from the influence the addition has on the performance. Thermal insulation systems line surfaces exposed to gas flow in several applications already, but the studied system differs from those in configuration, because of the mesh, and in conditions, which are more severe in car exhausts.

This thesis covers the performed research into the identified knowledge gaps regarding friction, heat transfer and wear, that prevent further development of this potential mass reduction solution. The main research question is: how can the friction, heat transfer and wear of an internally lined exhaust system be quantified, and what do the eventual results mean for the associated mechanisms and the feasibility of the concept?

All three aspects influence the performance of a fibre reinforced exhaust system and all are the result of the interaction between the gas flow and the thermal insulation. For many boundary types, the interaction between the flow and the flow domain boundary is generally understood. However, the concept under consideration combines features from several special boundaries and the combined effect on the interaction is yet unknown. An experimental approach was chosen, as numerical modelling was considered more challenging and less effective than developing new experimental setups and procedures.

One setup was developed to measure both the friction factor and heat transfer rate. The samples were formed by straight pipe sections with different insulation configurations. The measurements require a relatively short exposure time and constant insulation properties can therefore be assumed. The effects of configuration changes were discerned through measuring the streamwise pressure drop over and radial temperature differences in different pipe samples for a range of flow states with different Reynolds numbers and non-dimensional pulsation frequencies. The configurations covered a range of mesh pitches, insulation densities, and insulation compression ratios.

The friction factor was found to be effectively constant with varying Reynolds number and non-dimensional pulsation frequency, while the variation with insulation density and compression was not significant. Moreover, the friction factors for both mesh pitches were in line with those reported in literature for similar geometries with steady flow and solid walls. Neither compliance nor the pulsations from the combustion engine seem to significantly affect the friction. Comparison of the samples using the derived thermal resistance showed a similar influence of the fluid-wall interface as for the friction. Contrary to friction, insulation compression did contribute to the thermal resistance; it increased the radiation resistance through fibre reorientation.

Another test rig was developed for the wear of the thermal protection; to subject it to conditions representative for in-service use, to quantify its wear rate and, to enable investigation of its behaviour and the occurring phenomena. This rig can accommodate a range of insulation configurations and is compatible with different flow sources. This test setup, the experimental procedure, its accuracy and representative results are presented. Different insulation failure mechanisms were identified and in most samples the damage seemed related to the presence of *shot*: relatively large ceramic elements inherent to the employed fibrous insulation.

Using the knowledge gained from the experimental work, the remaining challenges and uncertainty in the realization of the concept were described. The identified challenges are related to durability, manufacturing automation and recycling, and to the final design, assembly and integration of the thermal protection.

The current realization of the concept has a straight pipe mass roughly equal to that of steel and does not form a mass reduction solution. As the design is not mature, further development could still result in a lower mass. The CO_2 emission during production is about as large as that of steel, when the concept shell is a thermosetting polymer. This emission is roughly equal to what could be saved during use if the exhaust were 10 kg lighter. Thermoplastic alternatives have a higher associated production emission and material cost. The material and forming cost of the thermosetting shell is comparable to that of steel and in some cases even less. The material cost of the the insulation is however several times more, making the concept as a whole more costly in terms of materials and processing.

The current work shows that the concept does not necessarily perform satisfactory or save mass for general use with all engine types. That goal is theoretically still achievable, but future efforts would probably better be focussed on more specialized or other applications of the concept.

Samenvatting

De huidige zorgen over opwarming van de aarde en klimaatverandering in Europa en andere delen van de wereld beïvloeden ook ontwikkelingen in de automobiel sector. Niet alleen zijn alternatieve energievormen en krachtbronnen in opkomst, maar vermindering van de broeikasgasuitstoot is voor auto's met een verbrandingsmotor ook een belangrijke factor in de ontwikkeling geworden. Aangezien personenauto's met zulke motoren waarschijnlijk nog enkele decennia zullen worden verkocht, zijn aanvullende mogelijkheden voor uitstootvermindering nog steeds welkom. Gewichtsbesparing zorgt voor een directe afname van de broeikasgasuitstoot per kilometer, zowel in de praktijk als in de bepaling van de officiele CO_2-uitstoot.

Dit proefschrift is onderdeel van een project dat tot doel heeft om een aanvullende mogelijkheid voor gewichtsbeparing bij personenauto's te ontwikkelen, specifiek door staal in het uitlaatsysteem te vervangen door vezelversterkte kunststof. Het principe achter deze oplossing is dat vezelversterkte kunststoffen betere mechanische eigenschappen per kilogram materiaal hebben dan staal. Echter, geen kunststof kan directe blootstelling aan uitlaatgassenstromen weerstaan vanwege de maximum gastemperatuur van 800 - 1000°C.

Toevoeging van thermische bescherming tussen het gas en de behuizing van vezelversterkte kunststof is daarom een noodzakelijke vergroting van de complexiteit. Gebaseerd op eerder werk van anderen, bestaat de thermische bescherming uit drie lagen: ten eerste, keramische vezelachtige isolatie, ten tweede, een weefsel dat de isolatie bekleedt en, ten derde, een stalen gaas voor mechanische ondersteuning. De extra complixiteit komt niet alleen door de toename van het aantal materialen en onderdelen, maar ook door de invloed van de toevoeging op de prestaties. Thermisch isolerende systemen bekleden aan gasstromen blootgestelde oppervlakken al in verschillende toepassingen, maar het beschouwde systeem wijkt af in configuratie, vanwegen het metalen gaas, en omstandigheden, welke meer extreem zijn in uitlaatsystemen.

Dit proefschrift omvat het uitgevoerde onderzoek naar de geidentificeerde gaten in kennis met betrekking tot stromingsweerstand, warmteoverdracht en slijtage, die verdere ontwikkeling van deze aanvullende mogelijkheid voor gewichtsbesparing verhinderen. De hoofdonderzoeksvraag is: hoe kunnen de stromingsweerstand, warmteoverdracht en slijtage van een uitlaatsysteem met thermische bescherming gekwantificeerd worden en wat betekenen de eventuele resultaten voor de geassocieerde mechanismen en de haalbaarheid van het concept van een uitlaatsysteem van vezelversterkte kunststof?

Alle drie aspecten beinvloeden de prestaties van een uitlaatsysteem van vezelversterkte kunststof en zijn het resultaat van de interactie tussen de gasstroom en de thermische bescherming. Voor verschillende grenssoorten, is de interactie tussen de stroming en de grensvlakken van het stromingsdomein globaal bekend.

Echter, in het concept onder beschouwing worden enkele bijzondere grenzen gecombineerd en hun gezamenlijke effect op de interactie is nog onbekend. Er is gekozen voor een experimentele aanpak, aangezien numeriek modelleren meer uitdagend en minder effectief werd geacht dan het ontwikkelen van nieuwe experimentele opstellingen en procedures.

Een opstelling is ontwikkeld voor het meten van zowel de wrijvingscoefficiënt als de warmteoverdrachtsnelheid. De proefstukken werden gevormd door rechte pijpdelen met verschillende configuraties van thermische bescherming. De metingen vereisen een relatief korte blootstellingsduur en daardoor konden constante eigenschappen worden aangenomen voor de isolatie. De effecten van configuratieverschillen werden onderscheiden door het meten van de stroomsgewijze drukval over en het radiale temperatuursverschil van verschillende proefstukken over een bereik van stromingsomstandigheden met verschillende Reynolds getallen en nondimensionele pulsatiefrequenties. De configuraties hadden verschillende gaasdraadintervallen, isolatiedichtheden en isolatie compressie ratio's.

De wrijvingscoefficiënt bleek effectief constant bij verschillende Reynolds getallen en nondimensionele puslatiefrequenties, terwijl de variatie met isolatiedichtheid en compressie niet significant was. Bovendien waren de wrijvingscoefficiënten voor beide gaasdraadintervallen in lijn met literatuurwaarden voor vergelijkbare geometriën met pulsatievrije stroming en massieve grensvlakken. Noch de lage stijfheid van het grensvlak, noch de pulsaties uit de verbrandingsmotor lijken daarmee een significante invloed te hebben op de wrijving bij deze thermische bescherming. Vergelijking van de proefstukken middels de afgeleide thermische weerstand liet een vergelijkbare invloed van het gas-wandgrensvlak zien als bij de wrijving. In tegenstelling tot bij wrijving, had isolatiecompressie wel invloed op de thermische weerstand: de stralingsweerstand nam toe door vezelheroriëntatie.

Een tweede testopstelling is ontwikkeld voor de slijtage van de thermische bescherming: om het bloot te stellen aan omstandigheden die representatief zijn voor gebruik in de praktijk, om de slijtagesnelheid te kunnen kwantificeren en om het gedrag en optredende fenomenen te kunnen onderzoeken. De proefstukhouder is geschikt voor verschillende isolatieconfiguraties en compatibel met verschillende stromingsbronnen. De testopstelling, de procedure, de nauwkeurigheid en representatieve resultaten zijn beschreven. Verschillende isolatiebezwijkmechanismen zijn geïdentificeerd en in de meeste proefstukken leek de schade gerelateerd aan de aanwezigheid van *shot*, relatief grote keramische elementenen die inherent zijn aan de gebruikte vezelachtige isolatie.

Gebruikmakend van de kennis die is opgedaan bij het experimentele werk, zijn de overgebleven uitdagingen en onzekerheden in de realisatie van het concept beschreven. The geïdentificeerde uitdagingen zijn gerelateerd aan duurzaamheid, productieautomatisering en recycling, en aan het detailontwerp, de assemblage en integratie van de thermische bescherming.

De huidige realisatie van het concept heeft een rechte-pijp-massa die ongeveer gelijk is aan die van staal en vormt daardoor geen gewichtsbesparingsmogelijkheid. Aangezien het ontwerp niet volwassen is, kan verdere ontwikkeling nog altijd tot een lagere massa leiden. De CO°C-uitstoot bij de productie is ongeveer even

groot als bij staal wanneer de kunststof een thermoharder betreft. Die uitstoot is ruwweg gelijk aan de besparing die gedurend het gebruik wordt bereikt met een 10 kg lichter uitlaatssysteem. Thermoplastische alternatieven hebben een hogere productie-uitstoot en hogere materiaalkosten. De materiaal- en vormingskosten voor een thermohardend kunststof behuizing zijn vergelijkbaar met die voor staal en in sommige gevallen zelfs lager. De materiaalkosten voor de isolatie zijn echter enkele malen hoger, waardoor het concept als geheel hogere materiaal en vormingskosten kent.

Het huidige werk laat zien dat het concept niet noodzakelijk voldoende presteert of massa bespaart bij algemene toepassing bij verbrandingsmotoren. Dat doel is theoretisch nog steeds haalbaar, maar toekomstige aandacht kan waarschijnlijk beter worden gericht op specialistische of andere toepassingen van het concept.

Nomenclature

Latin symbols

A	Area (m^2)
A_v	Absorptance of the gas (-)
c_p	specific heat at constant pressure (J kg^{-1} K^{-1})
D	Diameter (m), without subscript: inner
f_D	Darcy-Weisbach friction factor (-)
k	Permeability (m^2)
Kn	Knudsen number, ratio of gas molecular mean free path over the characteristic length (-)
L	Length of measurement segment (m)
$\dot{m}$	mass flow rate (kg s^{-1})
N	Number of measurements in the set for a mean value (-)
Nu	Nusselt number (-)
p	Pressure (N m^{-2})
p_{mesh}	Wire pitch of the mesh (mm)
Pr	Prandtl number (-)
$\mathbf{q}$	Heat flux vector (W m^{-2})
q	Dynamic pressure, Chapter 2 (N m^{-2})
q	Heat transfer rate, Chapter 3 (J s^{-1})
R	Radius (m)
Re	Reynolds number (-)
Re_K	Permeability Reynolds number (-)
S_{a_b}	Standard deviation of the error of type a of the variable of interest from source b
T	Temperature (°C or K)
t	Time (s)
t_{ini}	Initial thickness (mm)
$\mathbf{u}$	Fluid velocity vector (m s^{-1})
u	Fluid velocity, streamwise direction (m s^{-1})
u_τ	Friction velocity (m s^{-1})
$U_{a,b}$	Uncertainty in variable a at confidence b (unit of a)
v_{amb}	Ambient convective air velocity (m s^{-1})
V	Volume (m^3)
Wo	Womersley number (-)
x	Coordinate in streamwise direction (m)

Greek symbols

β	Coefficient of thermal expansion (K^{-1})
ϵ	Energy dissipation rate per unit mass ($m^2\ s^{-3}$)
ε	Strain (-)
λ	Thermal conductivity ($W\ m^{-1}\ K^{-1}$)
μ	Dynamic viscosity ($N\ s\ m^{-2}$)
ν	Kinematic viscosity ($m^2\ s^{-1}$)
ω	Angular frequency of the pulsations ($rad\ s^{-1}$)
ω^+	Wall-normalized frequency (-)
Φ_{inc}	Rate of viscous dissipation for an incompressible fluid (s^{-2})
ρ	Density ($kg\ m^{-3}$)
σ	Stefan-Boltzmann constant ($W\ m^{-2}\ K^{-4}$)
τ_w	Wall shear stres ($N\ m^{-2}$)
χ	Volume compressibility ($m^2\ N^{-1}$)

Subscripts

amb	Ambient air property
avg	Average
b	Bulk gas flow property
B_a	Bias or systematic error of the variable from source a
cond	Conduction
conv	Convection
in	Inlet
ini	Initial
ins	Insulation
out	Outlet
P_a	Random error of the variable from source a
r	Radial
rad	Radiation
θ	Circumferential
wall	Fluid domain wall, interface with the insulation

Abbreviations

AES	Alkaline-Earth Silicate
NEDC	New European Driving Cycle
RCF	Refractory ceramic fibre
STS	Space Transportation System
WLTP	Worldwide Harmonised Light Vehicle Test Procedure

1 Introduction

1.1. Rationale

Since their invention in the late nineteenth century, passenger cars have become the dominant mode of transport for an increasingly large share of the population. While the first models were custom-made and only affordable for the wealthiest of people, with standardization and series production they slowly developed into a form of transport for the masses. By providing faster, cheaper and more flexible transportation than horse or train, cars became, for many, synonymous with *freedom*.

A large contribution to the advent of the automobile came from developments in energy storage and conversion. Early twentieth century, gasoline-, steam- and electricity-powered vehicles were for sale on the market, each able to propel a vehicle faster, further and cheaper than a horse. Due to the low price and high specific energy and volumetric energy density of gasoline, the internal combustion engine was able to offer superior performance at the lowest price per driven distance and started to dominate the market [1].

Furthermore, big cities welcomed cars because of the promise of improvement in environment and public health. Because, by replacing horses, cars would rid the city of manure-breeding flies, wind-blown manure particles, and the noise of clattering horseshoes [2]. And indeed, these horse-related urban problems are something of the past.

However, internal combustion engined vehicles have their own effect on the environment and associated problems. Some of these problems have been tackled whereas others have proven harder to solve. For instance, the emission of noise and carbon monoxide has successfully been reduced through the legislation-enforced introduction of mufflers and catalytic converters in exhaust systems. Additionally, for vehicles with direct-injection engines, particulate filters can reduce particulate matter emission by roughly 99% [3]. In general, increasingly strict limits have been set on the emission of combustion products for road vehicles in the EU over the past

1

decades [4, 5].

The attention for the emission of one specific combustion product has increased over the past two decades: that of the greenhouse gas CO_2. Limiting greenhouse gas emissions in general has become a substantial factor in policy and road transportation is receiving part of that attention. In 2018, passenger cars and light-duty vehicles together were responsible for 18% and 20% of the total CO_2 emission in the EU and US respectively [6, 7]. Especially in the EU, legislation has created an incentive for vehicle manufacturers to reduce the CO_2 emission of new vehicles [8], which cannot be accomplished through an addition to the exhaust system and thus requires other solutions.

As a result, currently sold passenger vehicles with a combustion engine[1] have a 10-20% lower actual CO_2 emission than fifteen years or longer ago [9, 10]. However, the demand for lower emissions continues with the introduction of increasingly strict targets for the coming years in the EU and United States [11, 12]. Also, the actual emission in The Netherlands was lowest in 2016-2017 and has increased again since [10].

The official CO_2 emission figures of car models are determined using standardized procedures in laboratories. The official (type-approval) emission values have decreased much more than the actual ones, increasing the difference between practice and the type-certification protocol. The relative difference between the official CO_2 emission and the actual value has increased from about 10% in 2004 to over 40% for petrol vehicles and about 50% for diesel in 2020 [10, 13]. The replacement of the official emission test standard in 2017 has had little influence on the type-approval emission values [14].

One of the ways to reduce the required energy and the corresponding actual CO_2 emission is to reduce the empty mass of a vehicle. By Newton's second law of motion, less mass means that less energy is needed for the same acceleration. Also, when the vehicle is not accelerating, a lower mass means a proportionally lower rolling resistance. Whether the effect of mass reduction is also reflected in the official CO_2 emission figures of car models, depends on the test procedure. The WLTP protocol that is compulsory since September 2017 and its predecessor the NEDC protocol, both take the vehicle mass into account although differently [14–16].

Mass reduction also has advantages when emission reduction is not the goal, in the words of Colin Chapman[2] [17]:

> Adding power makes you faster on the straights. Subtracting weight makes you faster everywhere.

For performance cars, the engineering focus on mass reduction therefore goes back much further than the turn of the millennium.

One very effective mass reduction method is the replacement of the main material (steel) with a material with higher specific properties such as fibre-reinforced plastic. Current Formula 1 cars show us that, if performance demands it, all car

[1] Excluding plug-in hybrid vehicles
[2] 1928-1982, founder of Lotus Cars

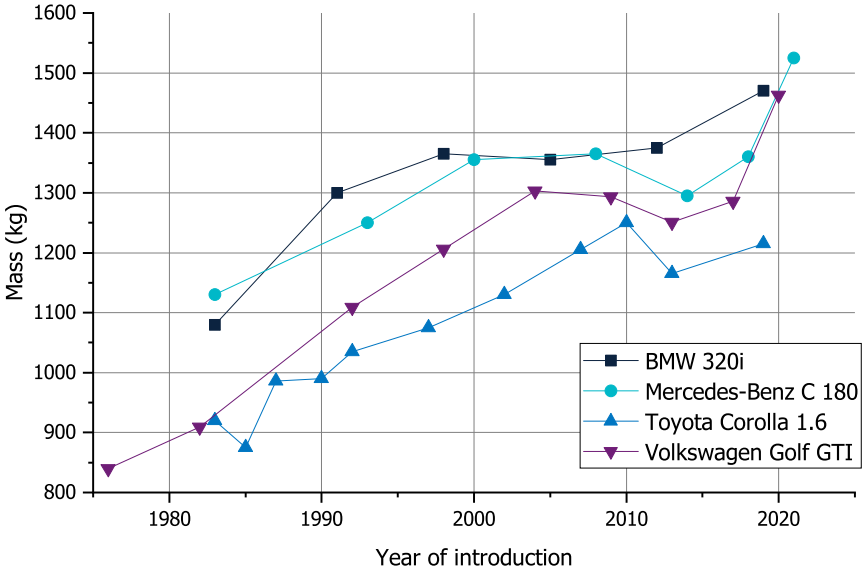

Figure 1.1: Vehicle empty mass vs year of introduction of several generations of mid-size passenger car models on the European market that have maintained a similar configuration.

chassis and body components can be made of fibre-reinforced plastics. More everyday models however still have most chassis and body components in steel; there seems to be insufficient incentive to overcome the generally higher cost associated with the change to fibre-reinforced plastics.

One could even think that the vehicle mass is not important in vehicle design, because the empty mass of passenger cars has generally increased with time. Looking at the evolution over time of the empty mass of four passenger vehicles that have been available on the European market in a mostly unaltered configuration, see Figure 1.1, it seems that despite a stagnation around 2010 there was a steady growth of the empty mass. Yet, it is hard to draw conclusions from this increase because vehicle design is a process with many variable and competing interests. Most of the weight gain can probably be explained by the simultaneous increase in vehicle size and in the number of safety and comfort systems.

There are models with large-scale application of fibre-reinforced plastic in the chassis and body. In niche models such as the Bugatti Chiron, BMW i3 and Alfa-Romeo 4C, the improved dynamic performance and the corresponding status apparently justified part of the higher cost. Whereas, for the twentieth century VEB Sachsenring Trabant it was definitely not the dynamic performance that dictated the choice for its reinforced thermosetting resin body, but rather the shortage of sheet steel [18].

Given the near-future need for further emission reduction for vehicles with combustion engines, it is likely that additional solutions are welcome.[3] Solutions that

[3]Electricity is making a comeback as an energy source for passenger cars, but combustion-engined

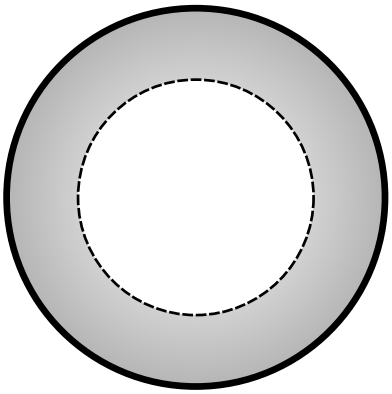

Figure 1.2: Schematic representation of the cross-section of the studied exhaust concept. The solid black line represents the fibre-reinforced outer shell, the white open area in the centre is the flow path for the exhaust gas, and in between is the protection layer that consists of two materials. First, low-mass fibrous insulation (grey) and second, a fabric liner (dashed).

concern replacing steel parts that are more complex and/or costly than body parts are deemed more promising. For that reason, the collaborative project between the department of Structural Integrity & Composites of the faculty of Aerospace Engineering of Delft University of Technology and BOSAL Emission Control Systems n.v., that this dissertation is part of, focusses on the feasibility of having fibre-reinforced plastics replace steel as the main material for the exhaust system. One benefit of this solution is that the exhaust system is functionally independent from the rest of the vehicle, so this change in material does not necessarily complicate the interface.

As exhaust gas temperatures typically reach 800 - 1000 °C, no (fibre-reinforced) plastic could endure direct exposure to exhaust gases. As a consequence, the addition of a low-mass thermal protection layer is critical to the concept studied in this project. A schematic representation of the cross-section of the exhaust concept is given in Figure 1.2. The hypothesis is that this combination of a protection layer and a load carrying shell could be a competitive alternative for steel in all components downstream of the catalytic converter.

Based on the earlier work by others [21–25], the protection layer comprises three main layers: firstly, a low-mass fibrous insulation, secondly, a woven fabric lining the insulation and thirdly, a steel wire mesh to keep the thermal protection layer in place. With this initial solution the insulation and liner are clamped between mesh and shell. Since this reintroduces steel to the systems and adds roughness

(hybrid) vehicles will most likely maintain a fair share of the market for quite some time to come. In 2021, battery electric vehicles accounted for 9% of new passenger car registrations in the EU, but globally their market share was smaller [19]. Especially in regions where the availability of fuel is better than that of electricity or where travel distances are very large, the market share of fully electric vehicles is expected to remain small for the near future. In 2030 the share of electric vehicles (including plug-in hybrids) of the global new vehicle market is forecast at about one-third [20]. There are also several hydrogen fuel cell vehicles available on the market, but their market share and annual sales growth is currently smaller than for battery electric vehicles [19].

to the flow interface, other options were also investigated as part of this project.

The materials in the layers are not new, but their combined application under the demanding conditions encountered in exhausts is. With this novelty comes uncertainty with respect to the performance. Consequently the work behind this thesis was initiated, with the idea of investigating some of the unknowns that are preventing finalisation of the design and the corresponding feasibility study. More specifically, the mechanisms and rates of heat transfer over and wear of the insulation system are unknown: for some aspects, neither literature nor test methods exist.

The flow state over rough, flexible and potentially also permeable (i.e. 'breathing') walls is highly complex and not fully understood yet. Studies have looked at aspects separately, both experimentally and numerically, resulting in many publications over the last two decades. Because of the focus on individual aspects, consensus on how the observed trends and effects interact is not established yet. The pulsating nature of combustion engines adds more complexity and uncertainty. Expressions for friction and heat transfer of regular exhaust systems do generally not apply to the introduced concept exhaust system.

On the other hand, friction and heat transfer are macroscopic properties compared to the smallest length scales of the flow and their rates can in principle be obtained empirically without measuring the intricacies of the flow. This requires established test methods for said configuration and conditions, but those do not exist yet. Given the unique combination of configuration and conditions, the mechanisms dictating the durability of the thermal protection system are as yet unknown. Empirical assessment could also provide insight into wear, but also for that no established test methods exist for exhaust conditions.

More insight into the feasibility of the lined composites exhaust concept is welcome in order to bring it closer to potential realization. With that, an additional solution to reduce the environmental impact of road transportation can potentially be realized.

1.2. Main aim

The main aim of the work described in this thesis is to quantify the three most important and yet uncertain aspects of the performance of a fibre-reinforced exhaust system, namely the flow resistance, heat transfer and durability. This will be done experimentally by using newly developed setups with as representative conditions as possible.

1.3. Outline

The literature review in Chapter 2 starts with an introduction to exhaust systems and then continues with the published works relevant to a fibrous wall lining a turbulent flow channel. Based on that literature, knowledge gaps, hypotheses and research questions are presented regarding the effects of configuration differences on the heat transfer rate, the wear, and the general interaction with the flow.

Based on the literature and formulated hypotheses, in Chapter 3 the flow-wall

interaction in an exhaust is reduced to a simple yet representative form to distil the critical boundary conditions. Based on these conditions, a test set-up for measurement of the back pressure and heat transfer was designed, manufactured and samples were tested. General trends observed in the results obtained using this test are then discussed.

An approach similar to that of the Chapter 3 is applied in Chapter 4, but this time the focus lies on the wear of the protection layer. Relevant boundary conditions were identified and using those a test set-up was designed, manufactured and used on a series of samples. Finally, trends derived from the results are treated.

In Chapter 5 the gained knowledge is employed to describe the remaining realization challenges, options and in some cases also potential developments. Subsequently, the exhaust concept is compared to a conventional exhaust system in terms of mass, CO_2-reduction and material cost.

Lastly, Chapter 6 discusses the obtained results and presents general conclusions and recommendations for further research and engineering.

References

[1] E. H. Wakefield, *History of the electric automobile* (Society of Automotive Engineers Inc, Warrendale, PA, USA, 1994).

[2] J. A. Tarr, *Urban pollution-many long years ago,* American Heritage **22** (1971).

[3] O. I. Awad, X. Ma, M. Kamil, O. M. Ali, Z. Zhang, and S. Shuai, *Particulate emissions from gasoline direct injection engines: A review of how current emission regulations are being met by automobile manufacturers,* Science of the Total Environment **718**, 137302 (2020).

[4] European Parliament and the Council, *Regulation (EC) No 715/2007 of the European Parliament and of the Council of 20 june 2007 on type approval of motor vehicles with respect to emissions from light passenger and commercial vehicles (Euro 5 and Euro 6) and on access to vehicle repair and maintenance information,* Official Journal of the European Union (2007), L171.

[5] European Commission, *Commission regulation (EU) 2016/646 of 20 april 2016 amending regulation (EC) no 692/2008 as regards emissions from light passenger and commercial vehicles (Euro 6),* Official Journal of the European Union (2016), L109.

[6] European Environment Agency, *EEA greenhouse gas - data viewer,* (2021).

[7] United States Environmental Protection Agency, *Inventory of U.S. greenhouse gas emissions and sinks 1990-2018,* (2020), EPA 430-R-20-002.

[8] European Parliament and the Council, *Regulation (EC) No 443/2009 of the European Parliament and of the Council of 23 april 2009 setting emission performance standards for new passenger cars as part of the Community's integrated approach to reduce CO_2 emissions from light-duty vehicles,* Official Journal of the European Union (2009), L140.

[9] M. Weiss, L. Irrgang, A. T. Kiefer, J. R. Roth, and E. Helmers, *Mass- and power-related efficiency trade-offs and co_2 emissions of compact passenger cars,* Journal of Cleaner Production **243**, 118326 (2020).

[10] R. Van Gijlswijk, M. Paalvast, N. E. Ligterink, and R. Smokers, *Real-world fuel consumption of passenger cars and light commercial vehicles*, Tech. Rep. R11664 (TNO, 2020).

[11] European Parliament and the Council, *Regulation (EU) 2019/631 of the European Parliament and of the Council of 17 april 2019 setting CO_2 emission performance standards for new passenger cars and for new light commercial vehicles, and repealing Regulations (EC) No 443/2009 and (EU) No 510/2011,* Official Journal of the European Union (2019), L111.

[12] United States Environmental Protection Agency and National Highway Traffic Safety Administration, *The safer affordable fuel efficient (safe) vehicles rule for model years 2021-2026 passenger cars and light trucks,* Federal Register **85**, 24174 (2020).

[13] L. Ntziachristos, G. Mellios, D. Tsokolis, M. Keller, S. Hausberger, N. Ligterink, and P. Dilara, *In-use vs.type-approval fuel consumption of current passenger cars in europe,* Energy Policy **67**, 403 (2014).

[14] N. E. Ligterink, P. van Mensch, and R. F. A. Cuelenaere, *NEDC - WLTP comparative testing*, Tech. Rep. R11285 (TNO, 2016).

[15] United Nations Economic Commission for Europe, *Concerning the Adoption of Uniform Technical Prescriptions for Wheeled Vehicles, Equipment and Parts which can be fitted and/or be used on Wheeled Vehicles and the Conditions for Reciprocal Recognition of Approvals Granted on the Basis of these Prescriptions,* (2013), regulation 101 rev 3.

[16] United Nations, *Addendum 15: Global technical regulation no. 15 worldwide harmonized light vehicles test procedure,* (2014), ECE/TRANS/180/Add.15.

[17] Lotus Cars, *Lotus philosophy,* Online, visited 27 February 2021.

[18] E. Rubin, *The trabant: Consumption, eigen-sinn, and movement,* History Workshop Journal **68**, 27 (2009).

[19] ACEA, *New car registrations by fuel type, european union,* Press release (2022).

[20] Deloitte, *Electric vehicles - setting a course for 2030,* Deloitte Insights (2020).

[21] B. Van der Wielen, *Feasibility Study of a Full Composite Exhaust System - Temperature Analysis of Light-Weight Exhaust Duct Concepts*, Tech. Rep. (2009).

[22] J. Klein Geltink, *Composite Exhaust Design for a High Performance Car*, Master's thesis, Delft Univerity of Technology, Delft (2010).

[23] L. Wagtho, *CompEx Prototypes and Joint Design*, Master's thesis, Delft University of Technology, Delft (2011).

[24] G. Ridolfi, *Composite exhaust system for lighter weight cars*, Master's thesis, Delft University of Technology, Delft (2012).

[25] T. P. Debrabander, *Durability Analysis of the CompEx System; Investigation on the durability of high temperature composites*, Master's thesis, Delft University of Technology, Delft (2012).

2

Literature on flow-wall interaction in conventional and lined exhaust pipes

In this chapter, the exhaust concept under investigation and the unknowns regarding its performance are detailed, after having been discussed generally in Chapter 1. This detailing is done using the available literature and with conventional exhaust systems as the starting point. First, the functions of exhaust systems are briefly discussed in Section 2.1. Second, the flow state in regular exhausts and its influencing factors is treated in Section 2.2. Third, in Section 2.3, the differences in flow boundary for the lined exhaust concept are discussed together with the (combined) effect that these differences have on the flow state and the flow-wall interaction. Friction, heat transfer and wear are treated individually in that discussion and, where applicable, relevant parameters are introduced. Lastly, in Section 2.4 the identified knowledge gaps are presented together with the research questions that form the basis for the remainder of this thesis.

2.1. Why having an exhaust system?

Having the exhaust gasses exit the engine in the engine bay itself would increase the local temperature to such an extent that it would reduce the engine thermal efficiency. In order to also keep the combustion products and heat away from the engine and interior air intakes, exhaust systems of road vehicles guide the exhaust gasses to or towards the rear of the vehicle.[1] While doing so, the heat still has to be kept away from the passenger or cargo compartment. If the geometry of the used exhaust manifold benefits from pulse interaction, then having an exhaust system can improve the cylinder filling efficiency and thus the engine performance [1].

[1] Here, the vehicle rear is defined with respect to the primary direction of movement.

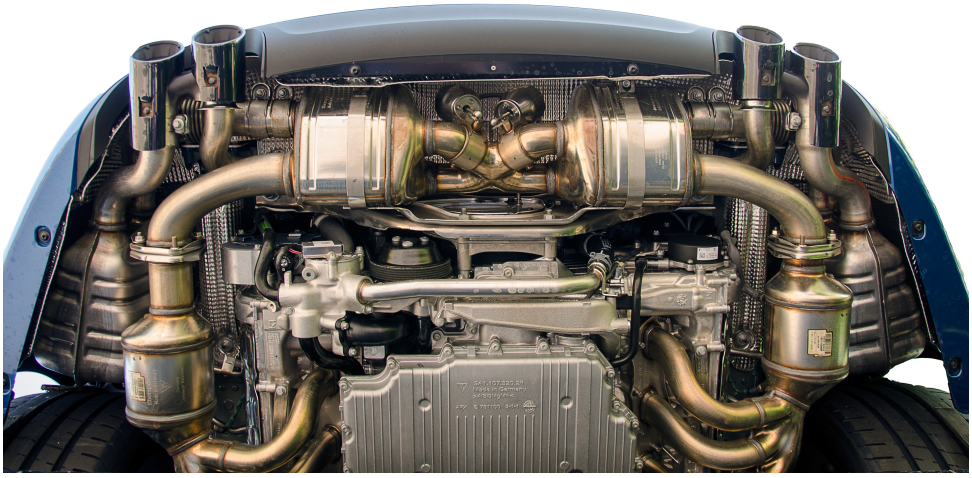

Figure 2.1: Exhaust systems of rear-engined cars, such as this Porsche 911 (997), are generally much more compact than those of front-engined cars. For this high-performance flat-six engine there are effectively two exhaust systems: one for the three cylinders on each side. CC0 Creative Commons image.

Besides improving the engine performance, exhaust systems are also used to comply with norms on some of the negative effects of combustion. Most exhaust systems therefore have several sections where piping is replaced with silencers for acoustic tuning or reactive and filter elements for emission control. As the emission control elements generally benefit from elevated temperatures, those are often placed very close to the engine, whereas the acoustic elements are at the downstream end because of the available space and lower temperature. The addition of these elements makes the gas flow in exhaust systems of rear-engined cars travel a much longer distance than just from the engine to the rear of the vehicle, see Figure 2.1 for an example.

In Figure 2.1, the exhaust manifolds are partially visible on the left and right of the engine block (bottom centre). The catalytic converter is placed as far upstream as possible to benefit from the highest thermal energy and thus at the very beginning of the common pipe section. Downstream of the catalytic converter are two more elements on each side and both are probably silencers. The silencers on the far left and right can be partially by-passed by actuating the valves that are visible in the top centre. The car components surrounding the exhaust system are protected by a heat shield. The next section treats the flow inside exhaust systems.

2.2. Conventional exhaust systems

This section aims to present an overview of the typical flow state inside exhaust systems of internal combustion engines and the interactions between the flow and the exhaust system wall in the form of friction and heat transfer. Typical characteristics are provided where of interest; for friction and heat transfer those are

mainly time-mean properties. The focus lies on a straight exhaust section with fully developed flow because that forms the starting point for the comparison with and development of the lined exhaust concept, however, most aspects apply to exhaust systems in general.

The overview starts with the properties of the source/inlet, then covers the flow domain (boundaries), and thereafter the resulting flow state and the corresponding interaction between fluid[2] and wall. Finally, the exhaust system aspects that were not extensively treated are described.

2.2.1. Combustion engine outflow

The flow exiting an internal combustion engine is a function of the combustion process and thus of the engine design. Only four-stroke combustion engines are considered, for which the exhaust stroke is the last of the 720° combustion cycle [1]. The timing of the combustion in the different cylinders is spaced equally over the two crankshaft rotations for a steady rotation rate. As a result, the firing and thus pulsation frequency is a function of the number of cylinders and the engine (rotation) speed only.

The elevated temperature of the exhaust gas, which dictates the need for an exhaust system, is the result of the relatively low thermal efficiency of internal combustion engines. Nowadays different engines types exist with different exhaust gas temperature ranges and compositions. The two main engine types are described here[3].

The first type is a naturally aspirated petrol engine that operates at an air to fuel ratio close to stoichiometry and has fuel injection into the inlet manifold. It has a relatively low efficiency and high exhaust gas temperatures, but the unwanted combustion products can effectively be tackled using a single (three-way) catalytic convertor. The exhaust gas temperature of such an engine ranges from 500 to 850 °C depending on the engine load (throttle setting) and can peak at about 950 °C [2].

The second type is an engine that has fuel injection directly into the cylinder (petrol or diesel), burns lean, meaning with more air than needed for ideal combustion, and has forced induction[4] with relatively high efficiency and low exhaust gas temperatures as a result. This engine type requires more complex exhaust gas aftertreatment to reach emission levels as low as an engine of the first type: an oxidation catalyst for CO combined with a selective catalytic convertor with urea injection for NO and NO_2 (NO_x) and a particulate filter for particulate matter [3]. The typical exhaust gas temperature range for this type is about 250 to 550 °C.

A defining aspect of internal combustion engine exhaust gas flow is its non-steady nature; the exhaust gas flow is essentially a superposition of cylinder exhaust waves and their reflections. Reflections of the primary exhaust pulse play

[2] In pipe flow the fluid can be either gas or liquid, whereas in combustion engine exhaust systems it is always gas.

[3] Some currently sold petrol engines have both types of fuel injection and can switch between combustion types depending on the required power.

[4] Increased cylinder inlet pressure because of a turbocharger or compressor.

an important role in a tuned exhaust system, because well-timed upstream travelling expansion waves increase cylinder outflow at little cost. During the rest of the combustion cycle however, the flow downstream of a single cylinder is less controlled and even backflow may occur. A relatively short length downstream of the engine, the exhaust pipes of individual cylinders join in a common duct[5]. For a four-cylinder engine the flow in the common pipe does not reverse, but the rate of flow does vary substantially [1]. Such a non-reversing pulsating flow classifies as *current dominated* according to Lodahl et al. [4], as opposed to *wave-dominated* flow.

Compared to acoustic waves, the pressure ratio of a typical exhaust pulse is much larger; Blair classifies them as *finite amplitude pressure waves* [1]. For a naturally aspirated four-cylinder engine, a typical exhaust pulse pressure ratio with atmospheric pressure is 1.5 just before and 1.2 in the common pipe section [1]. The strength of the pulsations is a function of the engine configuration and load level; a turbo-charger, for instance, reduces the downstream pulsation strength substantially. Downstream of the exhaust gas after-treatment systems the pressure amplitude is generally a few percent of the atmospheric pressure.

This amplitude is nevertheless substantially larger than the pressure fluctuations occurring in turbulent flow. Lowson and Schewe both showed that pressure fluctuations in turbulent flow are of the order of 5-10 N m^{-2} [5, 6], which is two orders of magnitude smaller than the pressure variations due to the exhaust pulses.

For each engine type, the exhaust gas temperature and mass flow rate is defined by the throttle setting and, to a lesser extent, the engine speed. More fuel is injected in the engine as throttle is increased, with more and hotter combustion products as a result. With higher engine speeds, more combustions per second take place, thereby increasing the mass flow rate. In general, the maximum mass flow rate of an engine scales with its peak power.

2.2.2. Exhaust system flow boundary

The exhaust gas flow is not just a result of the engine, it is equally well influenced by the downstream boundary conditions. This section therefore focusses on the general configuration of passenger car exhaust systems and specifically those aspects relevant to the flow.

Due to its temperature stability, formability and relatively low material and manufacturing cost, stainless steel is the material of choice for current passenger car exhaust systems [7]. For most industrially produced steel pipes the surface roughness is rather homogeneous and this is also the case for exhaust pipes. The actual average surface roughness size depends on the surface finish, but for stainless steel it is relatively easy to reach a micrometer level average roughness height. The wall thickness is crucial to the mass and some aspects of durability, but less to the flow. It is generally of the order of $1.0 \cdot 10^{-3}$ m.

The diameter is, together with the wall thickness, the largest determining factor in the mass of the exhaust system. On top of that, it also determines the mean flow

[5] In the case of performance engines, there are sometimes effectively two exhaust systems and thus two common ducts. An example is shown in Figure 2.1.

velocity for a given mass flow rate. As the velocity directly affects the turbulence level and the back pressure, the diameter follows from a trade-off between back pressure and mass. As a first impression, one can say that it is chosen such that the time-mean velocity ranges from ~10 to ~100 m s^{-1}, between idle and full load. The corresponding Reynolds number is at least 10^4.

Exhaust system configurations vary depending on the engine location, the engine type and the type of vehicle (passenger, performance or light-duty). This has to do with the design priorities, the functionality and emission legislation. Most current-day vehicle exhaust systems have at least a catalytic converter and a silencer.

If all of the above is taken into account, then the mass of exhaust systems can attain quite a range of values, even when the various exhaust gas after-treatment systems are excluded. It is generally of the order of tens of kilograms.

2.2.3. Pipe flow

Flow-wall interaction of pipe flow in general is discussed first and then the implications for exhaust flow are treated.

The region of the flow domain affected by a wall, the boundary layer, increases in thickness along the wall [8]. In a pipe, it takes a relatively short streamwise length for the boundary layer to reach a thickness equal to the pipe radius and thus to occupy the whole cross section. From that point onward, the mean flow state has become streamwise distance independent, or fully developed [9]. As momentum and temperature have different spatial distributions, their boundary layers differ and so do the required streamwise distances to full development. For both, different entrance geometries result in different such *entry lengths*.

Over time, many entrance configurations have been studied and as a result, empirical correlations are available for the increased friction and heat transfer over the entry length after bends and other pipe entrance geometries [10]. Most studies of influences on pipe flow however focus on the fully developed region and unless otherwise noted, the material covered in this chapter treats fully-developed flow.

The thermal and momentum boundary layer are different but nevertheless related as both are the result of interaction between wall and fluid. As a boundary, the pipe wall imposes a no-slip and wall-blocking condition to the flowing fluid. These two conditions are however not sufficient to describe interaction between the fluid and wall; the small-scale surface geometry is also necessary.

The wall roughness details influence, firstly, the local interaction with the fluid and, with that, they define the near-wall flow state and thus the total wall shear stress. And secondly, if there is a temperature difference between the fluid and the wall, then a nett transfer of thermal energy takes place through collisions of fluid molecules with the boundary. The (dominant) convective part of this heat transfer is a direct function of the flow state and consequently, the wall roughness details also affect the convective heat transfer rate.

The height of the wall roughness relative to that of the viscous sublayer determines the effect of the pipe surface on the turbulent flow; depending on whether the roughness is much smaller, comparable or larger, the near-wall flow state clas-

sifies as smooth, transitional or rough, respectively [9]. As these flow-states are distinctly different, so are the corresponding magnitudes of friction and convective heat transfer and their Reynolds number-dependencies.

To the author's knowledge, no analytical models exist that capture the complicated nature of turbulent flow sufficiently well to allow derivation of the magnitude of friction or convective heat transfer as a function of the Reynolds number. However, a century of studies has resulted in an impressive set of correlations for both magnitudes [10, 11]. Most of these correlations are valid for one of the three interaction regimes and with time, some have been developed with a very high closeness of fit with experimental data. Examples are the Prandtl, Karman and Nikuradse PKN correlation for friction and the Gnielinski modification of the Petukov, Kirillov and Popov correlation for heat transfer, both for smooth pipes.

In these correlations, friction in pipe flow is expressed in non-dimensional form using so-called friction factors. As only general flow and pipe parameters are required for their computation, friction factors enable comparison of different roughness types using for instance the Moody diagram. Two commonly used friction factor definitions are those of Darcy-Weisbach and Fanning. In this thesis the Darcy-Weisbach friction factor is used which is defined as [12]: $f_D = (\Delta p/\Delta x)\,(D/q)$ where $\Delta p/\Delta x$ is the pressure gradient, D is the diameter of the pipe and q is the dynamic pressure.

Since the elaborate friction experiments of Nikuradse with pipe walls lined with sand-grains of different sizes, sand-grain roughness has been the standard reference [12]. Most correlations in the sources mentioned earlier describe the variation of the sand-grain friction factor with Reynolds number and roughness size in one (or more) of the three regimes. As a consequence, the equivalent sand-grain roughness size that results in the same amount of friction can be determined for roughness that differs in terms of shape, size and spatial distribution.

In general, most friction factor correlations were established using isothermal flow and distributed isotropic roughness. Other roughness types have also been studied, but these are much harder to capture using general correlations as additional variables play a role, such as the roughness aspect ratio or pitch.

The correlations for convective heat transfer generally express the rate in non-dimensional form using the Nusselt number, which is the ratio of the convective to conductive heat transfer rate [10]. Since heat transfer also depends on the near-wall flow state, it not surprising that the Nusselt number correlations follow the same interaction regimes as friction [13]. Also similar to friction, heat transfer correlations have been established mostly for pipe surfaces with distributed isotropic roughness. It is furthermore important to note that the bulk of heat transfer studies was performed with small temperature differences, avoiding the influence of a significant variation in fluid properties.

Before moving on to exhaust flow, there is one last measure for the wall-fluid interaction that is worth mentioning: the friction or shear velocity. This artificial velocity is effectively the wall shear stress expressed in the form of a velocity [14]: $u_\tau = \sqrt{\tau/\rho}$. The friction velocity is the normalizing factor in the velocity defect law, which represents the universal velocity distribution in the outer region of boundary

layer flow. This means that with the friction velocity one can determine the velocity profile from a certain distance away from the wall up to the pipe centreline using the velocity defect law, the pipe diameter and centreline mean velocity [8]. The friction velocity is also part of the viscous wall unit (ν/u_τ), which scales the thickness of the viscous sublayer.

2.2.4. Exhaust system gas flow

Exhaust gas flow is, in principle, a subset of turbulent pipe flow, but, as mentioned in Section 2.2.1, it differs in several respects to the generally studied isothermal, steady flow. It is thus worthwhile to determine the relevant regimes and dissect the effect the differences might have on the flow-wall interaction and corresponding correlations. The exhaust wall roughness of micrometres is small enough to classify the wall as smooth over the full engine output range (of temperature and mass flow). This is understandable from an engineering perspective, as the smooth regime results in the lowest friction for a given mean mass flow rate.

To understand the effect of the high fluid temperature, first an estimate of the temperature differences is made. The temperature of the exhaust system wall is the result of the balance between its convective heat transfer with the much hotter gas inside and the much cooler air outside. In that conjugate heat transfer problem, the thermal resistance of the steel wall itself is negligible. Additional complexity stems from the vehicle velocity dependence of the external convective velocity. For now the focus lies on the most common situation: a moving vehicle. In that case, the relative velocity and thus the heat transfer rate are largest and consequently the largest temperature difference between wall and exhaust gas occurs. The exhaust system wall is then about 200 °C less hot than the bulk exhaust gas [2]. At such heat transfer rates, the temperature drop of the exhaust gas along the length of the exhaust system can be substantial; an axial temperature drop of about 70 °C/m in a straight pipe is possible.

With the aforementioned radial temperature difference, the fluid-wall interaction inside an exhaust system becomes a function of the variation in thermophysical fluid properties. As especially the near-wall flow state is altered, the friction and heat transfer correlations for isothermal flow then require correction. Such corrections were developed predominantly in the 70's, amongst others by Petukhov and Gnielinski [15, 16]. However a discrepancy in the magnitude of the influence was observed between analytical predictions and experimental results [15]. The exact cause of the difference is hard to point out, but generally the analytical expressions resulted in a larger effect than the experimental results. Either way, the effect is consistently similar in sign for friction and convective heat transfer, which is in line with their shared dependence on the wall-fluid interaction. Based on Wendland his exhaust experiments with conventional petrol engines, we can assume a gas temperature of 800 °C and a wall temperature of 600 °C [2]. If we then use equation (64) of Petukhov for the heat transfer and equation (66) for the friction as a first estimate, then the friction factor and convective heat transfer rate in exhaust flow are, respectively, 6 and 5% larger than with constant fluid properties. The influence is thus limited.

Table 2.1: Comparison of thermophysical properties of exhaust gas and dry air at 550 and 800°C. The exhaust gas composition is based on stoichiometric combustion of octane with air (17°C, 30 %RH and 1015 hPa).

		Exhaust gas		Dry air	
Property	unit	550 °C	800 °C	550 °C	800 °C
Density	$kg\ m^{-3}$	0.426	0.328	0.430	0.331
Dynamic viscosity	$kg\ m^{-1}\ s^{-1}$	$3.6{\cdot}10^{-5}$	$4.3{\cdot}10^{-5}$	$3.8{\cdot}10^{-5}$	$4.5{\cdot}10^{-5}$
Kinematic viscosity	$m^2\ s^{-1}$	$8.4{\cdot}10^{-5}$	$1.3{\cdot}10^{-4}$	$8.9{\cdot}10^{-5}$	$1.4{\cdot}10^{-4}$
Prandtl number	-	0.73	0.74	0.71	0.73
Specific heat at constant pressure	$J\ kg^{-1}\ K^{-1}$	1223	1293	1102	1154
Thermal conductivity	$W\ m^{-1}\ K^{-1}$	0.060	0.075	0.059	0.072

Irrespective of the exact temperature distribution, quantifying the flow and interaction variables requires an estimate of the thermophysical properties of exhaust gas. For that estimate, exhaust gas can be considered an ideal gas. Only water vapour deviates slightly from the ideal, but not significantly at the temperatures and (partial) pressures under consideration [17]. Table 2.1 shows several thermophysical properties of both exhaust gas and dry air at two representative temperatures.

The presented properties were obtained from temperature-dependent correlations [18] for the individual gas components combined using mixing rules [19]. The exhaust gas partial pressures were estimated using assumed stoichiometric reaction of octane [20] with (humid) atmospheric air [21]. Compared to room temperature, the viscosity is higher and the density lower; the combined effect is a lower level of turbulence at the same mass flow rate. The largest effect of the different composition with respect to air is an increase in the heat capacity at constant pressure.

The exhaust gas properties for combustion with an air to fuel ratio matching stoichiometry are used throughout this thesis. This combustion type was chosen as it results in the highest exhaust gas temperatures and is therefore thermally most demanding for exhaust systems. The property estimate and later analyses are therefore valid for petrol engines that operate with port-injection and not for engines with direct injection or with exhaust gas recirculation (EGR).

The thermophysical properties mentioned above are relevant for the fluid dynamics, however, due to the composition of exhaust gas, also non-convective physical mechanisms such as radiative heat transfer could be significant. Both combustion products, water vapour and carbon dioxide are capable of absorbing and emitting thermal radiation [10]. Radiation interaction with these gases is even more complex than with solids, because of for instance the non-continuous wave-length range and the fact that the interaction depends on the shape of the gas domain. Using the VDI Heat Atlas chapter dedicated to gas radiation, it is possible to estimate the contribution of radiative heat exchange between wall and gas to the total heat transfer [22].

The pulsed engine outflow is only relevant for the exhaust gas flow and related

effects if there is interaction between the pulsations and turbulence. This is only the case if the pulsation amplitude is substantial enough and its frequency is sufficiently close to the frequency range of the turbulent flow. The former has already been established, but the frequency compatibility has to be checked. The lowest frequency relevant to the flow, is that of the largest turbulent eddies and it can be estimated as the ratio of the friction velocity to that of the pipe radius [23]. For the exhaust flow of the experiments described in Chapter 3, $2u_\tau/D$ amounted to 34-128 s^{-1} which was of the same order as the engine firing frequency 130 s^{-1}. If we also use the more recent classification of the forcing frequency in wall units, $\omega^+ = \omega\nu/u_\tau^2$, then exhaust gas flow falls under the intermediate, high or very-high frequency regime depending on the engine load [24]. This generally means that different parts of the flow are influenced by the pulsations.

A short note on the nature of pressure waves in gases: the pulsation changes as it traverses the exhaust system [1]. First of all, the pulse pressure variation (i.e. the pulse shape) changes because of the density dependence of the speed of sound. Secondly, the local pressure variation is a superposition of forward and backward travelling waves. The backward travelling waves are mostly primary reflections that arise from details of the exhaust system such as bends and cross-section changes.

If adding an oscillation to turbulent flow alters the flow, then it could also affect the friction. However, increased and decreased friction factors have been reported in studies, depending on the relative frequency and amplitude of the pulsations, for instance by Kirmse and Tardu et al. [25, 26]. Later, Lodahl et al. [4] covered a very wide range of parameters in their tests and thus managed to identify regimes with no influence, a decreasing and an increasing influence of pulsations on the friction compared to the steady-flow value. In the current-dominated regime, which includes exhaust flow, the friction was unaffected. All these studies covered sinusoidal pressure variations.

Whether the convective heat transfer is affected in a similar fashion by pulsations as the friction is not well-established yet. A series of articles has been published where a pulsator of some kind was added to a turbulent air flow setup without the ability to determine the effect on the flow in terms of oscillation shape and amplitude [27–32]. As a result, the effect of those pulsations on the heat transfer could not be placed in perspective nor be compared to the effect on the friction. In wave-dominated flow (e.g. in pulse-combustors) substantial increases in heat transfer have been reported. For sinusoidal pipe flow, Ludlow et al. showed that the heat transfer enhancement increased substantially with pulsation amplitude in the wave-dominated regime [33]. Hardly any articles cover heat transfer in current-dominated pulsating flow. However, the trend in the results of Ludlow et al. indicates that, in line with friction and within the experimental accuracy, the heat transfer equals the steady flow value for the current-dominated regime. In this sense, the increase in heat transfer that Wendland reports for tailpipes of car-mounted exhaust systems is remarkable, but not necessarily conflicting as it also includes pipe bends [2].

So far, no study with sufficiently-controlled pulsating turbulent pipe flow has contradicted the correlation between friction and heat transfer. In other words,

a pulsation-induced increase in friction was accompanied by an increase in heat transfer; if the friction was unaffected then so was the heat transfer. This is in line with their shared relation to the near-wall flow.

2.2.5. Other exhaust system aspects

Other factors that influence exhaust system gas flow that have not been treated yet are disturbances to the fully-developed flow state such as curves, bends and (acoustic and composition) emission control components. The need for a Convective Augmentation Factor (CAF) reported by Wendland to account for the difference in heat transfer rate, shows that a straight pipe section is not fully representative for an actual exhaust system [2]. On top of that, car-mounted exhaust systems have generally different external conditions than systems in idealized pipe flow studies. For instance, the velocity of the external flow varies substantially between the road and chassis side and so does the surface type and temperature for radiation heat exchange. Although the influence of these factors is not necessarily negligible, it is expected to be similar for both the conventional and lined exhaust concept and are thus not further treated in this thesis.

2.3. Boundary interaction in a lined exhaust

Having introduced the friction and heat transfer for conventional exhaust systems and the aspects of the flow that influence it using literature, the attention can now be shifted to the composite exhaust concept that was introduced in Chapter 1. As the exhaust system wall of the concept differs from that of a regular exhaust, so could the flow and the interaction of the flow with the wall. For the development of the composite exhaust it is necessary to understand the interaction (friction and heat transfer) sufficiently well, therefore in this section the knowledge on the flow state and wall-flow interaction for that case is presented and knowledge gaps are indicated.

Besides friction and heat transfer, wear of the wall is another important result of the interaction for the lined exhaust system. For regular stainless steel exhaust systems wear due to the thermal and mechanical loading by the flow is generally negligible, but this is not necessarily the case for lined systems. Therefore also the knowledge state regarding wear is presented.

In Section 2.3.1 the differences between a conventional and composite exhaust that could be relevant to the interaction with the exhaust gas flow are discussed individually. Next, in Section 2.3.2 an overview is presented of the available literature regarding the interaction between the composite wall and exhaust gas flow (i.e. with the differences of Section 2.3.1 combined) and knowledge gaps are identified where applicable. The engine outflow is unaltered, so the description of Section 2.2.1 also applies for lined exhausts.

2.3.1. Boundary differences

In short, the alternative wall configuration under investigation is lined with fibrous thermal insulation material that is kept in place by a fabric layer and steel wire

mesh. Several aspects of this flow interface differ from that of a regular exhaust or those used in general pipe flow studies. The main differences between this flow domain boundary and the smooth steel wall of a conventional exhaust system are:

- the mesh wires that fixate the thermal protection layer are relatively large elements and, because of their spacing, the wall roughness classifies as non-distributed or discrete;
- the insulation material and fabric are relatively flexible and as a result, the flow boundary in between the wires could respond to pressure variations;
- the open space in the fibrous insulation and the non-zero permeability of the lining fabric could enable interaction between the gas in the composite wall and in the bulk of the flow;
- the added thermal resistance will result in a smaller temperature difference between the wall surface and the fluid, thus reducing the fluid temperature variation.

Next, for each of these differences individually, the available knowledge on the influence on the interaction of the wall with the exhaust gas flow is described.

The wire elements are of a sufficient size to cause more disturbance in the near-wall flow than the smooth wall of steel exhaust pipe. As the corresponding turbulent transport is increased, the velocity gradient at the wall is smaller [9]. As a result, the mean velocity is lower for the same pressure drop and the friction thus larger.

Just as ribs and grooves, the wire mesh wires holding the insulation in place can be seen as discrete roughness elements. Like most discrete roughness configurations, besides the roughness height, their spacing and geometry are additional variables for the flow interaction [14, 34, 35]. For steady flow, the effect of such roughness on friction and heat exchange is well-studied for heat exchanger performance. No universal friction factor correlation exists because of the additional variables and one has to resort to datasets such as ESDU 79014 [36] or individual articles describing particular configurations [37]. A similarly complex geometry dependence holds for convective heat transfer to walls with discrete roughness elements [9], although the increase compared to a smooth wall is smaller than for friction [38, 39].

Concerning the influence of pulsations, not many studies treating current-dominated (i.e. non-reversing) pulsating flow with rough walls were found. Bhaganagar and Jelly et al. used Direct Numerical Simulation (DNS) to study the friction of sinusoidal roughness under pulsating flow and generally found similar time-mean friction values as without pulsations [40, 41]. Since the current application spans the same frequency regimes, it is possible that the time-mean friction of the (wire-mesh) lined wall is also unaffected by the pulsations.

Compared to a steel pipe, the insulation layer underneath the wire mesh has a relatively low stiffness. If the out-of-plane stiffness of the flow boundary is relatively low and its deformation, and thus potential interaction with the flow, is no longer negligible, then it can be considered compliant. Such flexible flow boundaries are

probably found more often in nature than in engineering applications. In dolphin skin, for instance, the compliance has a drag-reducing effect [42].

For laminar flow, the effect of boundary-compliance on the delay of transition to turbulence is well-established, but for fully turbulent flow the understanding of the effect of compliant walls is still under (active) development. Up to this point, either no effect or a drag increase was reported depending on the (relative) properties of the compliant wall [43–45]. Whether there is significant interaction, and of what form, depends on the combined properties of the wall-fluid system. The stiffness, damping and mass of the wall and the magnitude and frequency of the pressure fluctuations determine whether there could be a non-trivial solution of the wall (and fluid) displacement. Often, the drag increases because the displacement of the compliant wall exceeds the viscous sublayer thickness, causing the intrinsically smooth boundary to become effectively rough.

No studies were found that had a compliant boundary and pulsating flow, so the combined effect is uncertain. However, the displacement of compliant walls is pressure driven and therefore pulsations can also alter the displacement and friction if the pulsation properties match those of the wall.

Porosity affects the flow-boundary interaction differently. It can cause a boundary to lose part of its blocking property and, on top of that, even its no-slip property. If the relative permeability of the insulation layer is high enough, then the moving fluid in the central part of the exhaust mixes with the fluid inside the wall resulting in substantial increases in friction and heat transfer [46–48]. Akin to discrete roughness, no general expressions for friction and heat transfer are available due to the number of involved variables (e.g. geometry, porosity and relative permeability). However, the Reynolds number dependence of this resistance differs from regular (no-slip) rough wall friction.

Also for permeable flow boundaries, no studies were found with pulsating flow, so whether the pulsations would alter the effect of a permeable boundary on the flow state and to what extent is uncertain. Theoretically, the pulsations could increase the mixing and therefore increase the effect on friction and heat transfer.

As the temperature difference between the fluid and (surface of the insulated) wall is smaller than in a conventional exhaust, so is the effect of the variation of fluid properties on the fluid-wall interaction. Since the influence was already small for regular exhaust systems, the influence should be even smaller and the focus thus lies on the boundary differences.

2.3.2. Effect of differences on friction and heat transfer

Understandably, the aforementioned differences were studied mostly independently, but in a lined exhaust all or several of these differences occur simultaneously. This section presents what knowledge exists on their combined effect and what knowledge gaps remain.

A compliant wall with discrete roughness elements is a rather abstract notion and could take several forms, it is therefore not surprising that no studies covering this general combination were found. Here, the focus lies on a relatively flexible fibrous insulation layer with an overhead wire mesh. Since there is general understanding

of the influence of the two aspects separately, the main question is could the two aspects influence each other? Part of that question can be answered using literature on the aspects themselves.

An often encountered mode of deformation of compliant walls in response to pressure variations in turbulent flow over a flat boundary is a two-dimensional streamwise wave [44]. The presence of the mesh wires hinders the propagation of such waves along the wall surface and thus the potential for interaction. Additionally, the mesh alters the exposure of the compliant wall to the overhead flow. Part of the compliant wall is in the wake of the wires and will respond differently. These two effects together, reduce the potential for interaction of a compliant wall with mesh wires with the flow compared to a compliant wall without mesh wires.

Simultaneously, the compliant wall could affect the interaction of the wire mesh with the overhead flow. Especially the dynamic parts of this flow state, such as vortex shedding [49], could be sensitive to (local) movement of the compliant wall. Analogous to interaction of compliant walls with regular boundary layer flow, such interaction requires that the properties of the pressure fluctuations (including the pulsations) and the wall are 'in tune'. This would affect both friction and heat transfer.

Discrete roughness and permeable boundaries individually cause more drag than a flat solid boundary. When both occur together in a boundary, interaction is possible according to simulations by Suga et al. In boundaries with sufficient in-plane permeability, the seepage flow[6] can reduce the pressure difference over (solid) ribs, thereby reducing the rib drag [50]. As a result, the drag of a boundary with these two aspects together is most likely smaller than the sum of both individual drag values. The same holds probably for heat transfer with a boundary featuring both aspects.

Compliant and permeable flow domain boundaries influence the flow through opposing mechanisms. The former through out-of-plane displacement of the boundary, thus activating the boundary, whereas the latter makes the boundary more diffuse, allowing interaction with the stationary fluid inside the porous wall. This makes a combined influence unlikely; which of the two will dominate in the case of a flexible and permeable boundary will probably depend on the magnitude of the relative permeability.

Lastly, there is the situation with all differences combined. In principle, simultaneous interaction between the (pulsating) flow and the compliant and potentially permeable wall with discrete roughness in the form of the wire mesh could lead to a unique flow state. However, no studies covering this situation were found.

2.3.3. Wear

Contrary to steel flow boundaries, fibrous insulation can wear substantially upon exposure to high-temperature turbulent flow. Durability of fibrous insulation un-

[6] When the boundaries are porous, the fluid movement is not restricted to the open part of the domain: in parts of the porous region the velocity will be non-zero inside. If there are discrete impermeable roughness elements, then the part of the flow that passes through the porous region underneath such elements is named 'seepage flow'.

der turbulent flow exposure is complex, its wear can result from a combination of mechanisms and depends on several influences, including the thermal history [51]. The addition of a fabric as a liner reduces the fluid-dynamic forces on individual fibres, but does not necessarily prevent wear [52].

Not many integral studies of damage to porous surfaces due to overhead flow were found and those available cover specific configurations that have limited relevance for the concept at hand [53]. Studies of erosion due to particle impingement can provide insight into potential influences, but are otherwise not representative [54].

2.4. Knowledge gaps

The main aim, described in Section 1.2, translates into the following main research question:

> How can the friction, heat transfer and wear of an internally lined exhaust system be quantified and what do the eventual results mean for the associated mechanisms and the feasibility of the concept?

An idea of the most important influences on the flow state of the concept exhaust is needed to be able to understand the performance of the alternative wall configuration and to estimate the effect of changes in this configuration. With that, directions for potential improvement could be determined.

In the previous section, it was shown that the interaction between the flow and the flow boundary is generally understood for smooth and solid boundaries and also for more complicated boundaries. However, the concept under consideration combines features from several special boundaries and the combined effect is yet unknown. As modelling would be challenging because of the complexity of the configuration and material properties, an experimental approach was chosen. Starting with constant insulation properties, i.e. ignoring insulation wear, the research questions related to friction and heat transfer are:

1. How can the friction and heat transfer rates of exhausts systems that are internally lined with fibrous insulation be quantified?

2. What can be concluded on the friction and heat transfer mechanisms based on their quantification experiments?

Besides the flow state, understanding the degradation of the insulation as a result of the exposure to the flow is also essential for sufficient performance of the concept. The corresponding research questions are:

3. How can the wear rate of an exhaust system that is internally lined with fibrous insulation be quantified?

4. What can be concluded on the wear mechanism based on the performed experiments?

Finally, it is worth examining the concept itself again. Mainly, because the potential of a composite exhaust system as an alternative for the conventional steel ones depends on more than friction, heat transfer and wear. In terms of concept feasibility it is worth looking at its mass, cost and CO_2 emission. Also, the realization up to this point can be revisited with the improved understanding of the conditions and performance to see whether there are alternative configurations that seem more promising. With that it is also necessary to look at remaining realization challenges such as those related to manufacturing.

5. What challenges and uncertainties remain for the realization of the concept?
6. What is the general performance (potential) of the concept in terms of mass, cost and CO_2 emission?
7. What configuration and application of the concept could have the largest potential, based on the performed work?

The answers to these research questions are treated in Chapters 3 to 6, mostly in the presented order.

References

[1] G. P. Blair, *Design and Simulation of Four-Stroke Engines* (Society of Automotive Engineers Inc, Warrendale, PA, USA, 1999).

[2] D. W. Wendland, *Automobile exhaust-system steady-state heat transfer,* SAE Technical Paper **931085**, 15 (1993).

[3] O. I. Awad, X. Ma, M. Kamil, O. M. Ali, Z. Zhang, and S. Shuai, *Particulate emissions from gasoline direct injection engines: A review of how current emission regulations are being met by automobile manufacturers,* Science of the Total Environment **718**, 137302 (2020).

[4] C. R. Lodahl, B. M. Sumer, and J. Fredsøe, *Turbulent combined oscillatory flow and current in a pipe,* Journal of Fluid Mechanics **373**, 313 (1998).

[5] M. V. Lowson, *Pressure fluctuations in turbulent boundary layers*, NASA Technical Note D-3156 (National Aeronautics and Space Administration, 1965).

[6] G. Schewe, *On the structure and resolution of wall-pressure fluctuations associated with turbulent boundary-layer flow,* Journal of Fluid Mechanics **134**, 311 (1983).

[7] P. A. Konstantinidis, G. C. Koltsakis, and A. M. Stamatelos, *Transient heat transfer modelling in automotive exhaust systems,* Proceedings of the Institution of Mechanical Engineers, Part C: Journal of Mechanical Engineering Science **211**, 1 (1997).

[8] F. T. M. Nieuwstadt, B. J. Boersma, and J. Westerweel, *Turbulence* (Springer, 2016).

[9] J. O. Hinze, *Turbulence* (McGraw-Hill, New York, 1975).

[10] R. Karwa, *Heat and Mass Transfer* (Springer, Singapore, 2017).

[11] F. W. Dittus and L. M. K. Boelter, *Heat transfer in automobile radiators of the tubular type,* University of California Publications in Engineering **2**, 443 (1930).

[12] J. Nikuradse, *Laws of Flow in Rough Pipes*, Technical Memorandum 1292 (National Advisory Committee for Aeronautics, 1950) translation of "Strömungsgesetze in rauhen Rohren." VDI-Forschungsheft 361. Beilage zu "Forschung auf dem Gebiete des Ingenieurwesens" Ausgabe B Band 4, July/August 1933.

[13] M. S. Bhatti and R. K. Shah, *Turbulent and transition flow convective heat transfer,* in *Handbook of single-phase convective heat transfer*, edited by S. Kakaç, R. K. Shah, and W. Aung (John Wiley & Sons, New York, 1987) Chap. 4.

[14] F. H. Clauser, *The turbulent boundary layer,* in *Advances in Applied Mechanics*, Vol. 4, edited by H. L. Dryden and T. Von Kármán (Academic Press Inc., New York, 1956) pp. 1–51.

[15] B. S. Petukov, *Heat transfer and friction in turbulent pipe flow with variable physical properties,* Advances in Heat Transfer **6**, 503 (1970).

[16] V. Gnielinski, *New equations for heat and mass transfer in turbulent pipe and channel flow,* International Chemical Engineering **16**, 359 (1976), translation of the original in German: Gnielinski, V. Forsch Ing-Wes (1975) 41:145.

[17] W. Wagner and H.-J. Kretzschmar, *D2 properties of selected important pure substances,* in *VDI Heat Atlas*, edited by VDI e. V. (Springer-Verlag, Berlin Heidelberg, 2010) 2nd ed.

[18] M. Kleiber and R. Joh, *D3 properties of pure fluid substances,* in *VDI Heat Atlas*, edited by VDI e. V. (Springer-Verlag, Berlin Heidelberg, 2010) 2nd ed.

[19] M. Kleiber and R. Joh, *D1 calculation methods for thermophysical properties,* in *VDI Heat Atlas*, edited by VDI e. V. (Springer-Verlag, Berlin Heidelberg, 2010) 2nd ed.

[20] S. McAllister, J.-Y. Chen, and A. C. Fernandez-Pello, *Fundamentals of Combustion Processes* (Springer-Verlag, New York, 2011).

[21] A. Picard, R. S. Davis, M. Gläser, and K. Fujii, *Revised formula for the density of moist air (CIPM-2007),* Metrologica **45**, 149 (2008).

[22] D. Vortmeyer and S. Kabelac, *K3 gas radiation: Radiation from gas mixtures,* in *VDI Heat Atlas*, edited by VDI e. V. (Springer-Verlag, Berlin Heidelberg, 2010) 2nd ed.

[23] B. R. Ramaprian and S. W. Tu, *Fully developed periodic turbulent pipe flow. part 2. the detailed structure of the flow,* Journal of Fluid Mechanics **137**, 59 (1983).

[24] P. K. Papadopoulos and A. P. Vouros, *Pulsating turbulent pipe flow in the current dominated regime at high and very-high frequencies,* International Journal of Heat and Fluid Flow **58**, 54 (2016).

[25] S. F. Tardu, G. Binder, and R. F. Blackwelder, *Turbulent channel flow with large-amplitude velocity oscillations,* Journal of Fluid Mechanics **267**, 109 (1994).

[26] R. E. Kirmse, *Investigations of pulsating turbulent pipe flow,* Journal of Fluids Engineering **101**, 436 (1979).

[27] A. Al-Haddad and N. Al-Binally, *Prediction of heat transfer coefficient in pulsating flow,* International Journal of Heat and Fluid Flow **10**, 131 (1989).

[28] M. A. Habib, S. A. M. Said, A. A. Al-Farayedhi, S. A. Al-Dini, A. Asghar, and S. A. Gbadebo, *Heat transfer characteristics of pulsated tubulent pipe flow,* Heat and Mass Transfer **34**, 413 (1999).

[29] M. A. Habib, A. M. Attya, S. A. M. Said, A. I. Eid, and A. Z. Aly, *Heat transfer characteristics and nusselt number correlation of turbulent pulsating pipe air flows,* Heat and Mass Transfer **40**, 307 (2004).

[30] A. E. Zohir, M. A. Habib, A. M. Attya, and A. I. Eid, *An experimental investigation of heat transfer to pulsating pipe air flow with different amplitudes,* Heat and Mass Transfer **42**, 625 (2006).

[31] E. Elshafei, M. Safwat Mohamed, H. Mansour, and M. Sakr, *Experimental study of heat transfer in pulsating turbulent flow in a pipe,* International Journal of Heat and Fluid Flow **29**, 1029 (2008).

[32] M. Simonetti, C. Caillol, P. Higelin, C. Dumand, and E. Revol, *Heat transfer investigation in engine exhaust-type pulsating flow,* in *Proceedings of the 4th International Conference of Fluid Flow, Heat and Mass Transfer (FFHMT'17)*, 138 (2017).

[33] J. C. Ludlow, D. J. Kirwan, and J. L. Gainer, *Heat transfer with pulsating flow,* Chemical Engineering Communications **7**, 211 (1980).

[34] S. Leonardi, P. Orlandi, and R. A. Antonia, *Properties of d- and k-type roughness in a turbulent channel flow,* Physics of Fluids **19**, 125101 (2007).

[35] K. A. Flack and M. P. Schultz, *Roughness effects on wall-bounded turbulent flows,* Physics of Fluids **26**, 101305 (2014).

[36] Engineering Sciences Data Unit (ESDU), *Losses caused by friction in straight pipes with systematic roughness elements*, Tech. Rep. 79014 (IHS Markit, 2007).

[37] N. Sheriff and P. Gumley, *Heat transfer and friction properties of surfaces with discrete roughnesses,* International Journal of Heat and Mass Transfer **9**, 1297 (1966).

[38] R. H. Norris, *Some simple approximate heat-transfer correlations for turbulent flow in ducts with rough surfaces,* in *Augmentation of Convective Heat and Mass Transfer*, edited by A. Bergles and R. Webb (The American Society of Mechanical Engineers, New York, 1970) pp. 16–26.

[39] D. Chung, N. Hutchins, M. P. Schultz, and K. A. Flack, *Predicting the drag of rough surfaces,* Annual Review of Fluid Mechanics **53**, 439 (2021).

[40] K. Bhaganagar, *Direct numerical simulation of unsteady flow in channel with rough walls,* Physics of Fluids **20**, 1 (2008).

[41] T. O. Jelly, R. C. Chin, S. J. Illingworth, J. P. Monty, I. Marusic, and Ooi, *A direct comparison of pulsatile and non-pulsatile rough-wall turbulent pipe flow,* Journal of Fluid Mechanics **895**, R3 (2020).

[42] T. I. Józsa, E. Balaras, M. Kashtalyan, A. G. L. Borthwick, and I. M. Viola, *Active and passive in-plane wall fluctuations in turbulent channel flows,* Journal of Fluid Mechanics **866**, 689 (2019).

[43] E. Kim and H. Choi, *Space-time characteristics of a compliant wall in a turbulent channel flow,* Journal of Fluid Mechanics **756**, 30 (2014).

[44] Q.-J. Xia, W.-X. Huang, and C.-X. Xu, *Direct numerical simulation of turbulent boundary layer over a compliant wall,* Journal of Fluids and Structures **71**, 126 (2017).

[45] J. Wang, S. S. Koley, and J. Katz, *On the interaction of a compliant wall with a turbulent boundary layer,* Journal of Fluid Mechanics **899**, A20 (2020).

[46] W.-P. Breugem, B. J. Boersma, and R. E. Uittenbogaard, *The influence of wall permeability on turbulent channel flow,* Journal of Fluid Mechanics **562**, 35 (2006).

[47] M. Chandesris, A. D'Hueppe, B. Mathieu, D. Jamet, and B. Goyeau, *Direct numerical simulation of turbulent heat transfer in a fluid-porous domain,* Physics of Fluids **25**, 125110 (2013).

[48] Y. Kuwata and K. Suga, *Lattice boltzmann direct numerical simulation of interface turbulence over porous and rough walls,* International Journal of Heat and Fluid Flow **61**, 145 (2016).

[49] C.-H. Liu and T. N. H. Chung, *Forced convective heat transfer over ribs at various separation,* International Journal of Heat and Mass Transfer **55**, 5111 (2012).

[50] K. Suga, S. Tominaga, M. Mori, and M. Kaneda, *Turbulence characteristics in flows over solid and porous square ribs mounted on porous walls,* Flow, Turbulence and Combustion **91**, 19 (2013).

[51] V. Heuer and G. Walter, *Wear of fibrous ceramic components caused by high velocity gas streams: Erosion mechanisms,* Ceramic Forum International / Ber. DKG **75**, 29 (1998), cfi-Ceram Forum Int.

[52] P. M. Sawko and H. E. Goldstein, *Performance of Uncoated AFRSI Blankets during Multiple Space Shuttle Flights*, NASA Technical Memorandum 103892 (National Aeronautics and Space Administration, 1992).

[53] B. Hofland, *Rock & Roll*, Ph.D. thesis, Delft University of Technology (2005), turbulence-induced damage to granular bed protections.

[54] V. Heuer, G. Walter, and I. Hutchings, *High temperature erosion of fibrous ceramic components by solid particle impact,* Wear **233-235**, 257 (1999).

3

Influence of a porous, compliant wall layer on friction and heat transfer in an exhaust

Successful application of fibre-reinforced plastics as the shell material for combustion engine exhaust systems, requires sufficiently accurate understanding of its influence on other vehicle systems. Its flow resistance is relevant for the engine performance and the heat transfer affects the vehicle underside and road surface. This chapter describes the empirical assessment of both using a newly developed test method.

This chapter is formed by the article *The influence of a porous, compliant layer with overlying discrete roughness elements as exhaust pipe wall on friction and heat transfer*[1]. Compared to the published text, only minor textual changes were made. The material from the appendix of this article can be found in Appendix A of this thesis.

3.1. Introduction

To date, the conventional steel exhaust system has contributed to control of the mass of non-electric road vehicles and thus their emissions. The exhaust system mass has generally reduced through a combination of improved design capabilities and steel compositions. However under the increasingly strict emission standards, such as those for passenger vehicles in the EU [2], there is a need for further mass reduction.

[1] Reurings, C., Koussios, S., Bergsma, O.K., Breugem, W.-P., Vergote, K., Paeshuyse, L. & Benedictus, R., Heat Mass Transfer (2020). https://doi.org/10.1007/s00231-020-02855-4 [1]

One of the options for exhaust systems would be to look for alternatives with increased specific performance, but those are not abundant. The use of a high-strength and high-density material such as steel is not driven by mechanical requirements, but mostly by the demanding combination of durability requirements. The peak temperatures of close to 1000 °C alone, already greatly limit the number of alternative materials.

Switching to multi-material solutions however, could enable a larger set of solutions with higher specific performance than the conventional steel system. More specifically: lining the exhaust with a low-mass and low-conductivity layer could thermally enable a much larger material set for the duct itself.

Understanding the effect of the addition of such a layer on the flow resistance and on the thermal resistance between the gas and duct under the non-steady exhaust gas flow of an internal combustion engine is crucial to this concept.

Friction and convective heat transfer are both fluid-wall interaction phenomena and thus dependent on the flow and wall state. They are macroscopic quantities and, as such, not all subtlety of the complex turbulent flow is of equal influence. It proved possible to establish relative simple correlations for friction and heat transfer in the canonical case of steady, turbulent pipe flow with smooth, solid walls and a small temperature difference [3]. For turbulent flows with more complicated boundary properties and geometries, establishing the friction and heat transfer rates has proved more difficult.

Because of its relevance to cooling systems and other industrial flow systems, friction and heat transfer for turbulent pipe flow has been of interest for at least close to a century [4, 5]. In many cases, the heat transfer, in the form of the Nusselt number, is correlated to the friction factor and consequently these aspects are often investigated together.

Bhatti & Shah [6] compared many of the correlations that were proposed over time for the friction factor and Nusselt number for steady turbulent flow in pipes with walls of homogeneous (sand-grain, k-type) roughness. In those cases the main factors of influence are the relative roughness height, the level of turbulence (Reynolds number) and the Prandtl number of the fluid.

For boundaries with discrete roughness, the spacing and geometry of the roughness elements also play a role. As a result, no general expressions for the friction factor for such cases exist and one has to resort to datasets such as ESDU 79014 [7] or individual articles describing particular configurations [8]. In principle, the same holds for the heat transfer to walls with discrete roughness elements, although Norris [9] introduced a general albeit coarse expression that covers quite a range of geometries.

In sinusoidally pulsating turbulent pipe flow, the effect on the friction factor depends on the amplitude and the frequency of the oscillation that is superimposed on the mean flow. The trend in the results of Lodahl et al. shows that in smooth pipes the friction is unaffected as long as the mean velocity is larger than the oscillating velocity amplitude, i.e. in the current-dominated regime. Wave-dominated flow, on the other hand, can substantially alter the mean friction magnitude [10]. Furthermore, the results from Bhaganagar suggest that also for rough walls the friction is

not affected by current-dominated pulsating flow, unless there is a specific length coupling with the roughness geometry [11].

To the authors knowledge, no studies have refuted the general correlation between friction and heat transfer for pulsating flow in smooth pipes. Analogous to friction, substantial increases in heat transfer have been reported for wave-dominated flow: for sinusoidal pulsations by Ludlow et al. [12] and for pulse-combustors see Meng et al. [13]. For current-dominated flow, no investigations towards the effect of sinusoidal pulsations on heat transfer were found. The trend of the results of Ludlow et al. towards that regime, however, indicates little deviation from the steady flow values. In that sense, the increase in heat transfer that Wendland reports for tailpipes of car-mounted exhaust systems is remarkable but not necessarily conflicting given their curvature [14].

If, contrary to all of the above studies, the out-of-plane stiffness of the flow boundary is relatively low and its deformation and potential interaction with the flow no longer negligible, then it can be considered compliant. Although the effect of boundary-compliance on the delay of transition to turbulence is well-established, for turbulent flow both friction increases and decreases have been reported without consensus on the interaction [15]. The reported effect on friction was however generally small ($< 10\%$) for smooth walls. No work on rough walls or its effect on heat transfer was found.

A porous wall can lose part of its wall-blocking and no-slip properties, depending on its relative permeability, resulting in mixing between the wall and bulk fluid with substantially increased friction and heat transfer as a result [16, 17]. General expressions for these increases are not possible due to the dependence on geometry, porosity and relative permeability [18].

The configuration of the lined exhaust wall in this study has several of these factors in combination and therefore covers new ground. Its porous and compliant wall surface is kept in place using a wire mesh that classifies as discrete roughness and it is exposed to the pulsating exhaust gas flow. Given the uncertainty in the influence of compliance and the non-sinusoidal nature of the pulsating flow, the friction and heat transfer of this configuration is already worth investigating, let alone because of the potential interaction between the three mentioned effects.

Next to the effect of the wall on the fluid-wall interaction, there is also the thermal resistance inside the porous layer that is of interest. Assuming that the permeability of the interface is indeed negligible, then the thermal resistance of fibrous insulation is in principle well understood for the density range of interest.

Between the solid and the gas phase in the insulation, there are four different modes of heat transfer possible: gas conduction, solid conduction, natural convection and radiation. Not all of these modes are equally relevant. At the densities and temperatures under investigation, for instance, natural convection and solid conduction are negligible. The main heat transfer mechanisms are thus radiation and gas conduction; especially the former is a complex mechanism: it depends highly on the optical properties of the fibres (as a function of wavelength) and on the geometry (fibre distribution and size) [19–21].

The two dominant mechanisms, radiation and gas conduction, have different

sensitivities to insulation compression. Gas conduction is at these high porosities effectively independent of the solid fraction, because the mean free path is substantially smaller than the mean distance between fibres (Kn $\leq$ 0.01) [19]. The effect of compression on the radiation resistance however depends on the resulting fibre distribution, because the fibres could rotate or translate or both with different results. If substantial rotation occurs, then a higher thermal resistance can be achieved with the same insulation mass. For mass critical applications such as these, it is therefore worthwhile to investigate the effect of compression on the thermal resistance.

The purpose of this work is to establish the yet undescribed combined influence of an exhaust pipe wall formed by a compliant layer with overlying discrete roughness elements exposed to pulsating turbulent flow on the friction factor and their combined thermal resistance and, at the same time, assess the effect of compression of the compliant layer on the thermal resistance.

This study examines these effects experimentally using a series of instrumented samples placed downstream of a combustion engine in a controlled environment. Through measuring the pressure drop and temperature difference over these samples for a range of flow states with different Reynolds numbers and non-dimensional pulsation frequencies, the effects could be discerned. The wall configurations of these samples cover a range of mesh pitches, compliant-layer densities, and compliant-layer compression ratios.

This articles is organized as follows: section 3.2 describes the samples, setup, and equipment, and the employed procedure and data processing. Subsequently, section 3.3 shows the obtained results and compares the trends to those from literature. Finally, section 3.4 provides the conclusions.

3.2. Materials and methods

The essence of the method is as follows: determine the friction and heat loss rate using, respectively, the static pressure and bulk gas temperature drop over samples that represent lined exhaust sections. A schematic representation of the test setup is provided in Figure 3.3 and a general overview of the different measurements is provided in Table 3.1. The computed friction factors were subsequently compared with reference values from literature to differentiate between various contributions. The subsequent sections detail the aspects of the samples, measurements setup, procedure and processing of the results.

3.2.1. Samples

In order to have a flow state relevant to exhaust systems, the sample's geometry was similar to a section of this envisioned application: a straight pipe lined with the multi-material wall under investigation. Such a axisymmetric sample is more difficult to manufacture than a flat one, but ideally offers the advantage of straightforward, one-dimensional heat transfer.

In the flow direction, the samples consisted of a lined section with connectors at its up- and downstream end. The central section of the sample was a 1-metre

Table 3.1: General measurement and analysis overview. The samples are an assembly of a cylindrical test section with a connector at each end.

Aspect:	Post-processing			
	Reference sample		Lined samples	
measurement	Input	Output	Input	Output
Friction: sample pressure drop	section pressure drop (theory)	connector pressure drop	connector pressure drop	section pressure drop
Heat loss: section gas temperature drop	$\dot{m}$, c_p	section heat loss	$\dot{m}$, c_p	section heat loss
Heat loss: external heat loss model	T_{amb}, v_{amb}, T_{shell}	section heat loss	T_{amb}, v_{amb}, T_{shell}	section heat loss

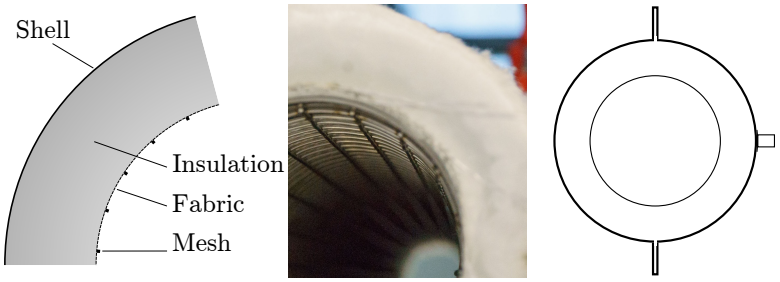

Figure 3.1: Schematic representation of a portion of the sample cross-section with components indicated (left), sample 18-1H-1 before adhesion of the connectors (middle), and schematic representation of a sample during testing with the shell flanges vertical and a gas thermocouple mount on one side (right).

long polymer cylindrical shell, internally lined with a porous ceramic fibre layer and a silica fabric. These were kept in place through a stainless steel mesh. In Figure 3.1 a schematic representation of the cross-section of the sample wall is given. The separate components of the sample are detailed in the paragraphs below.

Firstly, the square mesh was made of stainless steel wires of 1.0 mm diameter placed at a pitch of 11.0 mm. The wires were not woven but welded; the axial wires were radially on the inside of the circumferential wires. The average outer diameter of the circumferential rings was 59.8 mm. At both ends, there was a steel pipe section welded around the mesh extending beyond it, ensuring alignment with the inner tube of the connector. For some of the samples, the streamwise pitch was increased to 23 mm by removing the wire segments between the axial wires of every second circumferential ring. Small parts of the removed rings thus remained at the welds, keeping the fabric at the same distance. For one sample, the mesh was replaced altogether by a 1.5 mm thick solid steel tube with an outer diameter of 60.0 mm.

Secondly, covering the outside of this mesh was a twill-weave silica fabric of

0.44 mm thick. To assess the possibility of interaction, the absolute permeability of the fabric was measured according to ASTM F778 [22] and found to be k = 2x10^{-11} m^2. According to Hahn et al. [23], the effective permeability of a wall in turbulent flow can be classified using the ratio of the effective pore diameter of the wall ($k^{1/2}$) over the wall length unit ν_b/u_τ, where ν_b is the kinematic viscosity of the fluid and u_τ the friction velocity: $u_\tau = \sqrt{\tau_w/\rho_b}$.

Thirdly, the fibrous ceramic material that formed the insulation layer had porosity exceeding 0.9, a mean fibre diameter of several μm and consisted primarily of silica. The material was in blanket-form and two different bulk densities were used: 96 and 128 kg m^{-3}. For the density range used in this study, the fibre volume fraction was between 3 and 4 %. To study the potential influence of the insulation material on the friction and heat transfer, different densities with different amounts of compression were tested. By radially compressing an amount of material to fit the space for the insulation, the density of this layer was increased. Not only could this alter the fibre distribution, it could also result in a reaction force pushing against its domain boundary, altering the compliance of the wall. The different sample insulation densities can be found in Table 3.2 together with corresponding amount of compression.

Each sample had several layers of either of the two densities, but because the layers do not slide relative to each other and tend to buckle locally when bent or compressed, the assembly proved arduous. The general result was consistently applied insulation around the circumference except at the longitudinal seam, where gaps were observed for one or more layers locally along the length. The insulation seam was always positioned at one of the shell flanges. In some cases the rotational symmetry of the heat transfer was affected by this locally reduced density and thermal resistance; shell temperatures of up to 30° C higher than the mean have been observed near the flange at high engine loads. Hence an additional method to derive the heat transfer rate was employed based on the external thermal resistance.

The limited compressibility of the material and its discrete thickness allowed just two configurations with compressed insulation, but it is nevertheless important to know the resulting material density. The strains corresponding to radial compression of a cylinder under internal and external pressure are described by the Lamé solution [24]. If the plane-strain solution is assumed and the Poisson's ratio taken as zero, then this solution can approximate the strains corresponding to the compression of a network of randomly oriented fibres, the result of which is depicted in Figure 3.2. The radial strain is largest at the inner radius and in general much larger than the circumferential strain, causing the fibres to reorient towards the plane perpendicular to the radial direction. Compression thus makes the insulation anisotropic with a fibre orientation bias towards the circumferential direction, perpendicular to thermal radiation coming from the fluid-interface. Also depicted in Figure 3.2 is an estimate of the volume change, which indicates that the volume (and thus density) change is practically homogeneous over the radius.

Fourthly, the duct, or shell, had an average outer diameter of 93.3 mm and a thickness of 1.0 mm. It was made of two halves to allow for installation of the inner

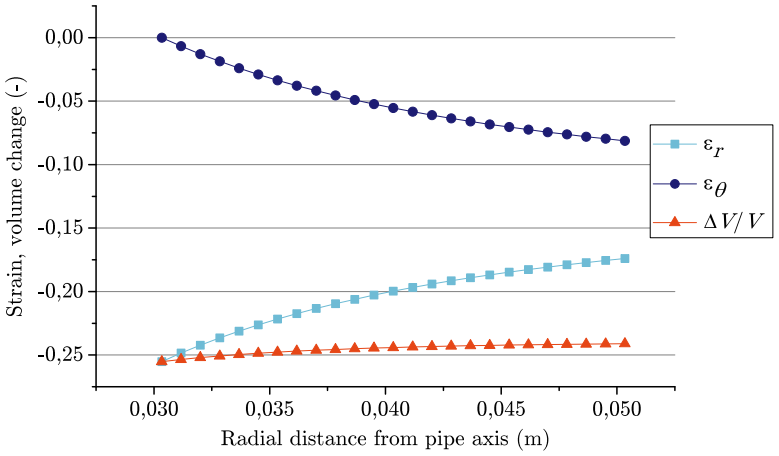

Figure 3.2: Estimation of the radial, ϵ_r, and circumferential strain, ϵ_θ, corresponding to the radial compression of 20-mm of insulation down to roughly 16 mm for a material with zero Poisson's ratio and plane strain. The third curve is the corresponding volume change: $\Delta V/V \approx (1+\epsilon_r)(1+\epsilon_\theta) - 1$.

layers. The 15 mm-wide longitudinal flanges of these two halves were subsequently bonded using a temperature resistant adhesive, see the right hand side of Figure 3.1 for an impression. The thermal conductivity of the shell material is of the order of 1 W m^{-1} K^{-1} which, combined with the limited connector temperature near the shell, makes axial heat conduction along the shell negligible compared to the radial heat transfer.

The adhesively bonded connectors provided the thermal and mechanical connection of the central part to the other elements of the setup. Essentially, these connectors consist of two concentric cylinders of the same diameters as the sample mesh and shell. At one end of the connector, the outer cylinder meets the inner one and there is a flange to attach it to other setup elements. The outer wall thus provides the mechanical connection to the polymer shell. The sole purpose of the inner wall is to guide the flow to the lined section; it has a helical structure allowing its segments to slide axially along each other, accommodating thermal expansion differences. This inner structure forms a flow boundary that is not completely smooth, because the gap between segments forms a rectangular groove.

To distinguish the effect of the mesh geometry, insulation density and compression on the friction and heat transfer separately, several configurations were manufactured and tested. An overview of the different samples and their designation is given in Table 3.2. The flow interface was varied between a smooth solid tube to a mesh with pitches of 11 and 23 mm, with a base insulation density of 128 kg m^{-3} without compression. The insulation compression and density were varied in two different ways in combination with the mesh pitch of 11 mm. First, to obtain the same insulation density as 128-16-H, but with substantial insulation compression and second, to have a considerably higher density. Each configuration except the one lined with the solid tube was manufactured and tested in duplicate

Table 3.2: Sample overview: mesh pitch, initial (pre-assembly) insulation thickness and density, sample insulation density, average radial strain and average volume change. The initial properties are according to factory specification and sample insulation compression properties follow from the Lamé solution with the initial density as input, see Figure 3.2.

sample	p_{mesh} mm	t_{ini} mm	ρ_{ini} kg m^{-3}	ρ_{sample} kg m^{-3}	$\varepsilon_{r,\mathrm{avg}}$ -	$\Delta V/V$ -
128-16-HS	solid	16	128	129	-0,01	-0,01
128-16-H	11	16	128	129	-0,01	-0,01
128-16-HR	23	16	128	129	-0,01	-0,01
128-18-H	11	18	128	149	-0,12	-0,14
96-20-H	11	20	96	127	-0,20	-0,25

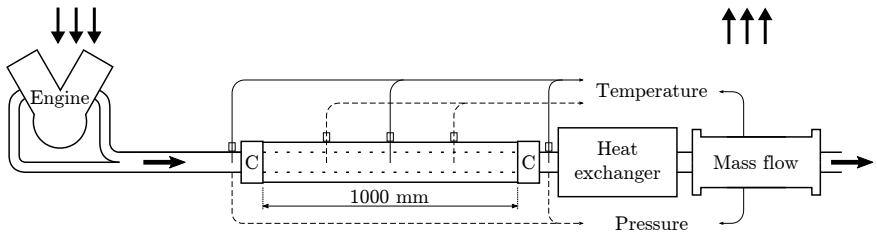

Figure 3.3: Schematic representation of the test setup with, from left to right, V6-engine, manifolds and interface pipe, sample with connectors ('C'), heat exchanger, and mass flow sensor. Also indicated are the locations of gas temperature and pressure measurement: differential measurement (dashed line) and point measurement (solid line). The test cell ventilation entry and exit locations are indicated by the two sets of three arrows.

to assess the consistency and scatter.

The sample with the solid steel inner wall serves as benchmark because friction and convective heat transfer in hydraulically smooth pipes with turbulent flow is well understood. Its wall lining is also definitively impermeable.

3.2.2. Setup

In the setup, each of the described samples was placed downstream of a dynamometer-mounted gasoline V6 engine. The first elements downstream of the merging point of the two engine manifolds were a flexible exhaust joint and a straight pipe section with several sensor ports, together spanning a streamwise length of about 750 mm. The sample in turn was mounted to this pipe through its connector with the shell flanges aligned vertically. A schematic representation of the setup is given in Figure 3.3; the sample orientation is shown schematically on the right side of Figure 3.1.

Coming out of the sample through the downstream connector, the exhaust gasses passed through a heat exchanger and a mass flow sensor and finally ended up in a large silencing vessel that exits into the atmosphere. The heat exchanger was placed downstream of the sample to reduce the exhaust gas temperature to within the validity range of the mass flow sensor. Because the cooling water flow

was actively controlled, the gas temperature could be preset and it was maintained at about 110 °C.

No pressure ports were placed in the lined section to prevent influencing the flow or temperature field. This meant that the static pressure ports had to be placed a few centimetres up- and downstream of the connectors. Both ports were connected to a single transducer to measure only the pressure difference.

The thermocouples for the gas temperature were positioned in the flow using dedicated steel mounts that were adhered to the shell after having drilled the required holes. They assured a similar depth for each measurement and air-tight placement. All three mounts were on the same locations on the circumference: at the top of a shell half, see the right hand side of Figure 3.1. The resulting flow penetration depth of the thermocouple sheath tip relative to the fabric was 38 mm. The longitudinal locations of the three mounts were at 250, 500 and 750 mm from the upstream edge of the 1000 mm shell. The instrumented length of the sample was thus half of its length: 500 mm and it was thus this length that was used in all relevant calculations.

As shown in Figure 3.3, the middle of the three gas thermocouples was used to measure the mean gas temperature and the other two for the temperature drop along the sample. Each thermocouple had three hot junctions along its exposed length, yet only those closest to the tip were used in the subsequent calculations because their temperatures proved most consistent. The only exception to that was the use of the temperatures from the three hot junctions in the central thermocouple to determine the radial gradient in Appendix A.2.

Attempts were made to measure the temperature near at the fabric inside the sample, but the radial temperature gradient was too large to measure accurately using thermocouples. Other in situ temperature measurement techniques were not available or not suitable.

Active ventilation ensured that the test cell air temperature was constant to about 1 °C for a certain test stage. The air circuit was an open one, meaning that the air was taken from outside. Given the time-span of the test, this meant that the inlet temperature was practically constant and in combination with the thermal mass of the test cell, this resulted in a stable ambient air temperature.

The inlet of the air flow is in the ceiling above the engine and the outlet also in the ceiling but above the mass flow sensor, see Figure 3.3. It was estimated that near the sample the air flow direction was both downward and axial. To prevent interference of the shell flanges with the external flow, the samples were mounted with the flanges vertical and thus aligned with the stagnation points of a cylinder in cross-flow.

Because of the vertical component of the air flow, the forced convection-dominated thermal resistance outside of the sample is not exactly rotationally symmetric. For consistent comparison, only shell temperatures measured at locations the furthest away from the flanges were used in the subsequent calculations. Looking at the right side of Figure 3.1, this means they were at the same height as the gas thermocouple brackets or opposite. Lengthwise, these shell thermocouples spanned the same range as the gas thermocouples. In detail, the hot junctions of

the two-wire thermocouples were taped to the shell in the middle between the gas thermocouple mounts and three more were placed exactly opposite these mounts, thus on the other side of the shell.

3.2.3. Equipment

The engine used to generate the turbulent gas flow is a 3.2 litre, naturally aspirated, four-stroke, petrol V6 (General Motors Company, USA) with a transversely mounted exhaust system. Each cylinder bank has its own manifold with integrated catalytic convertor. The exits of these two manifolds meet in a Y-intersection and downstream of that the flow can be classified as non-sinusoidal, non-reversing and having a Womersley number ($\mathrm{Wo} = R\sqrt{\omega/\nu_b}$) of at least 70 [25].

A hydraulic dynamometer (FroudeHofmann, now Froude, USA) was used to regulate the engine speed and power. It regulates the engine rotational speed with an accuracy of 1 RPM, which corresponds to an accuracy of 0.04% for the speed of 2600 RPM that was used in all results reported here. The engine output was controlled through the throttle and this was reflected in the torque, which was measured at 1 Nm accuracy, which corresponds to 0.6 - 5 %, for the applied range of the engine loads.

The mass flow sensors employed were of the calibrated pitot type, requiring pressure transducers for the static and dynamic pressure. Two different diameter flow sensors were used to have a dynamic pressure of sufficient magnitude relative to the employed transducer accuracy. Both were calibrated to an accuracy of 1 %.

All pressures (static pressure difference over the sample and the absolute dynamic and static pressure of the mass flow sensor) were measured using a DMQ*-DT pressure transducer (μmess GmbH, Germany) with an error of 0.2 mbar. An anomaly was observed in the static pressure drop readings for all samples at Reynolds numbers below $2{\cdot}10^4$, probably because of interaction between the transducer internal averaging and the non-steady flow. Consequently, only the pressure drop values obtained at Reynolds numbers of roughly $2{\cdot}10^4$ and higher were used to determine the friction factors.

To determine the connector friction factor and to prove that the anomaly was sensor related, the test with 128-16-HS was performed using a pressure sensor that did not show anomalous behaviour at $\mathrm{Re} < 2 \cdot 10^4$, namely a GE DPI 705 (General Electric Company, US) with a full scale error of 0.07 mbar. The result of that test is shown in Figure 3.6.

All exhaust gas temperature measurements were performed using sheathed, special tolerance K-type thermocouples (Thermo Electric, the Netherlands), yet in terms of geometry and data acquisition there were differences. All the exhaust gas flow temperature measurement inside the sample was performed using thermocouples with an Inconel outer sheath of 3.2 mm in diameter and 0.5 mm in thickness and housing three individual sheathed thermocouples with their junctions at a 10-mm interval from the outer sheath tip. Between the up- and downstream sample thermocouple, the junction pairs were wired for differential measurement[2], as in-

[2] In hindsight this did not improve the accuracy by much because it introduced an additional error through the non-linear temperature-voltage relation of the K-type on top of the lower thermocouple tolerance

dicated in Figure 3.3. The data acquisition for these thermocouples was performed using a Keithley Integra 2701 with a 7708 switch card (Tektronix, USA). For the differential temperatures, a 0 °C simulated cold junction was used resulting in a data-acquisition error of 0.2 °C; for the absolute temperatures, the automatic cold junction compensation resulted in a 1.0 °C error. Over the range of gas temperatures tested, the manufacturer calibrated tolerance in the absolute temperature measurement for the employed K-type thermocouples ranged from 2.2 to 3.2 °C. An analysis of the total temperature uncertainty can be found in Appendix A.1.

A set of regular manufacturer tolerance K-type wire thermocouples was used to measure the shell temperature on both sides of the sample and also near the flanges. Their wires were spot welded to form the hot junctions. Using the Froude-Hofmann system, the data acquisition error was 1.0 °C. Furthermore, at the shell temperatures encountered the individual thermocouple tolerance was 2.2 °C.

The air temperature in the cell was measured directly underneath the ventilation inlet at the engine intake, and at the ceiling away from the air stream; in both cases using an RTD with an accuracy of about 1.0 °C. The atmospheric pressure and humidity were also measured.

All measured quantities were recorded at sampling rate of 1 Hz, with the exception of the exhaust gas temperature measurement inside the sample which was at 0.5 Hz.

3.2.4. Procedure

For all data presented here, the same set of thermocouples, the same engine and the same test cell was used. Furthermore, the gas temperature sensors were placed in the same streamwise order.

Depending on whether the small or large diameter mass flow sensor was in place, the corresponding engine sequence that was programmed in the dynamometer software was run. Each sequence consisted of a set of stages with varying engine loads but always the same engine speed (2600 RPM). Effectively the engine load, and consequently the mass flow rate and gas temperature, was increased with successive stages according to the maximum dictated by the mass flow sensor. Having finished the first sequence, the mass flow sensor was swapped for the other diameter one and the other sequence was started without changing anything else.

Combining both sequences, six unique stages were run with the mean gas temperature and Reynolds number varying between 600 and 800 °C and $1{\cdot}10^4$ and $3{\cdot}10^4$, respectively. Figure 3.4 shows the bulk gas velocity and gas temperature as a function of the engine torque, which is representative for all samples. Even though the engine speed, and thus its firing frequency, was kept constant, all other fluid and flow properties did change with engine load. As a consequence, the wall-normalized frequency ω^+ ($= \omega\nu_b/\bar{u}_\tau^2$) also varied with engine load, more specifically, for the sample of Figure 3.4 it decreased from 0.040 to 0.003 with the engine torque increasing over the sketched range. The overscore on the friction velocity indicates the time-mean value.

of 1.1 °C.

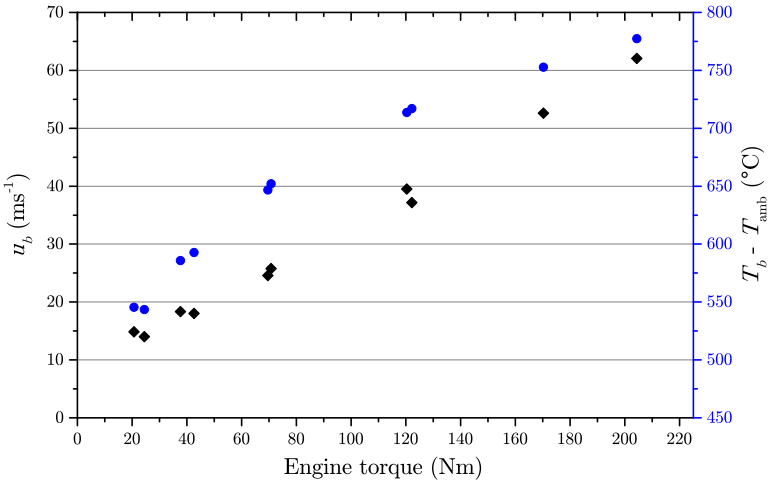

Figure 3.4: The bulk gas velocity (diamonds, left axis) and gas temperature (circles, right axis, relative to ambient) as a function of engine torque at constant engine speed for sample 18-H-1.

Several checks for consistency between and within the sequences were performed for each sample. Firstly, both sequences could be compared because the first stage was the same. Secondly, within each sequence the last stage had the same engine settings as the first. Repeating a stage with the same sample on the same day resulted in gas and shell temperatures that were within a few degrees.

The common first stage that subjects the samples to the largest gas temperature change, was used to determine the duration needed for convergence towards thermal equilibrium. Initial tests showed that duration of this stage of 20 minutes is sufficient to have a shell temperature that differs less than 1.0 °C from its exponential asymptotic value (obtained using a least-squares fit). This stage duration was adopted for all stages in the engine sequence, because the temperature increments become smaller for the successive stages.

The raw data also shows that there was scatter in the engine output in terms of torque and gas temperature; for this reason all measured quantities were time-averaged over the last minute of a stage in the post-processing. The average standard deviations of the gas and shell temperature over the last 60 seconds of each stage of both sequences were 1.0 and 0.6 °C, respectively.

3.2.5. Data processing and analysis

The assumptions behind and methods used to approximate or derive the thermophysical, friction and heat transfer properties are defined in this section. First, the thermal equilibrium of the gas thermocouple is treated to provide an indication of the temperature difference between it and the gas. Second, the thermophysical properties of the flue gas, which differ from dry air, are discussed. Third, the employed diameter for the flow domain of the samples with mesh lining is treated together with the average flow velocity. Fourth, the friction factor calculation is

outlined. Fifth, the axial heat balance of the flue gas is presented together with the resulting heat loss rate. Because of inconsistency observed in this heat loss rate between similar samples, an alternative heat loss rate estimation was also employed. The sixth subsection treats this alternative heat loss rate method. It includes the electrical analogy for radial one-dimensional heat transfer to relate the two methods and it also treats the thermal resistance model of the environment that it is based on.

Thermocouple deviation

The equilibrium temperature of a sheathed thermocouple tip in a gas flow results predominantly from the balance between forced convection and radiation and it could thus deviate significantly from the gas temperature depending on the influence of the radiation. If radiation contributes substantially, then the extent of this deviation depends on the infrared transparency of the gas flow, because that defines whether the radiative heat exchange is with the wall or the gas.

In order to estimate the temperature difference between that of the sheathed thermocouples and the gas itself, the heat balance of the thermocouple was modelled one-dimensionally. Details and results of this model can be found in Appendix A.2. In the end, a temperature-dependent correction was applied to the thermocouple gas temperatures, see Figure A.3.

Thermophysical properties

The combustion process that takes place in the cylinders of the engine alters the composition of the exhaust gas and thus the difference in properties compared to dry air was determined. It was assumed that the exhaust gas composition, used in all subsequent property calculations, could be approximated by the result of the idealized stoichiometric reaction between humid air and gasoline (in the form of octane, C_8H_{18}).

The molar fraction of water in the humid air was calculated using the method of Appendix A.1 of Picard et al. [26] with the measured air pressure and humidity as input. Its density can be obtained using the ideal gas law because at the temperatures and pressures under consideration, the resulting flue gas qualifies as an ideal gas [27].

The specific heat capacity, dynamic viscosity and the thermal conductivity were all obtained using correlations for the temperature-dependent gas component properties and a suitable mixing rule [27, 28][3]. As a result, the specific heat of the exhaust gas obtained in this manner is about 12% higher than that of dry air at the same temperature and pressure. This is the largest relative deviation from dry air for all mentioned thermophysical properties.

In all subsequent calculations the properties of the exhaust gas flow are based on these expressions.

[3] In D3.1 Table 8 the *D*-coefficient of H_2O should have a minus sign.

Diameter, flow velocity and Reynolds number

For both Reynolds number and friction factor computation, a diameter describing the flow channel is needed. For all the samples with a mesh interface, the diameter is not trivial. For these samples all subsequent computations that involve the diameter of the flow domain, D, the outer diameter of the mesh of 59.8 mm, i.e. the interface with the fabric, was employed.

The time-mean bulk flow velocity was based on the mass flow rate as follows:

$$u_b = \frac{\dot{m}}{\rho_b \pi \left(\frac{D}{2}\right)^2} \tag{3.1}$$

where D is the diameter of the flow duct and ρ_b is the average density of the exhaust gas. Similarly for the mean bulk flow Reynolds number:

$$\mathrm{Re}_b = u_b D / \nu_b = \frac{4\dot{m}}{\rho_b \nu_b \pi D} \tag{3.2}$$

where ν_b is the kinematic viscosity of the bulk fluid.

The combined uncertainty in the mass flow rate is dominant for both the bulk velocity as the bulk Reynolds number and as a result the uncertainty of all three is in the range of 2-4 %, depending on the engine load.

Friction factor

The friction factor definition used in this study is that of Darcy-Weisbach:

$$f_D = \frac{\Delta p}{L} \frac{D}{\frac{1}{2}\rho_b u_b^2} \tag{3.3}$$

where Δp is the pressure drop over streamwise length L in a pipe with diameter D.

To obtain the friction factor of the lined sections of the samples of interest, the contribution from the sample connectors has to be subtracted from the total pressure drop, see Figure 3.3. The pressure drop of these connectors can be obtained using the reference sample, because the friction factor of a smooth pipe is well-covered in literature. The employed expression for the friction factor of a smooth pipe in steady turbulent flow is the Techo et al. [3] explicit form of the Prandtl, Karman and Nikuradse correlation. This expression for non-pulsating flow should be applicable as exhaust gas flow is current dominated and according to Lodahl et al. the friction factor for smooth pipes is then not affected by the pulsations [10]. The fact that the pulsation is not sinusoidal should not matter much in the current-dominated regime.

Additionally, the pressure drop due to the gas flow thermocouples was determined by running the experiment with and without them installed.

The friction factors obtained for the connectors and thermocouples can subsequently be used to establish the pressure drop of the lined section of the other samples because these components are the same.

The flow entering the sample through the first connector should be close to or completely fully developed. The development length in steady flow for the turbulent Reynolds numbers at hand ranges from 14.0 to 17.1 hydraulic diameters according to the expression of Zhi-qing (see Table 4.12 of Bhatti and Shah) and Kirmse showed that similar lengths hold for the pressure gradient in pulsating flows [6, 29]. The circular section leading up to the sample connector has a length of about $12.5D$ and ahead of that, the duct is still circular and mostly straight for another few diameters but it does include the Y-intersection of the two manifold exits. The flow must thus at least be close to fully developed.

In all samples there is a sudden change in wall geometry from the connector to the centre section and vice versa, and that has a certain effect on the measured total pressure drop. Siuru and Logan have shown that for the transition from smooth to rough in turbulent flow, the transition length is a few roughness heights, which is negligible compared to the total length of the connector[30]. Even if the transition length for the change from rough to smooth is a few diameters, then that is still relatively short compared to the total connector and lined section lengths. In the samples with the lined section with discrete roughness, the transition is from rough to rough, which is a smaller difference than from smooth to rough and the effect is then also assumed small.

Heat loss rate

Another aspect of the flow is its temperature drop and that can, in certain cases, be related to its heat loss. If we apply the first law of thermodynamics in rate-form to an axial segment of the fluid domain inside the sample and then assume steady-state conditions, no changes in latent energy, no thermal or mechanical energy generation, an ideal gas, and both negligible pressure variation and viscous dissipation, then it reduces to the well-known form [31]:

$$q = \dot{m} c_{\mathrm{p}} (T_{b,\mathrm{in}} - T_{b,\mathrm{out}}) \tag{3.4}$$

where q is the heat loss rate of the fluid over the instrumented length of the sample in W, $\dot{m}$ is the mass flow rate in kg s^{-1}, c_{p} is the specific heat for constant pressure in J kg^{-1} K^{-1}, and $T_{b,in}$ and $T_{b,out}$ represent the bulk temperature in °C (or K) of the fluid entering and exiting the segment, respectively.

If furthermore the axial conductivity is assumed negligible, then only the radial heat flux remains. Equation 3.4 can thus be used to relate the heat loss through the wall of the test section to the bulk temperature drop of the gas. The uncertainty of this rate under the stated assumptions is treated in Appendix A.1.

Most of the stated assumptions are easily verified, but given the relatively large temperature, velocity and friction, a negligible contribution of viscous dissipation is not obvious. Consequently, an estimate of its magnitude was made in Appendix A.3. The result of this estimate is that at the highest engine load the temperature change through viscous dissipation could exceed 10% of the measured temperature drop. At that flow state, the true heat loss is thus somewhat larger than what is obtained from Equation 3.4 because part of the temperature drop was compensated by viscous heating.

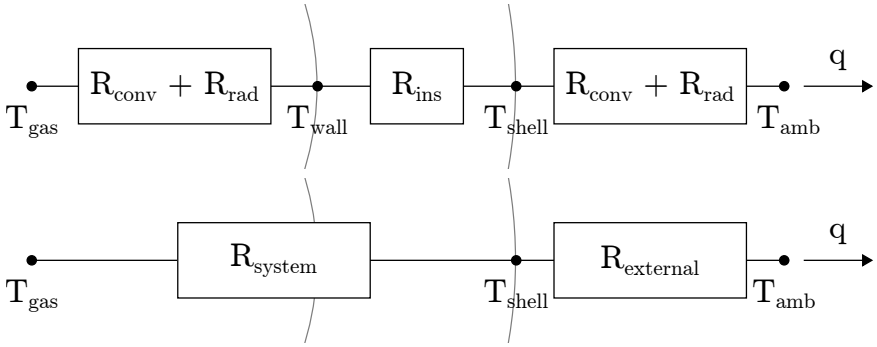

Figure 3.5: Schematic representation of the resistance elements in the electrical analogy of the radial heat transfer. Between the gas and wall there is the combination of convection and radiation, within the insulation the dominant mechanisms are lumped into one effective resistance R_{ins} and outside the sample, the external resistance is a combination of forced convection and radiation. In the absence of T_{wall}, the thermal resistances between the gas and shell can be lumped together into one system resistance R_{system} (bottom representation).

Alternative heat loss rate method

Figure 3.5 shows the electrical analogy of the one-dimensional radial heat flow in the lined section of the sample. The resistance elements in this analogy are the temperature-dependent thermal equivalents (unit: K W^{-1}) of electrical resistance [31]. The thermal resistance of the outer polymer shell and that of the steel inner tube in case of sample 128-16-HS are assumed negligible and thus excluded.

Because the test environment of the samples was always the same, a model of the external thermal resistance can provide an additional measure of the heat loss based on just the temperature of the shell and that of the environment. The main heat transfer mechanisms, and thus those that constitute this model, are forced convection and radiation.

Convective heat loss is often described in terms of the Nusselt number:

$$q_{\mathrm{conv}} = \mathrm{Nu}\lambda_{\mathrm{amb}}/D_{\mathrm{shell}}(T_{\mathrm{shell}} - T_{\mathrm{amb}})A_{\mathrm{shell}} \tag{3.5}$$

where λ is the thermal conductivity of the air and the subscripts *shell* and *amb* indicate the sample shell and environment, respectively.

The employed expression for the Nusselt number of a cylinder in turbulent cross-flow was that of Churchill and Bernstein [3]:

$$\mathrm{Nu} = 0.3 + \frac{0.62\mathrm{Re}_{D\mathrm{shell}}^{1/2}\mathrm{Pr}^{1/3}}{\left[1+\left(\frac{0.4}{\mathrm{Pr}}\right)^{2/3}\right]^{1/4}}\left[1+\left(\frac{\mathrm{Re}_{D\mathrm{shell}}}{282000}\right)^{5/8}\right]^{4/5} \tag{3.6}$$

to which the Gnielinski correction for non-isothermal fluid properties [32] was applied because use of the film temperature was deemed inaccurate given the sizeable temperature difference and where Pr (= $\mu c_{\mathrm{p}}/\lambda$) is the Prandtl number.

To model the radiation it was assumed that the area of the sample (cylinder) was much smaller than that of the enclosing space, allowing a simple expression for radiative heat exchange [33]:

$$q_{\text{rad}} = \varepsilon_{\text{shell}} \sigma \pi D_{\text{shell}} L (T_{\text{shell}}^4 - T_{\text{amb}}^4) \tag{3.7}$$

where σ is the Stefan-Boltzmann constant. The emissivity value of 0.93 for glass-epoxy from Berlin et al. [34] was employed.

The only unknown in the model that could not be reasonably estimated is the ventilation velocity. It was thus obtained for each sample by correlating the heat loss from the gas flow temperature drop through a least-squares fit to the heat loss from the external model, where the latter is a function of the ventilation velocity based on expressions 3.6 and 3.7. For these fits, the stages with an estimated viscous dissipation contribution exceeding 5% were excluded. The smallest of the obtained ventilation velocities was employed in the model, ensuring the smallest influence of insulation flaws on the result.

3.3. Results & discussion

3.3.1. Friction

To obtain the friction factors that are of interest, namely those of the lined sections of the samples presented in Table 3.2, requires the friction factors of the other components. This is treated first, in line with Table 3.1. For the reference sample the pressure drop corresponding to the smooth section was subtracted from the measured total back pressure of the sample, both with and without gas thermocouples, to determine the contributions of the connectors and gas thermocouples separately. The resulting Darcy-Weisbach friction factor f_D of the connectors is shown in Figure 3.6 as a function of Reynolds number. Also shown in this figure is the smooth-wall friction factor according to the explicit form of Techo et al. used to compute the smooth section pressure drop.

The connector friction is effectively constant over the tested range of Reynolds numbers and non-dimensional frequencies ω^+. The magnitude of the connector friction factor is furthermore consistent with the Reynolds number-independent value obtained from the ESDU 79014 data set [7] for steady flow: f_D = 0.06, where the helical elements of the connector were represented as rectangular ribs. The equivalent sand-grain roughness of the connector was obtained using the diameter and Nikuradse's expression for the relative roughness as a function of the friction factor [3]: e/D = 0.031 and k_s = 1.7 mm. This is larger than the estimated groove depth of 1 mm, but within expectation because of the larger flow influence of discrete roughness elements. This is also reflected in the roughness regime classification using the Moody diagram [3]: the connectors are in the transition regime for the three lowest Reynolds numbers and fully rough for the highest one. The curve of constant relative roughness is, even in the transitional regime, relatively flat over the Reynolds number range of interest, which is in line with the lack of Reynolds number dependence in Figure 3.6.

The current results for the connectors indicate that the conclusion of Bhaganagar [11] based on direct numerical simulation, namely that the friction of a surface

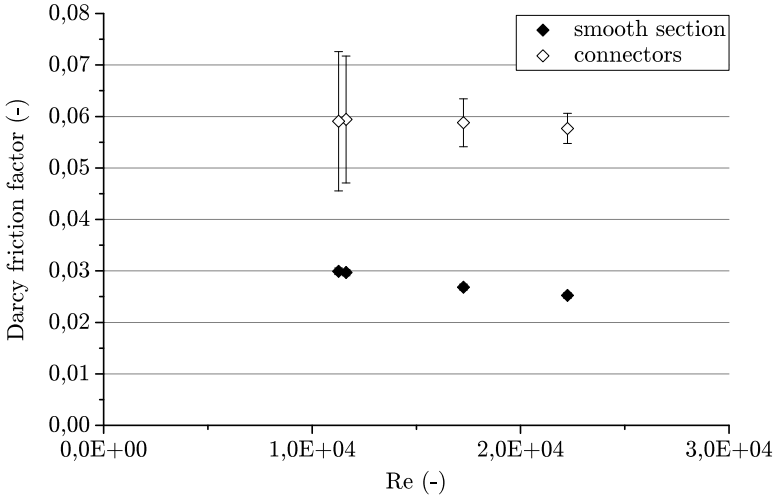

Figure 3.6: Subtraction of the back pressure of the smooth section of 128-16-HS-1 from the total static pressure drop without the gas thermocouples in place allowed determination of the friction factor due to the connectors. Both are shown here with corresponding error bars.

with periodic roughness is unaffected by pulsating flow as long as there is no specific length coupling between the oscillation amplitude and the geometry of the roughness, also holds for discrete roughness of larger size and spacing.

The effect of the gas thermocouples on the friction is much smaller than that of the connectors and also constant with Reynolds number.

Having the contribution to the pressure drop of the other components, now the friction of the lined sections of the other samples can be determined. The contribution of the connectors and the thermocouples to the total pressure drop was smaller than the pressure drop over the lined section, even for the samples with the largest mesh pitch. The average lined-section friction factors, including error bars, of all sample types are graphically compared in Figure 3.7 and a few things stand out.

Firstly, similar to the connector friction factor in Figure 3.6, the friction factors of the samples listed in Table 3.2 are, within the error, constant with Reynolds number and with the simultaneously varying non-dimensional frequency. Within the accuracy of these tests, the discrete roughness section thus seems to be equally insensitive to the pulsations as the connector.

Secondly, the porous compliant wall seems to have little influence. Replacing the solid smooth wall with a wire-mesh at the same insulation density (128-16-H) results in a tripled friction factor, which, in terms of magnitude, is in the range of that observed in literature for solid walls in steady turbulent flow lined with similar roughness types. For instance, using the methodology of ESDU 79014 [7] for semi-circular ribs and circular threads results in $f_D = 0.070 \pm 0.014$ and $f_D = 0.094 \pm 0.014$, respectively. Similarly, Sheriff and Gumley [8] report $f_D = 0.084$ for a wall lined with a 1-mm wire at a pitch of 10 mm. These sources lacked the longitudinal wires

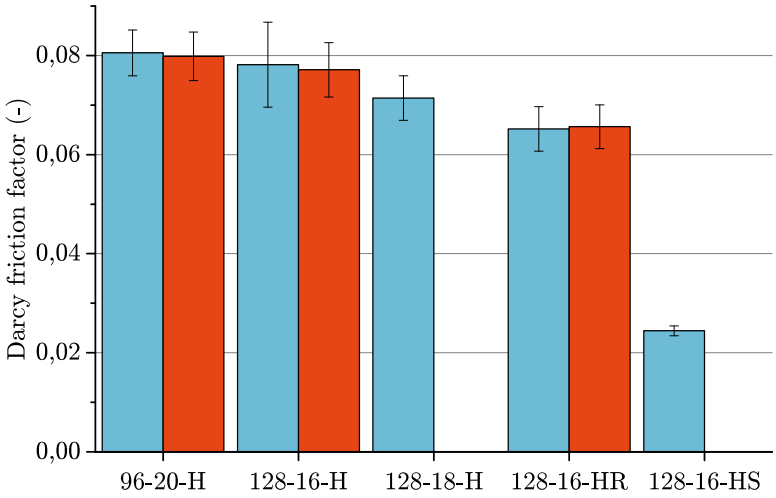

Figure 3.7: Darcy-Weisbach friction factors of the lined sections of samples of all types with corresponding error bars. Multiple bars indicate multiple samples of the same type. The labels are according to Table 3.2.

to form a mesh like the sample has, but their influence should be smaller than that of the circumferential ones. The equivalent sand-grain roughness size of 3.5 mm for 128-16-H is substantially larger than the mesh wire diameter of 1.0 mm and confirms the larger (form) drag of discrete roughness elements compared to closely-spaced ones. Together this suggests that the discrete roughness could, as for the connectors, be the dominant factor.

Thirdly, the friction of samples with an increased circumferential wire pitch is also not substantially affected by the pulsating flow or the underlying compliant, porous wall. The friction factor of 128-16-HR is 16% lower than with the smaller pitch and same insulation density. This decrease is in line with that observed in ESDU 79014 for circular thread walls with the same pitch increase: -16%. This also points to the discrete roughness as the dominant factor.

Fourthly, there is a small decrease in friction factor visible along the left three sample types in Figure 3.7 with increasing insulation density. This could be due to the porous, compliant wall material underneath the roughness elements. Direct interaction between the fluid in the insulation and in the flow is not expected because the ratio between the effective pore diameter of the liner and the wall length unit, the permeability Reynolds number $\mathrm{Re}_K = k^{1/2}u_\tau/\nu_b$, is about 0.1 for the employed fabric which is too small for the wall to be effectively permeable according to Breugem et al. [16]. Another mechanism that could affect the friction is the compliance of the wall, but only in between the mesh wires and with the right coupling with the normalized frequency. Since both the frequency and the wall properties (through the temperature) vary over the test sequence, it could explain part of the intrasample variation in friction between test stages, but not a consistent difference between samples. A last mechanism that could affect the friction is the curvature of

the fabric in between the mesh wires: through a decrease in the volume in between the drag could decrease. This would be expected largest for the samples with the largest compression, 96-20-H, but because those report the highest friction factor this mechanism cannot be responsible. Either way, for the current range of flow and wall properties the influence of the compliant wall is small compared to that of the roughness, but otherwise indecisive.

3.3.2. Thermal resistance

Without feasible means to accurately measure the wall temperature in this configuration without influencing the wall-fluid interface or the heat transfer, the convective heat transfer cannot be analysed independently. That does however not affect the ability to compare the different samples in terms of the combined thermal resistance of the insulation and the wall-fluid interface, R_{system}, see Figure 3.5. For all samples, the total heat loss used to compute the resistance with was obtained from the earlier described external resistance model using the local shell temperature. The total thermal resistance of different configurations is compared and correlations to the friction, insulation density, and compression differences are studied, see for instance Figure 3.8.

As mentioned in the introduction, the interest lies in both the thermal resistance between the fluid and the wall and the thermal resistance of the insulation. As such, it is worthwhile to estimate the relative contributions to R_{system}. This is possible for the reference sample as the system resistance is known just as for the other samples and its fluid-to-wall resistance can be estimated based on available literature.

The resistance between fluid and wall comprises a convective and radiative component and these are well described for the smooth ducts of 128-16-HS. Its convective resistance was calculated using the Nusselt number expression of Gnielinski for a smooth solid circular ducts (Table 8.3 of Karwa [3]) and the net radiative thermal energy exchange rate between a gas and wall was computed according to [35]:

$$q = A\sigma \frac{\varepsilon_{\text{wall}}}{1-(1-\varepsilon_{\text{wall}})(1-A_v)} \left(\varepsilon_b T_b^4 - A_v T_{\text{wall}}^4\right) \tag{3.8}$$

where ε_b and A_v are the emissivity and absorptance of the gas mixture and $\varepsilon_{\text{wall}}$ represents the emissivity of the wall. Of the gas components only water and carbon dioxide were taken into account as a function of their partial pressure, the temperature and equivalent layer thickness. The results show that the contribution of the radiative heat transfer cannot be ignored, because its contribution to the total heat exchange from gas to wall varies between 11% and 24%.

The relative contributions of the fluid-to-wall and insulation resistance can be compared through the ratio of the resulting thermal resistances. At low engine load the ratio of $R_{\text{ins}}/(R_{\text{conv}} + R_{\text{rad}})$ is 6, meaning that the insulation is dominant. As both the insulation and fluid-to-wall thermal resistance of 128-16-HS-1 depend on the engine load and decrease a similar amount in absolute terms, the ratio increases to 13 at the highest engine load, meaning the insulation resistance is even more dominant.

The system heat transfer of the samples with the same density and compres-

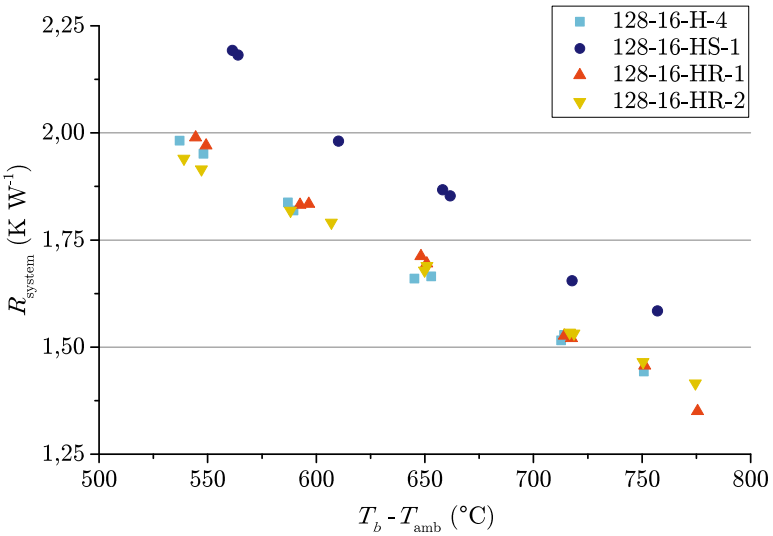

Figure 3.8: Thermal resistance of the system, i.e. between gas and outer shell, for the samples with different flow interfaces but the same insulation density as a function of the temperature difference between the gas and ambient ($T_b - T_{amb}$).

sion as the solid-walled one is shown in Figure 3.8 and the effect of the altered flow interface on the heat transfer is clear. The wire-mesh sample has a thermal resistance that is 13% less at the lowest engine load (and temperature difference) and 11% at the highest. This difference is substantially smaller than the factor three difference in friction and this is in part due to the relatively small contribution of the fluid-to-wall resistance and in part because the convective resistance for the discrete roughness sample will be smaller due to the increased friction. Also, the increase of the mesh pitch has no distinguishable effect on the system thermal resistance. The data points of 128-16-H and -HR in Figure 3.8 clearly overlap. The decrease in friction and the corresponding increase in convective resistance is simply too small to affect the system resistance significantly. In short, for the samples with the same insulation density and compression the trends for the heat transfer are consistent with those for friction when taking into account the relative magnitude of the fluid-to-wall resistance and this consistency substantiates the idea from the friction analysis that there are no substantial effects due to the interaction between the pulsating flow, the compliant wall and the wire roughness.

On the other hand, the samples with a similar insulation density as 128-16-H, but with significant compression (96-20-H) have a distinctly larger thermal resistance, see Figure 3.9. The average thermal resistance difference of the 96-20 samples with 128-16-H increases from about 7% larger at low engine loads to 11% larger at the high engine loads. As the flow interface is similar in terms of geometry, which was confirmed by a comparable friction factor, the difference must be due to the insulation compression. Also, as gas conduction cannot explain the difference because it is insensitive at these densities, the effect has to be due to radiation.

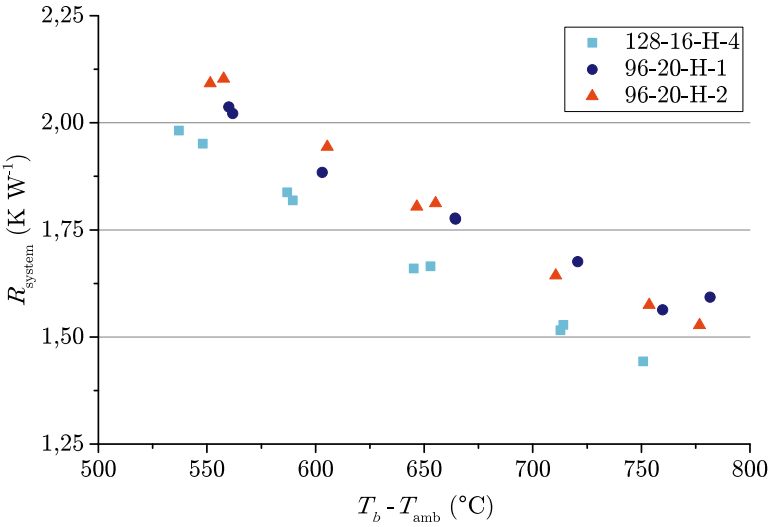

Figure 3.9: System thermal resistance of the benchmark sample, 128-16-H-4, and those with the same density but substantial insulation compression: 96-20-H.

Indeed, the radiation resistance can be related to the compression of the insulation. Firstly, the gas side insulation temperatures are high enough for radiation to contribute substantially to the total heat transfer. Secondly, inherent to the mechanism, the distribution and orientation of the fibres is of direct influence on radiation heat transfer [36]. The nett unidirectional compression can cause alignment towards the direction perpendicular to it, i.e. perpendicular to the radial (and thus radiation) direction, increasing the radiation resistance compared to the non-compressed sample. As the contribution of radiation to the total heat transfer increases with temperature, so does the difference in R_{system} between the two samples. Hence, the slight divergence of the resistance lines of the two samples with increasing temperature difference between the gas flow and the surroundings. This indicates that compression of the here employed fibrous insulation results in reorientation of the fibres that is beneficial to the radiation resistance, meaning that by a higher thermal resistance can be achieved at the same insulation mass through compression of an initially lower density material.

Finally, samples 128-18-H, with the highest density but less compression than the previously discussed samples, have the highest thermal resistance: 10% and 20% larger than that of 128-16-H-4 at low and high engine load respectively, as is shown in Figure 3.10. Again, the flow interface and friction factor were similar between these samples, so the cause lies in the insulation. More specifically, the difference must have been in the radiation, because also this insulation density is too low to affect the gas conduction. As already shown, compression increases the radiation resistance and so does an increase in density [20]. The volume reduction was, with 14%, considerably smaller than for 96-20 and yet the thermal resistance increase has roughly doubled, this means that the density or the combination has

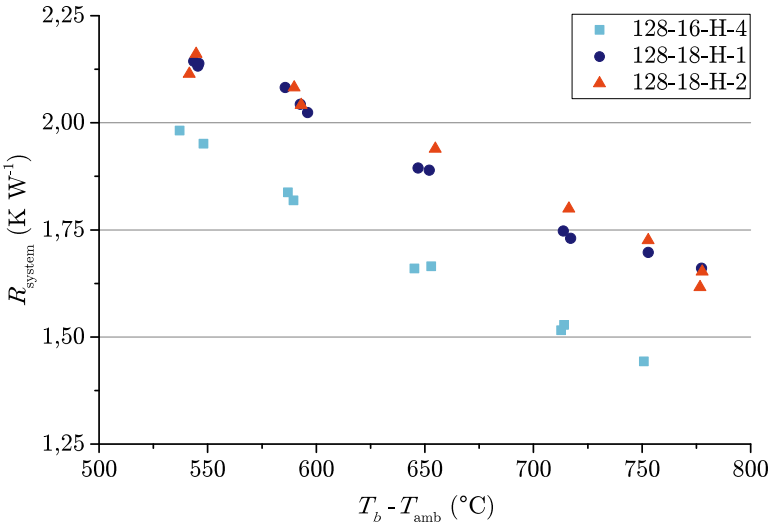

Figure 3.10: System thermal resistance of the benchmark sample, 128-16-H-4, and those with both insulation compression and higher density: 128-18-H.

a larger effect than compression alone.

A future differentiation between the effect of density and compression can be made using a more simple setup that allows more combinations of density and compression, such as the one employed by Daryabeigi et al. [20], since the current work indicates that the overhead gas flow is not of direct influence.

3.4. Conclusions

This article describes an experimental campaign that discerns the influence of different aspects of alternative combustion engine exhaust system walls on the friction factor and thermal resistance. These alternative wall configurations consisted of an outer shell, lined with a porous, fibrous insulation layer that was kept in place using a silica fabric and a steel wire-mesh. The insulation density, the amount of insulation compression and wire-mesh pitch were varied. In the same test, also the total thermal resistance of these configurations was determined, thus including the effect of density and compression. Samples were tested over a range of Reynolds numbers and non-dimensional frequencies relevant to combustion engine exhaust gas flow.

Over the tested range of Reynolds numbers and pulsation frequencies, the friction factor was found constant for the lined sections. Additionally, it did not vary significantly with insulation density/compression. For both wire pitches, the measured friction factors are in line with those reported in literature for similar geometries, but with steady flow and solid walls. Together this indicates that the discrete roughness is the dominant factor and that there is no substantial contribution or interaction of the non-sinusoidally pulsating flow or the compliant wall in between

the roughness elements.

The heat loss was determined using a model of the external resistance together with shell temperature measurements. The influence of the fluid-wall interface configuration was in line with that observed for the friction factor. Besides the interface, not only the insulation density, but also the compression of the fibrous insulation substantially increased the radiative heat transfer resistance. It is hypothesized that this happens because the compression leads to insulation fibre reorientation.

Besides the use of this work for alternative exhaust systems and although the investigated configuration is rather specific, its results have further implications. For instance, the observed lack of interaction between wall-compliance, pulsations and discrete roughness within the experimental error could serve as a start for the design of future experiments that involve such potential interactions. Furthermore, given the small number of publications on the friction of compliant walls, this work could add to the general understanding of the phenomenon. Lastly, the effect of fibrous insulation compression opens room for an investigation into the coupling between compression and fibre reorientation.

References

[1] C. Reurings, S. Koussios, O. K. Bergsma, W.-P. Breugem, K. Vergote, L. Paeshuyse, and R. Benedictus, *The influence of a porous, compliant layer with overlying discrete roughness elements as exhaust pipe wall on friction and heat transfer,* Heat and Mass Transfer **56**, 2367 (2020).

[2] European Commission, *Commission regulation (EU) 2016/646 of 20 april 2016 amending regulation (EC) no 692/2008 as regards emissions from light passenger and commercial vehicles (Euro 6),* Official Journal of the European Union (2016), L109.

[3] R. Karwa, *Heat and Mass Transfer* (Springer, Singapore, 2017).

[4] F. W. Dittus and L. M. K. Boelter, *Heat transfer in automobile radiators of the tubular type,* University of California Publications in Engineering **2**, 443 (1930).

[5] S. Kakaç, R. K. Shah, and W. Aung, eds., *Handbook of Single-Phase Convective Heat Transfer* (John Wiley & Sons, 1987).

[6] M. S. Bhatti and R. K. Shah, *Turbulent and transition flow convective heat transfer,* in *Handbook of single-phase convective heat transfer*, edited by S. Kakaç, R. K. Shah, and W. Aung (John Wiley & Sons, New York, 1987) Chap. 4.

[7] Engineering Sciences Data Unit (ESDU), *Losses caused by friction in straight pipes with systematic roughness elements*, Tech. Rep. 79014 (IHS Markit, 2007).

[8] N. Sheriff and P. Gumley, *Heat transfer and friction properties of surfaces with discrete roughnesses,* International Journal of Heat and Mass Transfer **9**, 1297 (1966).

[9] R. H. Norris, *Some simple approximate heat-transfer correlations for turbulent flow in ducts with rough surfaces,* in *Augmentation of Convective Heat and Mass Transfer*, edited by A. Bergles and R. Webb (The American Society of Mechanical Engineers, New York, 1970) pp. 16–26.

[10] C. R. Lodahl, B. M. Sumer, and J. Fredsøe, *Turbulent combined oscillatory flow and current in a pipe,* Journal of Fluid Mechanics **373**, 313 (1998).

[11] K. Bhaganagar, *Direct numerical simulation of unsteady flow in channel with rough walls,* Physics of Fluids **20**, 1 (2008).

[12] J. C. Ludlow, D. J. Kirwan, and J. L. Gainer, *Heat transfer with pulsating flow,* Chemical Engineering Communications **7**, 211 (1980).

[13] X. Meng, W. de Jong, and T. Kudra, *A state-of-the-art review of pulse combustion: principles, modeling, applications and r&d issues,* Renewable and Sustainable Energy Reviews **55**, 73 (2016).

[14] D. W. Wendland, *Automobile exhaust-system steady-state heat transfer,* SAE Technical Paper **931085**, 15 (1993).

[15] Q.-J. Xia, W.-X. Huang, and C.-X. Xu, *Direct numerical simulation of turbulent boundary layer over a compliant wall,* Journal of Fluids and Structures **71**, 126 (2017).

[16] W.-P. Breugem, B. J. Boersma, and R. E. Uittenbogaard, *The influence of wall permeability on turbulent channel flow,* Journal of Fluid Mechanics **562**, 35 (2006).

[17] Y. Kuwata and K. Suga, *Lattice boltzmann direct numerical simulation of interface turbulence over porous and rough walls,* International Journal of Heat and Fluid Flow **61**, 145 (2016).

[18] M. Chandesris, A. D'Hueppe, B. Mathieu, D. Jamet, and B. Goyeau, *Direct numerical simulation of turbulent heat transfer in a fluid-porous domain,* Physics of Fluids **25**, 125110 (2013).

[19] K. Daryabeigi, *Heat transfer in high-temperature fibrous insulation,* Journal of Thermophysics and Heat Transfer **17**, 10 (2003).

[20] K. Daryabeigi, G. R. Cunnington, and J. R. Knutson, *Combined heat transfer in high-porosity high-temperature fibrous insulation: Theory and experimental validation,* Journal of Thermophysics and Heat Transfer **25**, 536 (2011).

[21] S. Zhao, B. Zhang, and X. He, *Temperature and pressure dependent effective thermal conductivity of fibrous insulation,* International Journal of Thermal Sciences **48**, 440 (2009), int J Therm Sci.

[22] ASTM International, *Standard Methods for Gas Flow Resistance Testing of Filtration Media*, F778, 2014.

[23] S. Hahn, J. Je, and H. Choi, *Direct numerical simulation of turbulent channel flow with permeable walls,* Journal of Fluid Mechanics **450**, 259 (2002), j Fluid Mech.

[24] S. P. Timoshenko and J. N. Goodier, *Theory of Elasticity*, 3rd ed. (McGraw-Hill, New York, 1987).

[25] G. P. Blair, *Design and Simulation of Four-Stroke Engines* (Society of Automotive Engineers Inc, Warrendale, PA, USA, 1999).

[26] A. Picard, R. S. Davis, M. Gläser, and K. Fujii, *Revised formula for the density of moist air (CIPM-2007),* Metrologica **45**, 149 (2008).

[27] M. Kleiber and R. Joh, *D1 calculation methods for thermophysical properties,* in *VDI Heat Atlas*, edited by VDI e. V. (Springer-Verlag, Berlin Heidelberg, 2010) 2nd ed.

[28] M. Kleiber and R. Joh, *D3 properties of pure fluid substances,* in *VDI Heat Atlas*, edited by VDI e. V. (Springer-Verlag, Berlin Heidelberg, 2010) 2nd ed.

[29] R. E. Kirmse, *Investigations of pulsating turbulent pipe flow,* Journal of Fluids Engineering **101**, 436 (1979).

[30] W. D. Siuru, Jr and E. Logan, Jr, *Response of a turbulent pipe flow to a change in roughness,* Journal of Fluids Engineering **99**, 548 (1977).

[31] T. L. Bergman, A. S. Lavine, F. P. Incropera, and D. P. Dewitt, *Fundamentals of Heat and Mass Transfer*, seventh ed. (John Wiley & Sons, 2011).

[32] V. Gnielinski, *G6 heat transfer in cross-flow around single tubes, wires, and profiled cylinders,* in *VDI Heat Atlas*, edited by VDI e. V. (Springer-Verlag, Heidelberg Berlin, 2010) 2nd ed.

[33] S. Kabelac and D. Vortmeyer, *K1 radiation of surfaces,* in *VDI Heat Atlas*, edited by VDI e. V. (Springer-Verlag, Heidelberg Berlin, 2010) 2nd ed.

[34] P. Berlin, O. Dickman, and F. Larsson, *Effects of heat radiation on carbon/peek, carbon/epoxy and glass/epoxy composites,* Composites **23**, 235 (1992).

[35] D. Vortmeyer and S. Kabelac, *K3 gas radiation: Radiation from gas mixtures,* in *VDI Heat Atlas*, edited by VDI e. V. (Springer-Verlag, Berlin Heidelberg, 2010) 2nd ed.

[36] S.-C. Lee and G. R. Cunnington, *Conduction and radiation heat transfer in high-porosity fiber thermal insulation,* Journal of Thermophysics and Heat Transfer **14**, 121 (2000).

4

Empirical assessment of wear of a fibrous wall lining an exhaust

Successful application of fibre-reinforced plastics as the shell material for combustion engine exhaust systems, not only requires sufficiently accurate understanding of the heat transfer through the thermally protective insulation, as treated in the previous chapter, but it also requires the insulation system to do so for a sufficiently long duration. Rather than studying that through long-term heat transfer performance, the durability was assessed separately in more detail. This chapter describes the empirical assessment of the durability and wear. The rather specific conditions required made none of the found test methods applicable and as such another new test setup was developed.

This chapter is formed by the article *Experimental method for investigating wear of porous thermal insulation systems exposed to realistic, hot, turbulent gas flow*[1]. Compared to the published text, only minor textual changes were made. The material from the appendix of this article can be found in Appendix B of this thesis.

4.1. Introduction

Sustainability is a major topic in the European Union and as a result there is substantial drive for improved energy efficiency. This is, amongst others, reflected in the priorities of the EU Horizon 2020 and Horizon Europe innovation programs and in the increasingly strict EU road vehicle emission legislation [2–4].

For road vehicles, the energy efficiency can be increased through lowering the vehicle mass. One possible way to do so is to replace conventional steel exhaust

[1] Reurings, C., Koussios, S., Bergsma, O.K., Vergote, K., Paeshuyse, L. & Benedictus, R., Wear (2021). https://doi.org/10.1016/j.wear.2020.203536 [1]

systems with a lower density material alternative, where, by employing thermal insulation, more materials become suitable alternatives despite the exhaust gas temperature. However, for the most cost- and mass-competitive insulation, ceramic fibres, this is a challenge in terms of performance and durability. This is to a large extent because of the combined long-term thermal and fluid-dynamic influences [5].

Improved understanding of wear of fibrous thermal insulation under combined thermal and fluid-dynamic influences can help in increasing vehicle energy efficiency, but it is also relevant to existing applications where insulation durability matters, such as in processing industry exhausts and ovens. More understanding of the degradation of insulation systems can also help in reducing the formation and release of the types and sizes of ceramic particles that can cause adverse health effects [6].

Realistic wear testing possibilities are crucial for developing and assessing ideas and models for the wear of fibrous insulation and also for validating designs and configurations. Testing on real systems is often not feasible because of the limited availability and associated cost and safety risk. Replacement experiments require representative fluid-dynamic and thermal conditions and realistic mounting of the insulation systems.

4.1.1. State of the art

There are some test rigs and methods already available; these are mentioned and analysed here. First, two from standards and then, three tests found in scientific literature. The analysis focusses on whether the test is suitable for high-temperature, high-turbulence gas flows and on the wear mechanism(s) identified, if reported.

Test standard E859 of ASTM focusses on the erosion of sprayed fire-resistive materials lining ventilation ducts, including sprayed fibrous materials [7]. Another erosion test is part of UL 181, which is a set of standardized tests for factory-made air ducts [8]. Both standards test the wear of material lining a duct by exposing it to an air stream and collecting fibres downstream using filters. The use of collection filters is a proven method for detecting lost fibres or fibre fragments. There is a lower limit to the captured fragment size though, so wear in the form of very small fragments can go undetected. For high temperature flow, the thermal resistance of the filter materials would have to be investigated. Also, the relatively large flows ducts and the use of collection filters is not well suited to high levels of turbulence and temperature, because of the capacity demand on the flow source.

In a set of articles Arnold, Heuer and Walter describe their measurement of wear of different configurations of fibrous insulation using a slit wind tunnel [9–11]. The thermal insulation formed both long sides of a rectangular flow channel, which was termed slit because of its small relative height of 20 mm. Their flow source was a natural gas burner and as a consequence, they achieved temperatures up to 1200 °C and a Reynolds number of $1.4 \cdot 10^4$ at that temperature and even higher at lower temperatures. The insulation wear rate was determined by counting and measuring using SEM the fibres that were sampled isostatically from the flow downstream. Accelerated embrittlement was achieved through thermal

ageing before the test, i.e. by heating the samples to temperatures close to their classification temperature for a certain time interval. The fibre counting using SEM is a rather cumbersome approach and the isostatic sampling is incompatible with pulsating flows as those generated by combustion engines. Only refractory ceramic fibre insulation without cover fabric or binder was tested and it was concluded that the main wear mechanism was loss of complete fibres. The minimum detectable fibre (fragment) size was not mentioned.

Sokov and Sokov [12] have published results of a test of a different type of insulation, namely rigid fibrous hollow cylinders. These fibres are sintered together and can withstand even higher temperatures. The mass change was measured after exposure to flows with temperatures up to 1800 °C. No mention is made of mass flow rate measurements, so the Reynolds number is unknown. The presented method seems incompatible with non-rigid fibrous samples, as no provision is made to house or support them. No mention was made of the mechanics behind the wear.

Mui and Clancy [13] developed a relatively simple laboratory setup to mimic the damage of fibrous insulation systems resulting from flow exposure. A room temperature pulsating air-jet was directed at the centre of a 15 x 15 cm sample under a 45° angle to create a repeated series of travelling waves across the cover fabric. It was used in conjunction with thermal cycling to compare samples with different coatings. This approach offers a lot of freedom in terms of insulation configurations, but the thermal and flow conditions at the sample surface are not necessarily representative for those in for instance pipe flow. Consequently, this test can be used to rank the resistance of materials under the specific test conditions, but the user must determine the degree of correlation with in-service results.

The focus of their investigation was on protective coatings, so only a brief mention of the damage of the uncoated sample was made. The waves passing through the cover fabric separated and ultimately ruptured its fibres. A few seconds after the first few fibres ruptured, a hole formed in the fabric. In the provided figure, these holes in the fabric seem to occur some distance away from the through-the-thickness stitches in the insulation system, where the fabric was less restricted in its movement.

Besides the above mentioned articles, there is little comprehensive literature on the degradation of fibrous insulation (systems) under influence of high temperature turbulent flow. Publications on separate influences do exist, but were usually done with a different aim and were therefore not exactly representative. The authors identified the following influences that can affect the response and thus potentially also the degradation of insulation systems: the system configuration [13, 14], its interaction with the flow [15–18] and the materials and their thermal history [19–21].

The wear test presented in this article simulates in-service conditions with the benefit of flexibility in terms of sample configurations and flow sources, including compatibility with pulsating flows as those generated by combustion engines. Furthermore, it enables simple access to the sample, making mass measurement and inspection with different techniques possible.

4.1.2. Aim and outline

A test for wear of fibrous insulation systems was designed and built that offers wall-like mechanical boundary conditions and well-defined flow conditions. During the development, the focus was on a test rig that could accommodate different insulation configurations with different mounting methods while compatible with different flow sources, including combustion engines.

The result is a test that allows wear quantification through its mass loss and visual identification of the sample state and potential damage accumulation through relatively easy intra-test inspection. The mechanical boundary conditions are such that the test rig can accommodate a range of insulation thicknesses and mounting methods. Also, as the test rig is independent of the flow source and easy to handle, the flow source can be used efficiently, because a second test rig can be coupled to the source while the first rig is, for instance, weighed, inspected or has its sample replaced.

This chapter firstly presents the test rig in detail, part of the test capabilities and the additional components required. Secondly, it presents the experimental procedure and thirdly, representative samples and results are shown. This includes mounting methods, mass change with time and visually observed damage mechanisms.

4.2. Hardware

4.2.1. Test rig

In essence, the test rig forms a closed flow channel with the sample surface forming part of the channel boundary. Along the sample, the flow channel cross-section is rectangular and it smoothly converges both up- and downstream to circular over a length of little over two pipe diameters. See Fig. 4.1 for an overview.

The insulation sample surface forms one of the two long sides of the rectangular flow section in the middle of the test rig, see Fig. 4.3 for a widthwise cross-sectional cut. The surface of other three flow channel walls is smooth steel. The rectangular section has the same hydraulic diameter as the up- and downstream circular sections, so the Reynolds number should not vary along the channel. The flow condition at the sample can thus be derived from the measurements downstream.

The test rig consists of two main components. The first and largest part of the test rig makes up the flow channel and widens on the sample side to form part of its enclosure, this is the top part in Figs. 4.1 - 4.4. The second part of the test rig forms the remainder of the sample enclosure, namely the bottom part in Figs. 4.1 to 4.4. In this easily replaceable part different mounting methods can be integrated. The bottom part is designed to be bolted to the top part. These bolt connections are through the part of the sample that extends beyond the flow channel, thus through its clamped edge, see Fig. 4.2.

As the sample is clamped beyond the flow channel, no special provisions are necessary for mounting it at the edge of the flow domain. Another consequence is that the sample is slightly more constrained near the sides, generally causing the wear to initiate widthwise in the middle, exactly where the flow conditions are

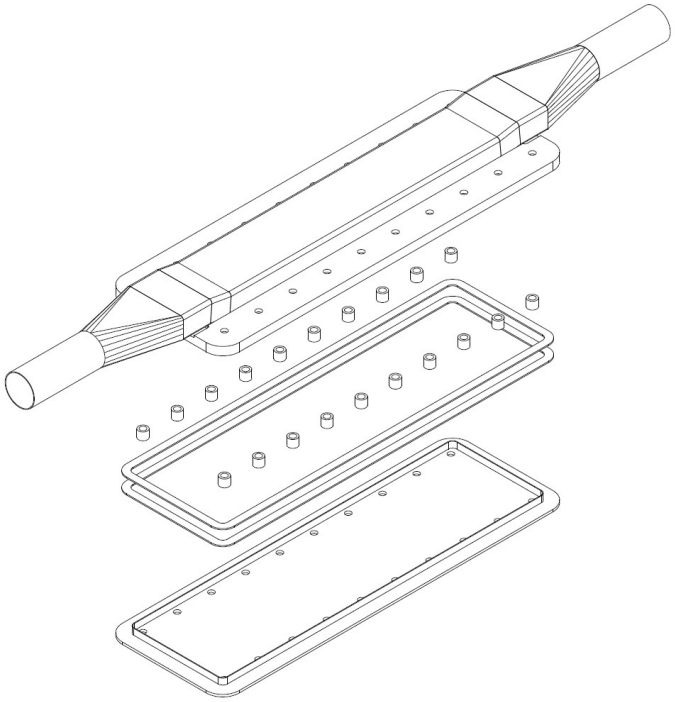

Figure 4.1: Exploded view of the test rig without sample. It consists of two main components: the flow channel itself together with the top and sides of the sample enclosure, and the bottom part of the enclosure to which the sample can be mounted. In between, spacers and gaskets are mounted to control the height available to the sample and seal the circumference, respectively.

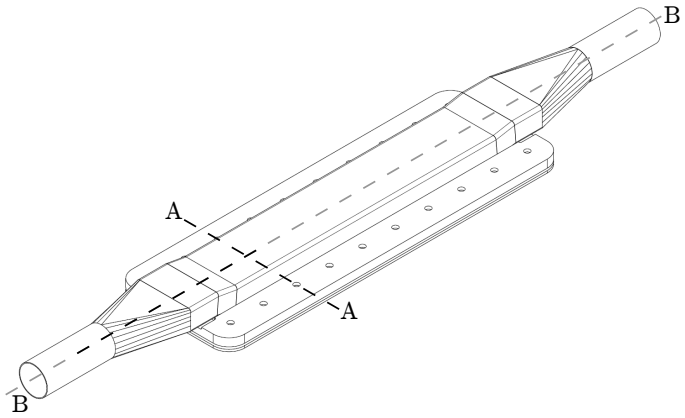

Figure 4.2: An isometric view of the test rig in closed form (nuts and bolts not shown). The dashed lines A-A and B-B indicate the cross-section axes of Figures 4.3 and 4.4.

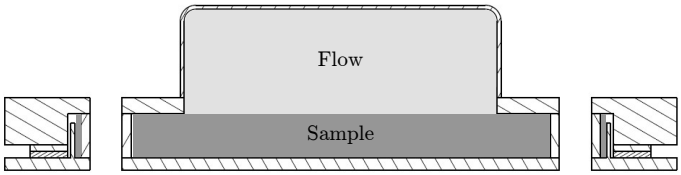

Figure 4.3: Widthwise cut of the test rig, see A-A in Figure 4.2. Visible are the top and bottom parts of the rig, spacing cylinders for the bolts and two stacked gaskets. The flow domain is indicated in solid light grey and the sample domain in solid dark grey.

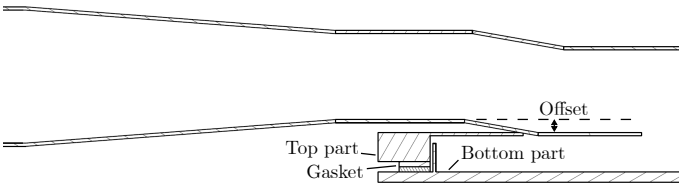

Figure 4.4: Partial mid-plane lengthwise cut of the test rig, namely the bold part of line B-B in Figure 4.2. From left to right, it spans from the cylindrical section to the rectangular sample section of the top part.

well-defined.

The distance between the top and bottom part that defines the sample thickness is set using spacer rings around the bolts. Together with the gasket around the edge of the sample enclosure, these provide sufficient airtightness. See Fig. 4.1 for the spacers and gaskets. In the current configuration, the minimum thickness available to the insulation is 11 mm.

The insulation samples that can be tested using the presented rig are flat, making installation relatively simple and the setup compatible with many different configurations. In the current test rig, the length of the channel boundary that is formed by the sample is more than four times the channel width. The dimensions of the exposed area are 434 by 100 mm. The total length and width available to the sample are 593 and 170 mm, respectively. Sufficient exposed length is, first of all, necessary to make the distance over which the fully developed flow can adapt to the change in wall roughness relatively small. Second, a sufficiently long sample is necessary to be able to test insulation with spatial patterns, e.g. periodic mounting points.

The test rig was designed in such a way that its stiffness and temperature distribution limit the test rig curvature during testing with high gas temperatures. This is the reason that beyond the exposed section of the sample, the channel slopes away to a vertical offset of about 15% of the height of the rectangular channel section, see Fig. 4.4. Also, the spacing rings and gasket around the sample enclosure provide sufficient airtightness to prevent unwanted secondary flow through the sample. The gaskets can be stacked to accommodate different spacer heights. As the pressure difference is generally low, the stacking of gaskets provides sufficient sealing.

Table 4.1: Main specifications of the here presented test rig.

Current max. gas flow temperature	800 °C
Mass change uncertainty	< 0.2 g
Test rig mass	~ 15 kg
Sample size	593.2 x 170 mm
In- and outlet pipe outer diameter	54 mm

The test rig was made of EN 1.4301 stainless steel, providing dimensional stability at high temperatures and resistance against different gas compositions, including flue gasses. The employed gaskets were made of mica and have a maximum service temperature of 950 °C. Thermocouples were spot-welded to the test rig at specific locations to monitor the temperature evolution along the flow channel, and to record the temperature difference between the top and bottom part. In the current configuration, the test rig has been used with gas temperatures up to 800° C. Higher gas temperatures up to 1000 °C are deemed possible, but require further investigation.

The design of the test rig is not set in stone, some aspects can be varied depending on the situation of interest. As already mentioned, the smaller bottom part can be easily replaced and adapted to different insulation mounting systems if necessary. Also, the dimensions of exposed sample area are not crucial and can be adapted to relevance, although a minimum exposure length is required to reduce the influence of entrance effects.

Furthermore, the thickness range available to the sample is not fixed. The sample thickness range of interest is primarily influenced by the insulation type and its mounting. Irrespective whether a porous sample forms a permeable or impermeable fluid boundary, the loads are largest near the flow-exposed surface [15]. The minimum possible sample thickness will therefore often be defined by the need for a realistic mechanical and thermal boundary conditions for the surface layer of the sample. When an internal combustion engine is used as a flow source, a larger sample thickness might be required for a realistic response than for steady turbulent flow because of the larger pressure variations.

The basic cylindrical connections of the test rig allow combination with different flow sources. The authors have used the test rig in combination with blowers, burners and combustion engines, but other sources are not excluded.

4.2.2. Experimental layout

The described test rig is the main component of the experimental setup, but it cannot function on its own. The experimental layout that was employed for the results presented in this article was as follows, from up- to downstream, Fig. 4.5: flow source, connection section with gas temperature measurement, test rig, connection section with gas temperature measurement and mass flow measurement. Additionally, downstream of this layout, the flow was led away from the test area to maintain a steady test environment. Furthermore, to keep the temperature of

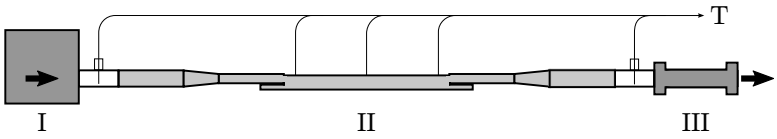

Figure 4.5: Schematic representation of the test setup with, from left to right, flow source (I), test rig (II) and mass flow sensor (III). Also indicated are the locations of temperature (T) measurement.

the test environment constant across time and space, active room ventilation was employed.

The analysis and study of wear requires sufficiently accurate knowledge of both sample and flow state. To assess the mass change of the sample after exposure using the afore described layout (without having to disturb the sample), the mass of the test rig including the sample was measured using a high-accuracy scale. A scale (Mettler Toledo) with a 15 kg capacity and an absolute measurement error of 0.5 g was employed. This accuracy is such that the mass has to be determined at room temperature, otherwise the buoyancy of the hot air inside will result in a bias. An uncertainty analysis according to Dunn [22] was performed to determine the uncertainty in the mass change determination of the sample, see Appendix B.

Using a heat exchanger and flow meter (ABB) the mass flow rate could be determined with about 1 % accuracy. Together with the temperature, measured using K-type thermocouples, this allowed the estimation of all relevant flow properties. Fig. 4.6 resembles part of the setup.

4.3. Experimental procedure

The experimental procedure employed to obtained the results presented in this article was as follows. In order to prevent unwanted secondary flow throughout and around the sample and to determine the virgin sample mass accurately, it is important that the sample is prepared correctly to fit the enclosure. This means sizing it to the casing and punching out the holes for the bolts and spacers. Once the virgin sample mass is determined, it can be installed. Accelerated thermal ageing of samples before testing is possible. This should be done before sizing the sample to the casing as the ageing generally results in non-negligible in-plane shrinkage. The remaining steps before exposure are closing the rig at the preferred sample thickness using the spacer rings, optionally measure the leak rate to check the gasket sealing quality, and then, lastly, determine the mass of the test rig including the sample.

Once this baseline mass has been determined, the test rig can be mounted in the described experimental setup. The sample can then be exposed to the set flow for the required duration. The conditions inside the test rig can be determined from the gas flow temperature in combination with the mass flow rate and from the temperature distribution over the casing.

To assess the mass change of the sample after the exposure, the test rig has to be dismounted and allowed to cool down to room temperature. In the meantime

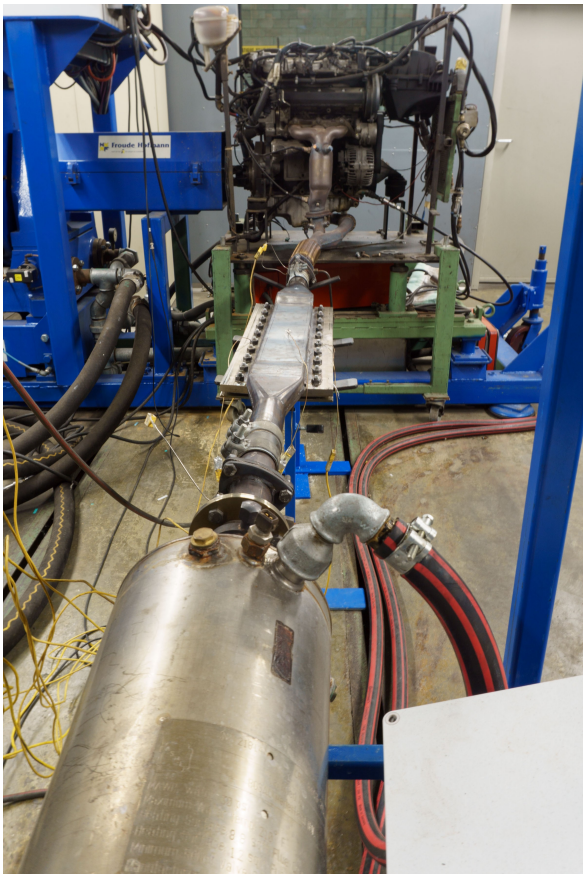

Figure 4.6: The test setup as employed with a combustion engine (figure rear): downstream of the engine manifold is first the test rig with sample (figure middle), then a heat exchanger (figure front) and third a mass flow sensor (not in figure).

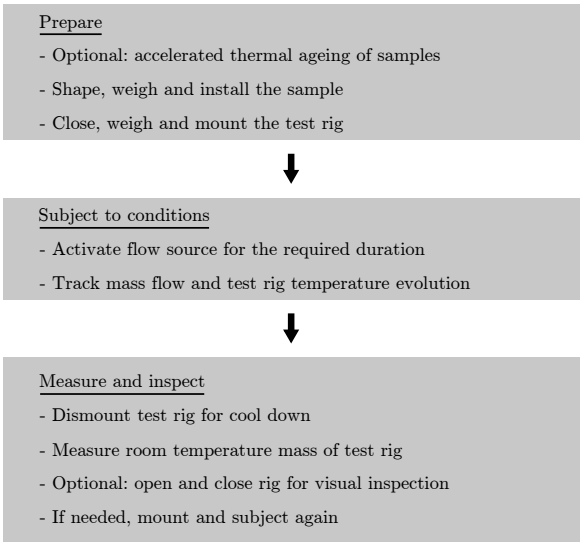

Figure 4.7: Measurement procedure.

a second test rig can be mounted to use the flow source efficiently. Once at room temperature, the mass of the test rig (including the sample) can be determined and thus the mass change with respect to the baseline mass. If required, the casing can be opened to visually inspect the sample or to apply inspection techniques. Subsequently, the casing can be mounted to the flow source again for further exposure. The whole procedure is schematically visualised in Fig. 4.7 and specifications are provided in Table 4.1.

4.4. Results & discussion

A non-exhaustive set of insulation systems that can be tested using the test rig is shown here as a representative example and subsequently, for some the mass change and visual change are discussed. These examples were exposed to internal combustion engine exhaust flow (the more severe end of the test spectrum).

Many types and configurations of fibrous insulation exist and many can be tested using this test rig, some of which are presented here. Besides the insulation material itself, most configuration differences are related to the mounting, i.e. keeping the insulating fibres in place. The solutions differ between applications, but do generally include a cover fabric or liner. Figs. 4.8 to 4.10 depict several mounting configurations.

Figs. 4.8 and 4.9 show a mounting method that requires no modifications of the bottom part of the test rig, namely using a fabric liner held down by a metal mesh that spans the surface. This method offers the possibility to determine the influence of surface elements and of varying degrees of mechanical support on the wear by varying the mesh wire thickness and wire pitch. Another option is to connect the

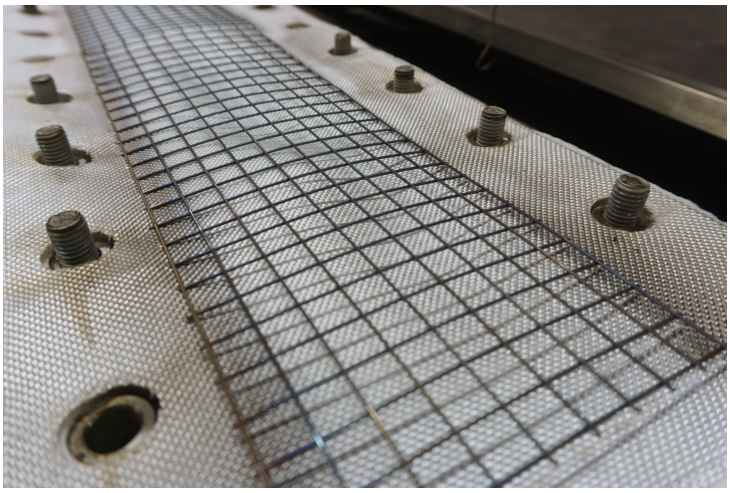

Figure 4.8: Example of sample mounting: a liner with overhead thin metal mesh.

liner to another fabric underneath the insulation and adhere that to the bottom, as shown in Fig. 4.10.

A range of insulation system samples was exposed to gas flow until visible damage to one of the parts had occurred and their configuration was similar to that shown in Figs. 4.8 and 4.9. Given the diversity in types of degradation and the fact that some of these do not occur at the interface with the flow, makes the authors refer to the degradation in general as *wear* rather than *erosion*. Figs. 4.11 to 4.14 show some of the failure mechanisms that occurred. In some cases it was not the insulation that degraded the most. As shown in Fig. 4.11, prolonged exposure proved too much for the mounting in this case with a thin mesh.

Additionally, when testing a sample that was not thermally aged before exposure, a tear occurred in the liner after about 10 hours, see Fig. 4.12. As this type of failure was not observed in samples with thermally aged liners, the tear was probably the result of fibre tension due shrinkage and insufficient capacity for contraction.

Fig. 4.13 shows a form of local insulation damage: cylindrical holes in the insulation underneath and perpendicular to the liner with a large 'shot' chunk inside. These holes suggest that these largest of shot elements do not just fall down, but keep moving around and with their large inertia, damage the surrounding fibre structure.

In most cases however, the tested insulation systems had distributed insulation damage, which is the type that can be better correlated with the mass change. Fig. 4.14 shows an example. With such extensive wear, the mass change can be corrected for the presence of shot chunks in the worn region, as they remain as residue at the bottom of the sample container. This can be done by determining their mass separately after sample removal.

Representative graphs of mass change with exposure time for several fibrous

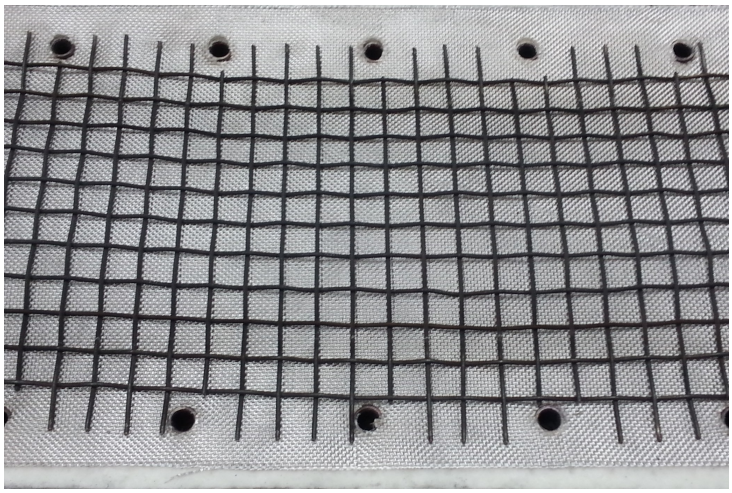

Figure 4.9: Example of sample mounting: a liner with overhead thick metal mesh.

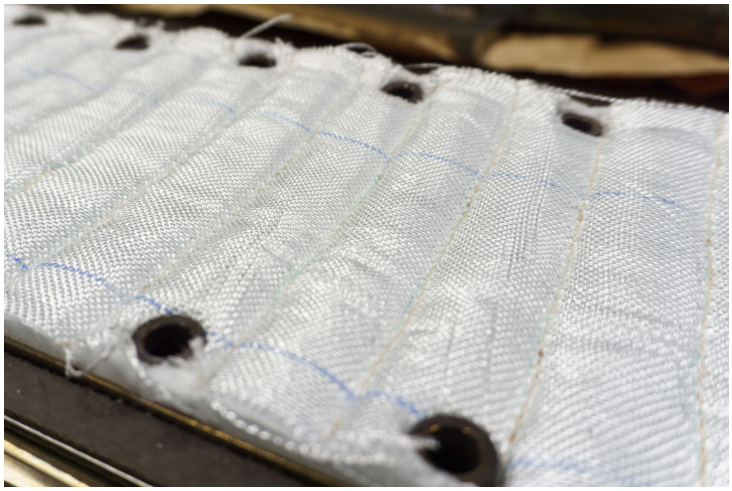

Figure 4.10: Example of sample mounting: locally, the liner is mechanically connected to the bottom.

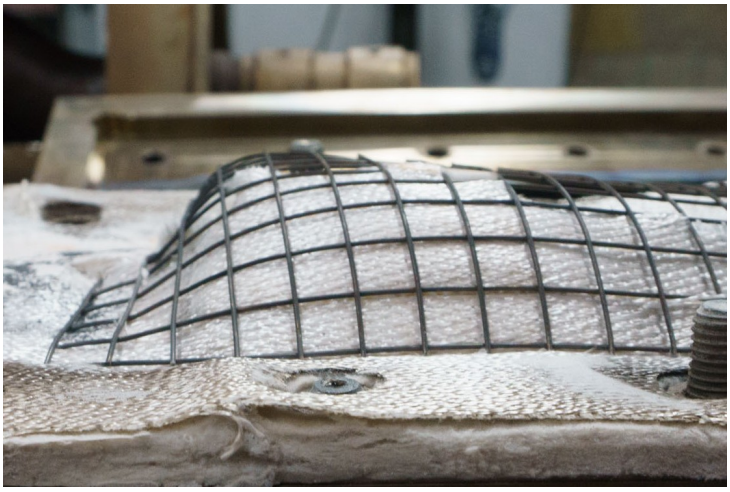

Figure 4.11: Example of mounting failure rather than insulation wear.

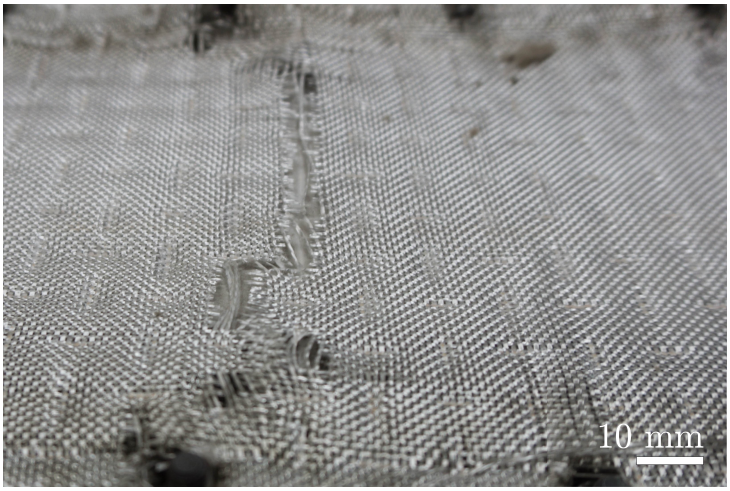

Figure 4.12: Example of protective liner damage.

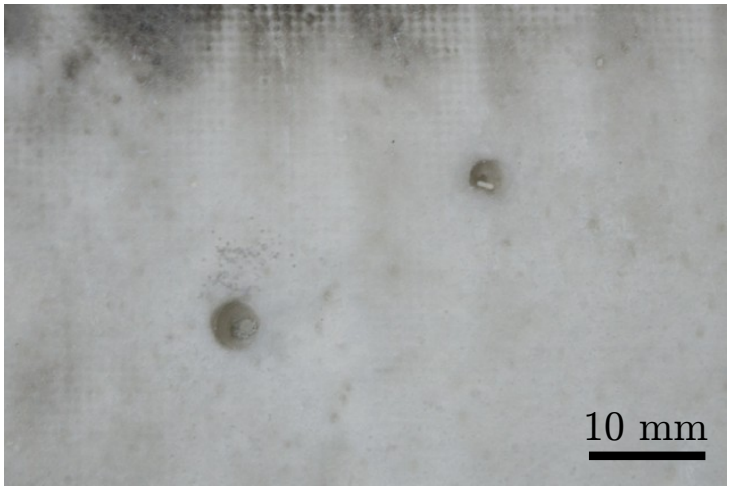

Figure 4.13: Local insulation damage (wormholes), photograph taken from the flow side with the liner removed.

Figure 4.14: Distributed insulation damage, photograph taken from the flow side with the liner removed.

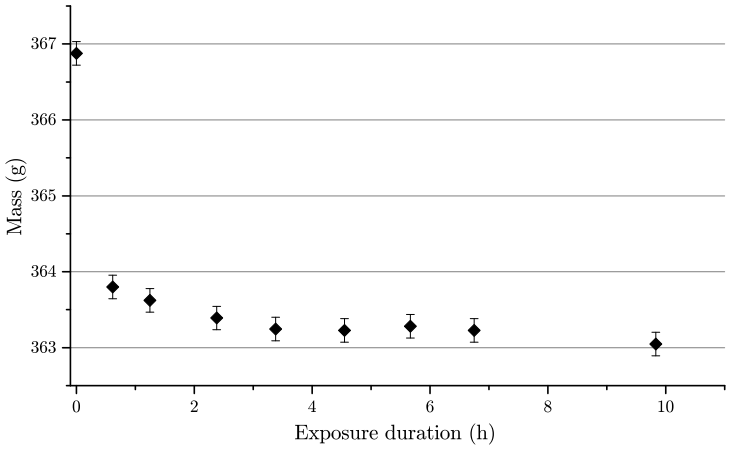

Figure 4.15: Sample mass as a function of exposure time for an un-aged sample exposed to combustion engine flow (T = 700 °C, Re_b = 2.8·10^4).

insulation systems are shown in Figs. 4.15 to 4.17. Error bars indicating the uncertainty, see A.1, are included. It is assumed that the gaskets and test rig do not change in mass.

The mentioned bulk Reynolds number is defined as $Re_b = u_b D/\nu_b$ and the range that was achieved with this flow source was 1·10^4 - 4·10^4. It was computed using the diameter D of the pipe up- and downstream of the sample and the bulk gas flow velocity u_b derived from the mass flow using the flue gas properties, amongst which the bulk kinematic viscosity ν_b. The range of the wall-normalized frequency of the pulsations with this flow source was $\omega^+ (= \omega\nu_b/u_\tau^2)$ = 0.003 - 0.040, where ω is the angular frequency of the pulsations and u_τ is the friction velocity.

The exposure duration of the un-aged sample in Fig. 4.15 is shorter because the sample developed a tear in the liner. To avoid interference of this local degradation with the general sample mass change, exposure was not continued. After the shown exposure durations, the liner and insulation of the samples of Figs. 4.16 and 4.17 both still lacked visible damage, proving the added value of the mass change measurement, as the absolute decrease was rather different. Additional techniques such as thermography could aid in identifying potential differences inside the insulation blankets.

Despite the difference in ageing, for all three samples of this insulation system, the observed mass change is of the order of a few percent of the sample mass. After an initial relatively large decrease the sample mass decreases more slowly with increasing exposure duration. This insulation system has blankets of amorphous ceramic fibre that contain manufacturing related residue called 'shot'. Compared to the average fibre diameter, these chunks of shot are huge and under pressure variations, the difference in inertia will very likely stress nearby fibres. One hypothesis on the initially larger mass decrease is that it results from the larger shot elements breaking loose and falling through the network early on.

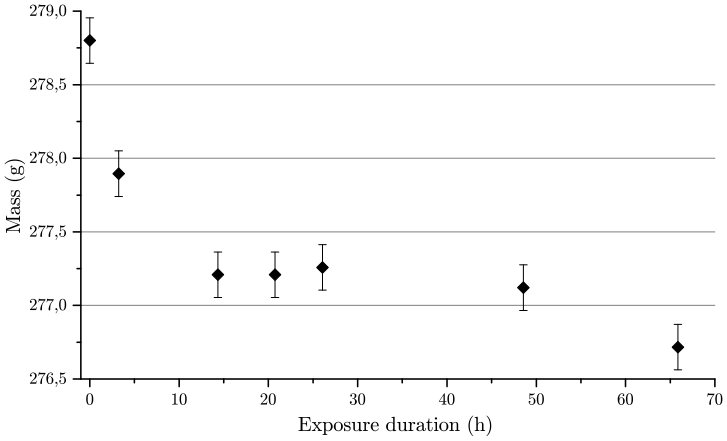

Figure 4.16: Sample mass as a function of exposure time for a thermally pre-aged sample exposed to combustion engine flow (T = 690 °C , Re_b = $2.8 \cdot 10^4$).

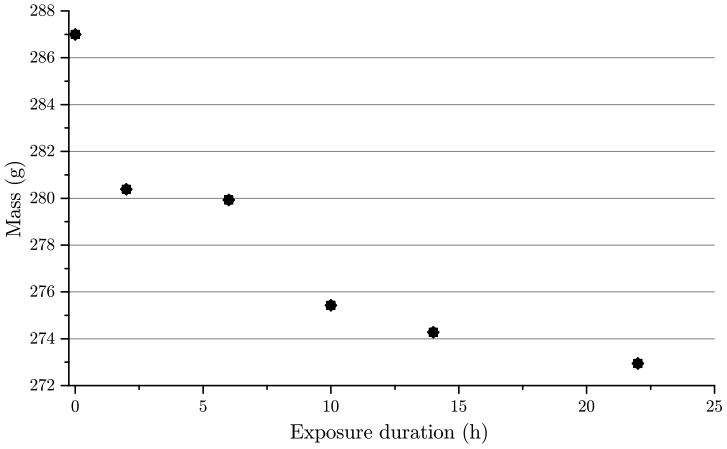

Figure 4.17: Sample mass as a function of exposure time for a sample with un-aged insulation and thermally pre-aged liner exposed to combustion engine flow (T = 760 °C, Re_b = $3.5 \cdot 10^4$).

Further research, for instance comparison with shot-free fibrous insulation and insulation characterisation using microscopy before and after, is needed improve understanding of degradation of this system. This test rig makes such research feasible. For other fibrous insulation systems, however, the observed mechanisms will not be equally relevant, because of different combinations of influences, and separate investigation might be needed.

4.5. Conclusions

A test rig for the wear assessment of fibrous high-temperature insulation systems exposed to realistic turbulent flow was designed and built. During the development the focus was a test rig that has mechanical and fluid-dynamic conditions representative for in-service use of thermal insulation systems lining ducts or channels with high-temperature turbulent gas flows from various sources, including those that generate pulsating flows such as combustion engines. The test rig, additional components and the experiment procedure have been introduced. The sample surface state can be visually inspected and its mass change measured without having to remove the sample from the test rig and additional techniques can be applied. Different samples have been tested under well-defined conditions, revealing different failure mechanisms and representative results have been outlined. The presented test rig can enable efficient further studies on degradation and wear of fibrous insulation systems.

References

[1] C. Reurings, S. Koussios, O. K. Bergsma, K. Vergote, L. Paeshuyse, and R. Benedictus, *Experimental method for investigating wear of porous thermal insulation systems exposed to realistic, hot, turbulent gas flow.* Wear **466–467**, 203536 (2021).

[2] European Commission, *Horizon 2020: Key enabling technologies,* .

[3] European Commission, *Commission launches work on major research and innovation missions for cancer, climate, oceans and soil,* (2019).

[4] European Parliament and the Council, *Regulation (EU) 2019/631 of the European Parliament and of the Council of 17 april 2019 setting CO_2 emission performance standards for new passenger cars and for new light commercial vehicles, and repealing Regulations (EC) No 443/2009 and (EU) No 510/2011,* Official Journal of the European Union (2019), L111.

[5] P. M. Sawko and H. E. Goldstein, *NASA Technical Memorandum*, NASA Technical Memorandum 103892 (National Aeronautics and Space Administration, 1992).

[6] T. P. Brown and P. T. C. Harrison, *Crystalline silica in heated man-made vitreous fibres: A review,* Regulatory Toxicology and Pharmacology **68**, 152 (2014).

[7] ASTM International, *Standard Test Method for Air Erosion of Sprayed Fire-Resistive Materials (SFRMs) Applied to Structural Members*, E859, 2011.

[8] Underwriters Laboratories, *Standard for Factory-Made Air Ducts and Air Connectors*, UL 181, 2013.

[9] F. Arnold, V. Heuer, and G. Walter, *Zur wirkung von strömungsbeanspruchungen auf die beständigkeit von fasernbauteilen in industrieöfen,* GASWÄRME International **45**, 285 (1996).

[10] V. Heuer and G. Walter, *Wear of fibrous ceramic components caused by high velocity gas streams: Erosion mechanisms,* Ceramic Forum International / Ber. DKG **75**, 29 (1998), cfi-Ceram Forum Int.

[11] V. Heuer, G. Walter, and F. Arnold, *Zu den einsatzgrenzen keramischer faserbauteile in thermischen anlagen bei hohen gasgeschwindigkeiten,* GASWÄRME International **47**, 325 (1998).

[12] V. N. Sokov and V. V. Sokov, *Fibrous nanocorundum products for use in a high-temperature gas flow,* Refractories and Industrial Ceramics **53**, 379 (2013).

[13] D. Mui and H. M. Clancy, *Development of a protective ceramic coating for shuttle orbiter advanced flexible reusable surface insulation (afrsi),* Ceramic Engineering and Science Proceedings **6**, 793 (1985).

[14] K. Keller, J. Antonenko, and K. H. Weber, *High-temperature insulations,* ESA bulletin **80**, 50 (1994).

[15] W.-P. Breugem, B. J. Boersma, and R. E. Uittenbogaard, *The influence of wall permeability on turbulent channel flow,* Journal of Fluid Mechanics **562**, 35 (2006).

[16] C. Manes, D. Pokrajac, I. McEwan, and V. Nikora, *Turbulence structure of open channel flows over permeable and impermeable beds: A comparative study,* Physics of Fluids **21**, 1 (2009).

[17] K. Suga, Y. Matsumura, Y. Ashitaka, S. Tominaga, and M. Kaneda, *Effects of wall permeability on turbulence,* International Journal of Heat and Fluid Flow **31**, 974 (2010), int J Heat Fluid Fl.

[18] C. Reurings, S. Koussios, O. K. Bergsma, W.-P. Breugem, K. Vergote, L. Paeshuyse, and R. Benedictus, *The influence of a porous, compliant layer with overlying discrete roughness elements as exhaust pipe wall on friction and heat transfer,* Heat and Mass Transfer **56**, 2367 (2020).

[19] I. Zaplatynsky, *Shrinkage of amorphous silica fibers,* in *Proceedings of the 7th Annual Conference on Composites and Advanced Ceramic Materials*, Ceramic Engineering and Science Proceedings Series, Vol. 44, edited by W. Smothers (John Wiley & Sons, 1983) pp. 492–501.

[20] V. Heuer, G. Walter, and I. Hutchings, *High temperature erosion of fibrous ceramic components by solid particle impact,* Wear **233-235**, 257 (1999).

[21] T. Tonnesen, P. Dietrichs, and R. Telle, *Linear shrinkage, resilience and microstructural changes in high temperature insulating wools in maximum use temperature range,* Advances in Applied Ceramics **104**, 249 (2005).

[22] P. F. Dunn, *Measurement and data analysis for engineering and science*, 2nd ed. (CRC Press, Boca Raton, FL, USA, 2010).

5

Concept analysis

It's relatively easy to make a prototype but extremely difficult to mass manufacture a vehicle reliably at scale. Even for rocket science, it's probably a factor of 10 harder to design a manufacturing system for a rocket than to design the rocket. For cars it's maybe 100 times harder to design the manufacturing system than the car itself.

Elon Musk, 2019

The focus of this chapter lies beyond heat transfer and wear; the challenges and uncertainty in the realization of the concept are described and the global concept feasibility is analysed. Realization challenges related to material, design and manufacturing are considered, including the remaining uncertainty around the durability of a lined exhaust. The description starts with the most crucial parts at the material level and then moves on to higher levels of detail and to other parts. For each identified challenge the options are described and for some stages of realization also potential future developments are highlighted, as they are either crucial or have the potential to substantially improve performance. Next, the potential of the concept in terms of mass reduction, CO_2-reduction and material cost reduction is determined. These are key aspects for the (economic) feasibility of the concept.

5.1. Realization challenges

As described in Chapter 1, the principle concept is to replace steel piping for high-temperature gas flows with fibre-reinforced piping that is thermally disconnected from the flow by a thermal insulation system.

As the conditions differ per part and layer, so do the requirements and does the number of feasible alternatives. It would stretch too far to discuss all possible alternatives. Only those that are deemed feasible or with sufficient potential are included.

5.1.1. Proven insulation systems

Since there are (and have been) applications with similar insulation systems, the wheel might not have to be entirely reinvented. The identified similar systems are briefly analysed.

Many types of high-temperature industrial processes feature thermal insulation, however not often exposed directly to gas flow. Exhaust silencers for stationary gas turbines are one exception to that; fibrous ceramics in pillow-form are mounted parallel to the exhaust flow. Although the insulation is applied for acoustic purposes, its surface is also exposed to parallel exhaust flow. The size of these silencers and pillows is however several orders of magnitude larger than that of the concept under consideration, still the configuration is generally similar [1]. Design details of these silencers are not publicly available, but it features needle mats and wool as insulation enclosed by a woven fabric. An additional liner is offered for improved protection.

In the past, the United States space organisation NASA fitted flexible insulation to the topside of the Space Transportation System (STS, also known as Space shuttle) to thermally protect it during re-entry of the Earth's atmosphere. This tiled insulation consisted of silica batting in between an inner and outer fabric; these two fabrics were mechanically connected through lines of stitches distributed over the surface of these blankets at a certain pitch [2]. The back fabric of these flexible tiles was adhesively bonded to the protected surface, so the load transfer was distributed [3]. The main failure mechanisms were fabric abrasion through wind erosion and fabric embrittlement [2]. No challenges were reported regarding the protection of curved surfaces or blanket interfaces. To the author's knowledge, no similar product is currently available.

Both applications show that insulating a surface using enveloped fibrous insulation from overhead flow is technically possible, although there are differences in terms of the duration and velocity of the flow and the curvature of the insulation. Neither existing application is similar enough to apply directly or to guarantee sufficient performance, but some features could also benefit the application at hand, such as the mechanical attachment of the insulation through stitching and adhesion employed by NASA.

5.1.2. The concept in more detail and inherent challenges

A passenger car exhaust is several meters long and less than a tenth of a metre in diameter. Furthermore, in current car design, the exhaust has to conform to the other elements present under the body of the vehicle resulting in designs with multiple bends. As a result, each car model has a unique exhaust layout and often even several different exhaust systems. Fortunately, the production quantities are still large enough to dedicate a production line completely to an exhaust system of a particular car model. It is assumed for now that production volumes for this concept are also large enough to design and manufacture an exhaust system dedicated to one car model.

The configuration of the concept will depend on the design priority. Between the designs with goals *absolute lowest mass* and *economically most attractive mass*

reduction, the amount, type and thickness of the insulation and the type of shell material could differ. Higher quality thermal insulation is generally more expensive and so is a lower thickness, more thermally stable outer shell.

On top of that, the outer diameter should be kept as small as possible as both the insulation and shell mass are related to it. With the fixed inner diameter, the insulation that can offer the largest thermal gradient per unit mass is thus preferred. The achievable insulation densities depend on the available insulation materials and, if compression is involved, also on the type of structural support.

Regardless of the design goal, there is a radial temperature difference across the insulation that is inherent to the concept. If materials with a non-negligible positive coefficient of thermal expansion are used, this temperature difference will cause a difference in thermal expansion with respect to the unheated state between both sides of the insulation. Depending on the exact configuration and the magnitude, this difference in expansion could create internal stresses or alter the inner geometry and affect the flow resistance or durability.

Furthermore, by limiting the heat from reaching the exhaust shell, the exhaust gas temperature at the exit or tail pipe is much higher than in its steel counterpart. In some cases the gas flow exit temperature could be so high that it could negatively affect nearby objects. This challenge is analysed later in this chapter, together with the other exhaust interfaces.

In the above analysis and the remainder of this chapter, the relationship of the concept with the underbody design of the car is ignored, since no information on that trade-off was available. It is assumed that the exhaust geometry can be copied from the metal counterpart (diameter and layout) and also that there is enough space underneath the car for an exhaust system with a larger external diameter such that the inner diameter can indeed be kept the same.

Conclusion As these challenges are not considered insurmountable and are inherent to the concept and thus also to all potential realizations, the challenges are carried forward to be discussed whenever the related component is treated.

5.1.3. Exhaust gas flow exposure

Given the crucial role of the insulation system, the potential materials for the insulation and liner are considered first. One of the challenges for the insulation and liner is to offer sufficient long-term resistance to the thermo-mechanical loading of the exhaust gas flow.

Temperature

At the maximum exhaust gas temperature of a regular naturally aspirated petrol engine, which is 1000 °C in the engine exhaust manifold, only a fraction of all materials is still in its solid phase and an even smaller set is still mechanically of engineering significance.

Not all materials with a continuous use temperature of at least 1000 °C are feasible candidates. On the one hand, this limit is conservative because downstream of the manifold and the catalytic convertor especially, the peak temperatures are

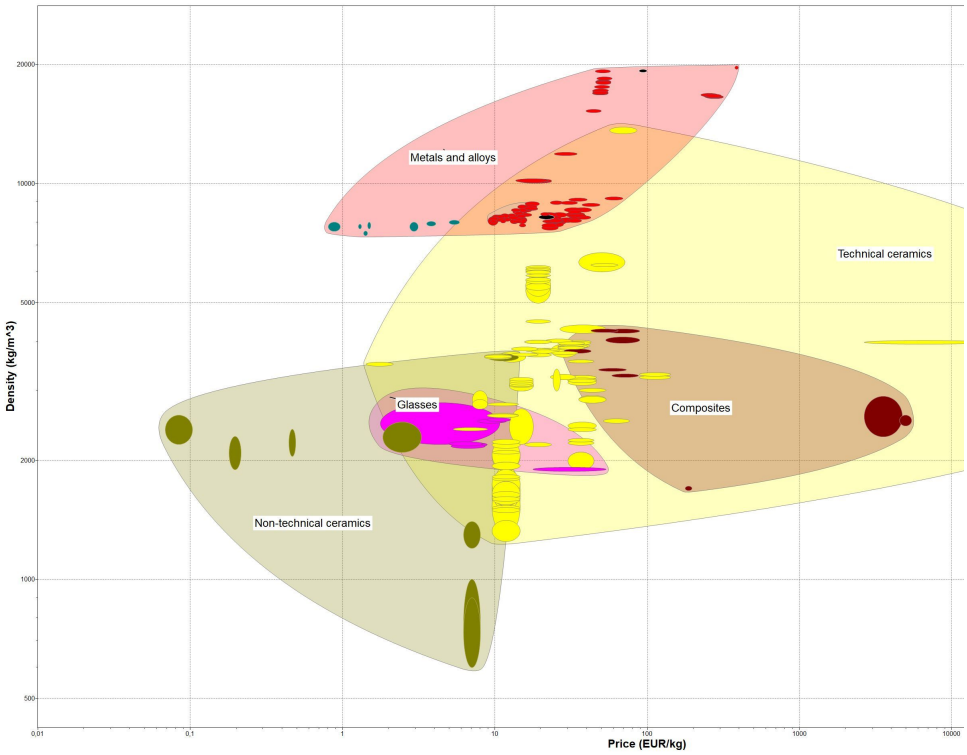

Figure 5.1: Graph of price vs density for materials with continuous use temperatures exceeding 1000 °C according to CES Edupack [4].

about 100 °C lower. On the other hand, the definition of the continuous use temperature is application specific and its value is therefore not necessarily realistic for the application under consideration. Nevertheless, a minimum continuous use temperature of 1000 °C is used as a first filter.

Chosen option and alternatives Figure 5.1 shows the material groups that have a continuous use temperature of at least 1000 °C from a database of (engineering) materials [4]. In short, the set of feasible materials is limited to metals and ceramics.

None of the metals in the set has a density of less than 7000 kg/m^3.[1] As the difference with the density of steel is relatively small, metals are not further considered for insulation because the potential for mass reduction is minor. Heat-resistant ceramics are therefore the candidate material set for insulation and liner. This set is a very diverse group, containing both amorphous and crystalline materials.

[1] Titanium is sometimes used in exhaust systems of high-performance road vehicles, but it can only be applied in lower temperature regions or a shorter lifespan has to be accepted.

Long-term mechanical performance: theory

The insulation and liner material in an exhaust system should not just be able to resist high temperatures, but they have to do so for a large number of short and long cycles and on top of that, possess sufficient resistance to the mechanical loading by the flow.

Although vehicle accelerations should not be ignored, most cycles of mechanical loading of the insulation system come from the exposure to fluid flow. With mean gas flow velocities reaching well over 200 km/h, turbulence Reynolds numbers of up to $5{\cdot}10^4$ and cylinder pulsations, the conditions are more harsh than in most industrial applications. The thermal cycles are mostly related to driving phases (acceleration, cruise, idle or parked) and have a much lower frequency than the pressure variations.

The focus lies on ceramic materials in fibrous form because of their higher thermal shock resistance (and strength) compare to the bulk form [5]. On top of that, fibrous ceramics in the form of a fibrous network (wool) are very capable thermal insulators. At solid volume fractions of about 5%, and corresponding low densities, free convection and solid conduction are limited. The resulting low effective conductivity makes ceramic wools commonly applied thermal insulators [6–8].

As fibrous ceramics are common in high-temperature applications, there is quite a range of fibre products available. However, the fibre diameter and fibre length for ceramic fabrics and insulation wools are as different as their target applications. As a result, fibres for fabrics and wool are made with different manufacturing processes and sometimes different materials, causing different properties and cost levels.

Fortunately, for all those (man-made mineral) fibres the same general properties are of importance: price, durability and acceptable health risks. The last is related to potentially adverse health effects because of inhalation of fibrous material, as for instance with asbestos. All three properties depend on the composition and phases of the material, through the processing temperature and energy, the material stability and properties at elevated temperatures, and the preferred fracture direction and biopersistence (durability of the fibres in human tissue), respectively.

The general relation between price and composition is simple: the higher the silica (SiO_2) content, the higher the cost and above that, the higher the alumina (Al_2O_3) content, the even higher the cost. In addition, complicating the composition by increasing the number of elements, tends to lower the liquidus temperature of the ceramic and thus the required processing energy. That is why E-glass, despite its alumina content, has a low price and low maximum use temperature. Another factor that influences the price is the length of the fibres. Fabrics require longer fibres than insulation wool and thus a more tightly controlled manufacturing process.

The table below lists some commonly available temperature-resistant fibre types, their composition and relative price. Table 5.1 also includes two typical composite reinforcement glass fibre types, namely E-glass and S-glass with continuous use temperatures of 600 and 815 °C respectively [9]. Note that alkaline-earth silicate (AES) fibres are only available in the form of insulation wool.

The ceramic fibre durability depends on the mechanical properties at elevated

Table 5.1: Composition, initial phase and price index of common heat-resistant fibres.

Fibre material	SiO_2 [wt. %]	Al_2O_3 [wt. %]	CaO + MgO [wt. %]	Initial phase(s)	Price index [9]
E-glass	60	13	22 + 3	amorphous	1
S-glass	65	25	0 + 10	amorphous	6
Alkaline Earth Silicate	~65	0	~29 + ~5	amorphous	
Silica	>99			amorphous	10
Aluminosilicate (RCF)	~50	~50		amorphous	
Aluminosilicate	~28	~72		amorphous + crystalline	
Alumina		>99		crystalline	150

temperatures and also on the change of those properties with repeated exposure to elevated temperatures. Initially, fibres with a relatively low alumina content (and high in constituents such as SiO_2, MgO, CaO) tend to be amorphous or partially amorphous, whereas fibres with larger amounts of alumina (> 70% alumina) are generally crystalline.

In both phases internal mobility increases with elevated temperatures[2] enabling mechanisms that reduce the fibre strength. In the amorphous phase it is the nucleation and growth of crystals and in the crystalline phase it is the growth of the already present crystals [9–13].

In the amorphous phase another mobility-related mechanism occurs at elevated temperatures: structural relaxation. According to Greaves and Sen, Zheng et al. and Fokin et al. structural relaxation is the transition of the glass to the supercooled liquid state corresponding to the elevated temperature [14–16]. Structural relaxation can cause fibres (and thus fabrics) to reduce in aspect ratio (length decrease but diameter increase) and there are even reports of fibre bundles fusing together. Both effects reduce the fibre flexibility and strength because of the increase in diameter [5, 17, 18]. Overall, crystalline fibres are stronger and retain more of their room temperature strength at elevated temperatures than (partially) amorphous fibres.

For the potential health risks of fibres, the first factors are the duration of their presence in human tissue and the effects during that presence. For this, the composition is relevant and thus also changes of that composition during the use [19]. In general, alkaline earth silicate is labelled as less biopersistent (biosoluble), whereas some aluminosilicates (RCF) and crystalline forms of silica are classified as (potentially) carcinogenic. A second factor is the fibre diameter and length [20]. If large enough, the fibres are considered non-respirable, as for fibres in fabrics for instance. Meaning that few of those fibres would end up in human lungs. Most insulation wools however have respirable fibres and the author therefore considers RCF insulation unacceptable for this concept. Also note that broken fibres, especially in the form of dust, tend to be respirable and care should be taken when

[2]Elevated temperatures are temperatures substantially higher than room temperature, but lower than the classification temperature and, if applicable, lower than the glass transition temperature.

handled.

Although the above analysis resulted in a relative ranking of candidate fibre materials, it did not provide a criterion for sufficient performance. For that, the conditions that the liner and insulation material have to endure are currently too uncertain. That some ceramic wools are durable enough for the exhaust environment, is proven by their common use as catalytic convertor substrate support mats. These mats are often made of fibres with about 50% alumina (Al_2O_3) [21]. Whether more affordable wools are also suitable, cannot be concluded without testing or modelling of those materials. A first impression was obtained from thermally accelerated ageing followed by mechanical loading according to the erosion test presented in Chapter 4.

Chosen option and direct alternatives The initial focus lies on the more affordable amorphous fibres, because the system with the most affordable fibre and yet sufficient performance is generally the most cost competitive. For the test campaign, pure 'glass' or silica fibre was employed for the fabric lining the fibrous insulation in the samples. According to the manufacturer, the application limit is 1000 °C, which is in line with the value of Wallenberger and Bingham [9].

For the insulation, pure silica might also be an option, but it is not generally available in wool form. One the reasons for that is probably that there is another insulation material that is more affordable and with a similar theoretical temperature range: alkaline earth silicate (AES), see also Table 5.1. According to the supplier, it has a classification temperature of 1200 °C and a maximum continuous temperature of 1000 °C.

Should the performance of either prove insufficient, then the next option would be fibres including alumina for both liner and insulation.

In theory it is possible to provide integrity to insulation using ceramics in other ways than with a liner. Fibrous insulation held together by a ceramic binder is also available on the market, in both sprayed and pre-impregnated blanket form. However, this solution not only has a higher mass, but the resulting ceramic solid is also susceptible to thermal shock. This is unwanted given the number of thermal cycles in the life of an exhaust system.

There are also other forms of high temperature thermal insulation than wool that require less support. Microporous insulation for instance, is a moulded rigid ceramic form of insulation that is also available in pipe segments. It has a generally lower thermal conductivity and higher density than high temperature insulation wool. It thus requires a smaller insulation thickness and shell diameter and its mass can therefore be roughly the same mass as of this concept. However, it has to be made exactly to size, it is much more expensive than fibrous insulation and it has very low resistance to liquids, so a watertight liner is needed.

Long-term mechanical performance: tests

The silica liner of the erosion samples in Chapter 4 performed adequately for the duration of those tests, except for the one that tore, probably because of shrinkage. There were some signs of wear at the contact points with the metal mesh, but not

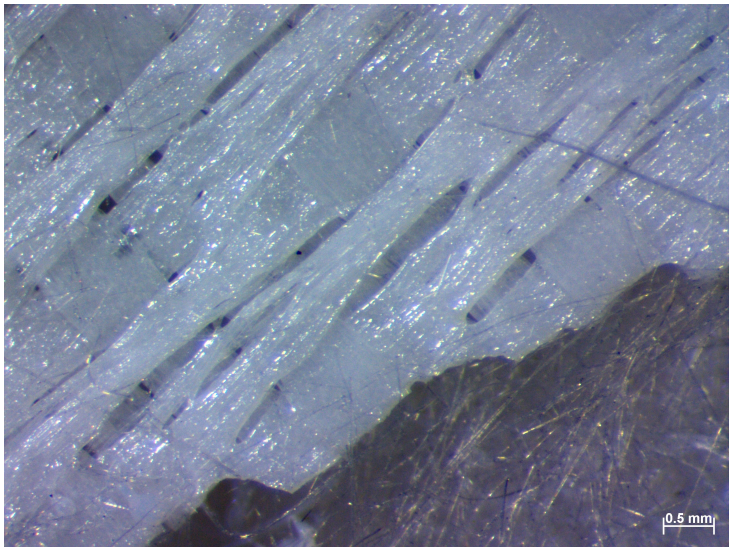

Figure 5.2: Optical microscopy image (8x) of an erosion sample after heat-treatment and flow exposure.

critical for the investigated duration. The next more affordable alternative, S-glass, is certainly not eligible. During thermal ageing at 950 °C its filaments had fused together, see figure 5.2.

Whether silica is sufficiently durable for the liner remains to be seen, it could be that another material from Table 5.1 is needed. Much will depend on the configuration of the insulation system and the influence of other factors that were ignored so far. A feasible concept would require a much longer product use time than tested so far.[3]

The samples used in the erosion tests had been artificially aged before flow exposure. Those 60 hours at 950 °C were not without influence, despite being below the continuous use temperature. Besides having shrank in the in-plane directions, both the liner and insulation had changed in their physical response to handling compared to before the pre-ageing stage: they seemed less compliant.

The change in compliance of the silica fabric was such that it could still be considered flexible, however, its in-plane shrinkage was substantial at 5%. The shrinkage did not continue in the samples, it seems to have a limit and occur primarily on the first exposure to elevated temperatures. The main mechanism was mostly likely structural relaxation, as also observed by others [5, 17].

The difference in mechanical response upon handling was larger for the AES insulation and it also seemed more brittle, but it shrank less than the silica liner. The shrinkage and change in response is most likely due to the combination of structural relaxation and crystallisation, the latter has been shown by others to occur in AES at temperatures below the classification temperature [11, 22]. However, the smooth

[3] If we assume a minimum lifespan of 300,000 km and an average velocity of 50 km/h then the use time is 6000 hours.

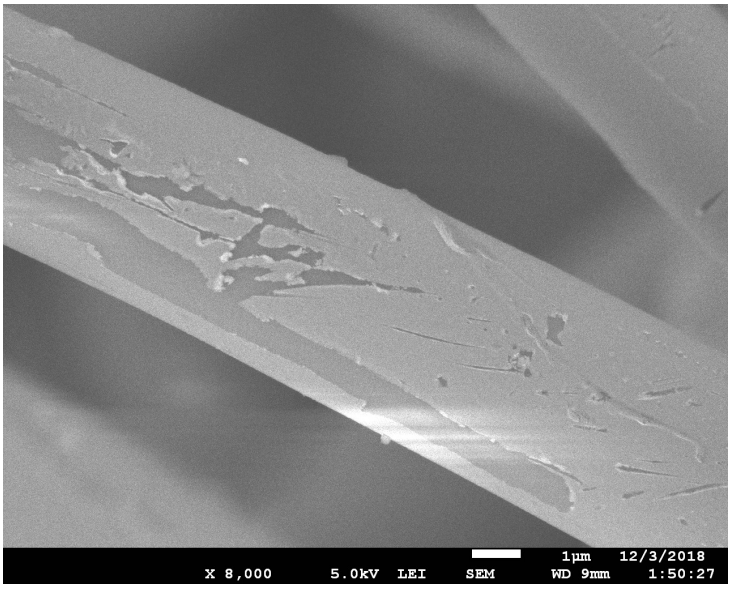

Figure 5.3: SEM image (8000x) of pristine AES insulation fibres.

fibre surfaces observed using a SEM cannot confirm the crystallisation (Figures 5.3 and 5.4). Although the response to handling is not a representative test, the impression and the potential mechanisms can help in understanding the damage due to erosion.

Besides the aforementioned changes of the fibres themselves, the performance of AES insulation is also influenced by its manufacturing method. AES fibres are produced from a melt with a large scatter in fibre length and diameter as a result [23]. On top of that, the droplets of molten glass that are spun to form fibres generally solidify before stretching out completely and become part of the final product. The set of these 'blobs' in the thermal insulation is called *shot*, see the microscopy images of Figures 5.5 and 5.6 for examples.

The common definition or classification of shot is based on size. According to the manufacturer, the average fibre diameter is 2.6 μm which makes the fibres volumewise many times smaller than these blobs with dimensions up to 300 μm. As a result, these shot elements take up a substantial fraction of the insulation mass despite the much larger number of fibres. According to the manufacturer, 35% of the AES insulation mass is shot of 45 μm or larger [23].

In erosion testing after artificial ageing, the performance of the insulation was in most samples the factor limiting the test duration. Different forms of insulation damage were observed in the AES insulation in the samples with silica liner and metal mesh, as already partially described in Chapter 4. First, there is local damage in the form of tunnels perpendicular to the insulation surface with a shot element inside. This was called wormhole in Chapter 4. Second and also mentioned in that chapter, insulation damage was observed at one or more locations along the sample

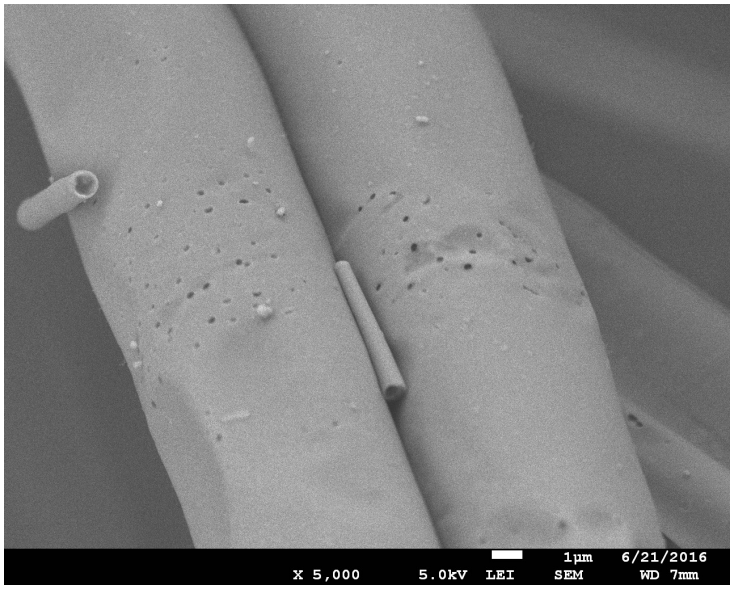

Figure 5.4: SEM image (5000x) of AES insulation fibres after thermal ageing.

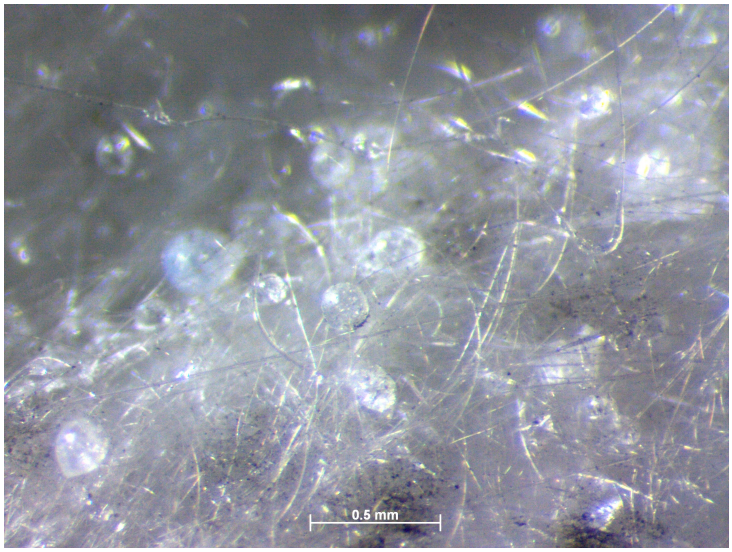

Figure 5.5: Optical microscopy image (8x) of AES insulation that was used in erosion testing, but was not heat-treated. The black spots in the image, for instance behind the scale bar, are probably soot resulting from the combustion process.

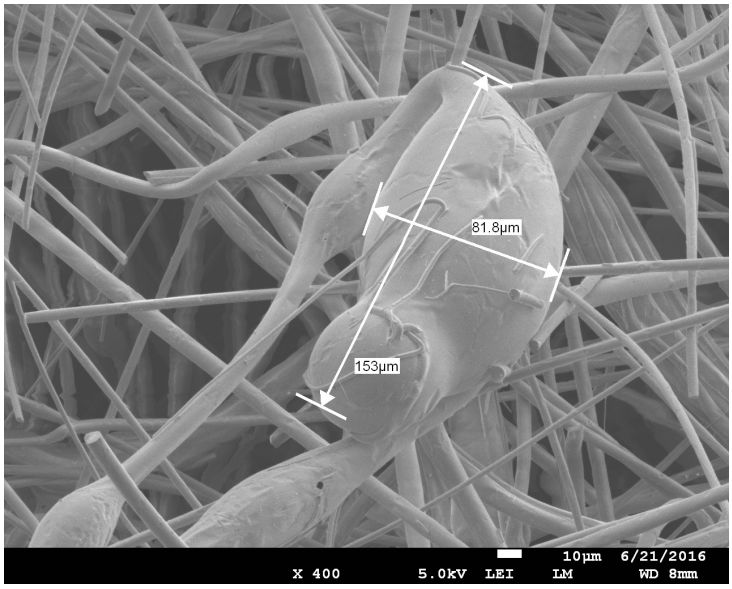

Figure 5.6: SEM image (400x) of AES insulation fibres with shot dimensions indicated.

centre axis. After testing, the larger elements of the insulation were found on the bottom of the sample container, see Figure 5.7.

Third, there were samples with no visible damage to the insulation, yet larger insulation elements were found underneath afterwards. In those cases the sample mass reduction was up to 5%. For a representative sample, see Figure 5.8 for the insulation top surface and Figure 4.17 for the corresponding mass change. These samples were discontinued for other reasons and it could be that this state precedes the damage state with visible damage.

In all three damage states loose *shot* particles were found, which meant they got separated from the fibrous network. It is hypothesised that this is due to the inertia and limited mechanical support of the shot elements in combination with variable loading, such as the pressure fluctuations in the flow. Similar degradation was observed in a vibration testing study of fibrous RCF-insulation with shot [24]. It is nonetheless hard to estimate to what extent the shot movement and detachment could damage neighbouring insulation fibres.

Since the test duration was relatively short compared to the actual application, this could mean that the insulation system with AES is not durable enough. It is expected that insulation types without shot would show smaller mass losses for the same exposure.

In short, both silica and AES candidate materials change due to long-term exposure to high temperature, pulsating, turbulent flow. Testing has revealed failure modes for both liner and insulation. The employed liner performed generally adequately, but more investigation is needed to assess whether its durability is sufficient for the full product lifetime. For the AES fibrous insulation there is not only

Figure 5.7: Residue at the bottom of the sample holder after erosion testing, consisting almost completely of large shot elements.

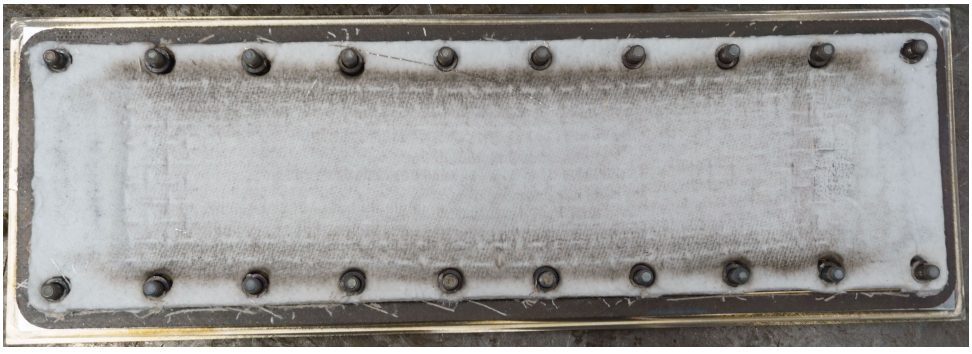

Figure 5.8: Insulation top surface (liner removed) of a sample after 22 hours of exposure to exhaust gas flow.

uncertainty, but it also generally formed the limiting factor for the sample durability.

In future work, it could be effective to reduce complexity by first studying the durability of the concept using shot-free materials. If that proves adequate, then AES can be tried again to see whether its performance could be improved by configuration changes.

5.1.4. Other insulation system challenges

The thermo- and fluid-mechanical loading on the insulation system is perhaps the most obvious one, but it is certainly not the only influence in exhaust systems. Other influences can also affect (and even dictate) the insulation durability and thus have to be mentioned.

First, there is the potential interaction with the substances in the exhaust system. As a result of the combustion process, there is a lot more water vapour present than in general ambient air. Together with other combustion products, such as acids, this water can condensate inside the exhaust during and after engine operation [25]. Glass properties are known to be sensitive to water vapour and, depending on the composition, also to acids [10, 12, 20, 26]. The combustion process depends on the engine type and load and in some cases also produces soot (solid carbon). Depending on the aftertreatment, this could be present in the exhaust gas flow too and could in theory also affect the insulation performance. In Figure 5.5, some soot deposit is visible. The test cycle employed during wear testing is not necessarily representative for the influence of these substances.

Second, there is additional mechanical loading due to driving. Besides accelerations due to vehicle-road surface interaction, there are accelerations related to changes of the vehicle velocity vector and impact events of road debris on the exhaust system. The frequency and magnitude of these loads differ from those of the loading by the gas flow. For the insulation system, these loads are expected to be inferior to that of the flow. For the outer shell, that could be different.

Third, there is the environmental influence when the engine is off. As ceramics can contain large amounts of water, the most predominant effect could be that of freeze-thaw cycles on the fibre integrity. This will also have to be investigated further.

None of these influences is expected to be deal breaking, as fibrous ceramics are already applied in exhaust systems (in silencers and catalytic convertors), but they could make one type more suitable than another.

On the practical side remains another challenge, namely establishing the thermal resistance of the insulation system. Although the thermal resistance between gas and shell can be obtained using the method presented in Chapter 3, the method did not prove suitable for separate determination of the resistance of the insulation system because the interface temperature could not be measured accurately enough. Fortunately, the results of Chapter 3 also indicate that there is probably little interaction, so the effective conductivity within the fibrous insulation can be studied separately. This is relevant because of two reasons: first, the insulation resistance is dominant compared to the thermal resistance of the boundary layer and second, it could be studied using samples that are less labour-intensive to

make than those used in Chapter 3. Since there are several effects yet to study, a more simple approach would be welcome. The insulation thermal performance is for instance affected by its density, compression and degradation.

Surprisingly, the test method that manufacturers of fibrous insulation use to report the conductivity of their product (ASTM C-201) is designed for refractories (insulation bricks) [27]. Its sample boundary conditions are not immediately suitable for fibrous samples. As a result, the inaccuracy of the conductivity determined using this test is uncertain. This can be overcome through the use of ASTM C-177 [28].

Another aspect of this challenge is the complex temperature dependence of the thermal resistance of fibrous insulation. Because radiation and conduction occur together, the effective conductivity is not just a function of the mean temperature, but also of the temperature difference.

5.1.5. Shaping and assembling the insulation system

Above, the external influences that pose a challenge for the different parts of the insulation system were treated and candidate materials were presented. Based on that, this section will look into the challenges that come with different ways of creating the insulation system.

One aspect that differs from the earlier mentioned proven insulation systems is the required curvature. The manufacturing of the samples described in Chapter 3 has shown that it is not straightforward to form the insulation to fit a surface with a small radius of curvature, such as a 90mm-diameter straight pipe. Bending an initially flat segment of the insulation system to fit such a curved surface will buckle the liner and even the insulation on the concave side.

To prevent this buckling when lining a curved surface, the different layers of the insulation system could be joined in their curved form. This was done to form the heat transfer samples from Chapter 3 by working outward from the wire mesh. To have a taut liner at operating temperatures, its shrinkage at first heating and its thermal expansion might also have to be taken into account.

An advantage of the curved insulation in a circular cross-section is that it inherently provides resistance against large-scale out-of-plane displacement of the insulation. The resistance comes from the in-plane compression that is required for the insulation to accommodate to the smaller circumference when it moves towards the centre of the duct.

This challenge is even larger for doubly-curved parts in bends. At the material level, both the wool and fabric are in principle compliant enough to be formed and combined with double curvature too, although not all weave-types are equally well-suited [29]. An alternative would be to cut them to (an optimized) shape.

Another alternative could be the use of a non-circular exhaust duct cross-section, something that was also briefly covered in earlier work [30]. If square or rectangular cross-sections are used, then bending of insulation is not necessary. Such cross-sections do however, have other consequences: more insulation joints, no inherent resistance to out-of-plane displacement and a higher mass for the same effective Reynolds number.

The insulation system also requires mechanical support: in order for it to function properly, it will have to be able to resist the pressure variations of the flow without separating from the shell, for instance. The shell serves as the backbone of the concept: it provides the structural rigidity to be able to suspend it under the vehicle body. To also provide mechanical support to the insulation and liner will require additional elements. Two types can be distinguished:

One already sketched and shown option is to introduce another structural element on the flow side of the insulation system, thereby clamping it to the shell. This was successfully done using a metal mesh in the samples for the tests of Chapter 3 and in most samples presented in Chapter 4, see for instance Figures 3.1 and 4.9.

Reintroducing steel in a concept that is to replace a steel system is not ideal, but it could be functional. Technologically it is a low risk solution, but the challenge is to make it affordable and durable. Despite the relatively low base material price, the complexity of the welded steel mesh cylinder used in Chapter 3 made it quite costly. The welded mesh could perhaps be replaced by a helical wire. However, further investigation would be needed to determine whether that is feasible and what would be an effective geometry, because the wire pitch of the insulation support influences its performance in terms of back pressure and wear.

Another option for providing support to the insulation is a mechanical connection to the shell. This approach is taken in most existing insulation applications, but uncertainties remain for the concept under consideration. Compared to mechanical support using a metal mesh, it poses stronger requirements on the insulation system, especially on maintaining integrity. Two variants can be discerned:

- The first variant is local attachment of the insulation, for instance through an array of metal wall anchors. Although such anchors are often used for industrial oven insulation, it is far from a plug-and-play solution for the concept under consideration. The first challenges are how to attach them to the composite shell and how to make them durable enough. Once that is tackled, one has to detail the connection with the insulation system, for instance with the shell- and flow-side liner.

- Distributed attachment is the second variant. An example is the earlier discussed Space Shuittle-concept of insulation enveloped by fabrics that are periodically stitched together[4] and then adhesively bonded to the protected surface. Those stitches were made with the stitching threads under tension, compressing the insulation and ensuring a taut liner and dimensional stability even under external compression. The largest challenge for this variant is the durability: the adhesive connection, whether polymeric or ceramic in nature, will have to endure the temperature, loading, moisture and other condensates. The stitches will also have to be numerous and durable enough. For the concept, the stitches can be made using the same material as the liner, avoiding additional complexity.

To get a first idea of the suitability and durability of stitches with exhaust flow, a flat sample was manufactured and tested using the erosion test, see Chapter 4. The

[4]Not unlike a duvet bed cover

curvature of the insulated composite exhaust pipe is in principle not a problem for current-day stitching technology. The double-curvature in bends, however, could be an automation challenge, but that also holds for the metal mesh. For structural efficiency, the stitches could be connected directly to the (dry) reinforcing fibres in the shell. That introduces other challenges though, by posing additional requirements on the assembly and manufacturing of the shell.

The employed material form also influences the aforementioned challenges related to the shaping and assembly of the insulation system. For the samples used throughout this thesis, the following forms of the chosen materials were used:

- The liner was a woven silica fabric, more specifically a 400 g/m^2 2/2 twill weave fabric. The twill weave makes the fabric more suitable for draping complex shapes than plain weave. Its permeability was measured and is such that the insulation system can be considered impermeable under most turbulent flows. Other available fabric types are plain weave and satin weave. Some manufacturers also offer pre-shrunk silica fabrics.

- The AES-insulation wool was employed in blanket form. Blankets were chosen for the ease of handling and the predefined insulation density. The employed blankets had specified densities of 96 or 128 kg/m^3 and thicknesses of 6 and 10 mm. The available density range is from 64 to 160 kg/m^3. Other available forms of insulation are: bulk (batting), paper, board, vacuum formed board and textile.[5]

Several lessons were learned form working with the blanket form for the experiments. First, a single 10 mm-thick blanket could not be bent to the heat transfer shell radius without buckling of the concave side, see Figure 5.9. This is not necessarily a problem, but it could affect the forces on the liner or the smoothness of the flow boundary. The resulting, locally increased insulation density could be responsible for the increased radiation resistance observed in the heat transfer experiments of Chapter 3.

Another, related lesson concerns the junction of insulation blanket ends when circumferentially lining a straight pipe: creating a junction of good quality is not straightforward. Despite trimming, fitting and the compliance of the blankets, some gap was present after closing the shell, judging from the locally increased shell temperature during the experiments described in Chapter 3. At least for blankets, some work remains in securing the quality of insulation junctions. Ideally, junctions in insulation and liner would be realized in such a way that their performance in terms of thermal resistance and durability would be no less than that of the rest. For liner junctions, this can probably be achieved through some overlap.

Both lessons also apply to doubly-curved surfaces, as encountered in exhaust system bends. Using insulation batting rather than blankets could make shaping easier, while making the insulation density harder to control. So far, the double-curvature in bends remains a major challenge, from both a geometrical and material

[5]Not all forms can meet the continuous use temperature of 1000°C.

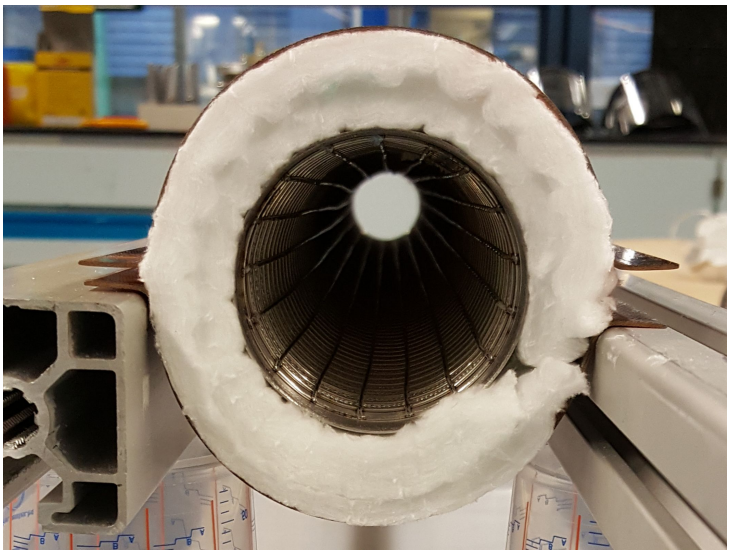

Figure 5.9: Buckling of insulation blankets on the concave side, photo taken during sample assembly.

perspective. Since manual installation of the materials is not an option from manufacturing rate and cost perspective, finding some form of automation is another challenge for the concept.

The third lesson that was learned, was that the density varied substantially across the employed insulation blankets. There is not only scatter in the insulation properties at the fibre level (shot), but for these blankets also at a much larger scale: mass measurements of punched out 50 mm-diameter samples of thermally aged but otherwise pristine blankets had standard deviations of up to 10 kg/m^3 (on a mean density of about 128 kg/m^3). Since the density affects the thermal resistance and probably also the durability, this would require a relatively high mean insulation density (and mass) to meet the minimum.

One perhaps easily overlooked challenge, is finding the preferred insulation density. At a first glance, the highest practically possible density seems preferable because it reduces the shell mass: the higher thermal resistance allows for a smaller shell radius at the same shell temperature. Furthermore at higher densities the fibrous insulation network could have more internal mechanical support. However, it is likely that there will be a difference in durability of the insulation system between stress-free higher insulation densities (as manufactured) and higher densities realized through compression of the insulation.

5.1.6. Shell design

The outer shell has been mentioned several times already, but has not been treated in detail yet. It provides the exhaust concept with rigidity and airtightness and it also has to be sufficiently durable.

The external influences it has to endure are the same as for the insulation sys-

tem, but not necessarily with the same intensity. Mechanically, the impact by road debris will be more influential, as the pressure pulsations and heat of the flow will be dampened by the insulation. Its exposure to moisture and acids is probably similar.

As the basis of the shell is a polymer, most effects of the external influences are different than in ceramics. Time, temperature and loading rate nevertheless influence the mechanical response of composites, as does moisture [31, 32]. Since (fibre-reinforced) polymers have been applied in high-temperature applications and also in other engine components, it is expected that there will be several feasible material options. The minimum wall thickness will be one of the aspects that will have to be considered in the durability study.

The manufacturing of the load-carrying shell of the exhaust system is deemed technically feasible in several ways. It is assumed that it can be manufactured in two full-length half-shells, as a set of modular half-shells or in one piece through for instance braiding. These options should be possible with both thermosetting and thermoplastic polymers and with continuous and short fibres, but with different manufacturing processes. Given the sensitivity to cost and the production series size and rate, short fibre moulding is a good candidate. Using a thermosetting polymer that has a two-phase cure (A and B-stage cure) could be beneficial as the second cure could be used to connect the half-shells, rather than using adhesives.

The largest influence on the performance and the cost of the polymer material of the shell will probably be the maximum shell temperature. Although maximum shell temperatures will be substantially lower than at the fluid-insulation interface, this will still be challenging as polymers have much lower limit temperatures than the considered ceramics. Understanding the heat transfer rate to the shell with sufficient accuracy will help with finding a good solution. The final shell material will have to be chosen by taking all relevant factors into account though, including also cost, availability and manufacturability.

5.1.7. Combining components

The main manufacturing options and limitations for the shell and insulation system have been discussed above. The question is now, what options remain when these components are considered together? One way or another, the insulation and the shell both have to be formed and combined. The manufacturing of conventional exhausts can be performed using proven techniques such as bending and welding. Compared to that, the concept under investigation has more uncertainty in its manufacturability, mostly because of its concentric configuration.

The main challenge lies in combining the insulation system and shell in a shape that is as slender and bendy as a car exhaust. The shell is so slender and its the diameter so small that lining it with something rigid over the full length with just access from the ends is not trivial. The assembly order thus has to be considered in the selection of the manufacturing system.

A first option is to divide the shell and/or the insulation system into multiple parts. This leaves more to assemble, but can make it more straightforward. This solution has the lowest technological risk, but adds some mass and complexity to

the components because of the added joints and interfaces. The access to the inside of the shell nevertheless improves dramatically by sectioning it along its length, i.e. using two full-length halve-shells. Additionally, the insulation system could also be made in sections. This would reduce the complexity of the manufacturing of the insulation system, as the bends could for instance be produced separately from the straight sections.

It could be effective to align the section interfaces of the shell and insulation, to end up with elements or building blocks. One could for instance make standard straight sections and bends. On the other hand, exhaust systems can have many sections, see for instance Figure 2.1, and the number of 'standard' components might be (too) large.

A second option to simplify assembly, is having dependent sequential manufacturing processes, i.e. form the shell around/over the insulation system. Although theoretically possible, this is far from proven technology and could only be possible with sufficient mechanical support, such as the configuration with a metal mesh. The insulation system, forming the mould for the shell, would have to be (made) stiff and relatively strong, although perhaps only temporarily. Although composite manufacturing technologies are generally quite complex and not very flexible, braiding could potentially deal with those constraints. In short, this option removes the need for assembly at the cost of additional constraints on the insulation rigidity and shell manufacturing.

A third option, although probably the least realistic, is to reduce the geometric complexity by designing the underbody of vehicles such that the exhaust can be straight. This is not a complete solution for assembly, but makes it a lot more simple.

5.1.8. Transitions, mounting and silencers

The insulated composite exhaust system has, in flow direction, two main interfaces or transitions: up- and downstream. Both are different and pose their own challenges.

Upstream there is the interface with the exhaust system that connects with the engine. To limit the complexity of and the demands on the composite system, the concept is only considered for the exhaust system downstream of the exhaust gas aftertreatment system (catalytic convertors and particulate filters). There, the exhaust gas pulsation pressure amplitude and temperature are lower than in the engine manifold. Nevertheless, a connection has to be made. The interface to the insulated composite exhaust system has to: (1) couple the outer surfaces to ensure airtightness, (2) thermally decouple the outer surfaces, (3) provide a relatively smooth transition between the inner surfaces that form the flow boundary, (4) depending on how both ends are mounted, potentially provide mechanical support, and (5) do so at the lowest mass and cost possible.

The heat transfer samples already required such an interface, which resulted in the following implementation. It was an adaptation of existing flexible connections for regular exhausts, which have a bellow-shaped outer tube and a spiralling telescopic inner tube. The main adaptation was that at the composite end, the

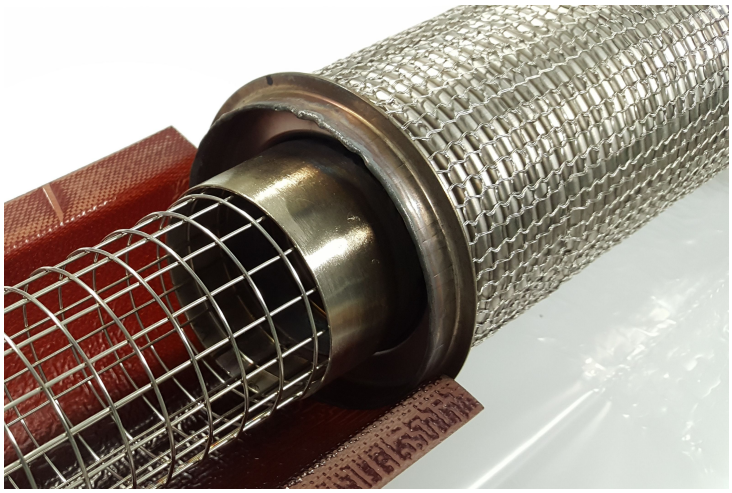

Figure 5.10: Cut-out view of the heat transfer sample interface between the composite section (left) and the connector (right).

inner and outer tube did not join again; the outer tube ended at the bellow outer diameter with a flange. See Figure 5.10.

The bellow provides thermal resistance through its long path length and large external surface area and, as an added advantage, it provides some rotational flexibility, decoupling the system from some of the engine movement. Its performance was sufficient for the experiments, yet it could be further refined and optimized. One aspect that has to be further investigated is the durability of the connection between the outer shell and the connector.

Downstream, the requirements are different. No coupling is required at the downstream interface, because the exhaust gasses can exit the exhaust system into the surrounding atmosphere. The main challenge at the tail pipe is related to one of the main reasons that exhaust systems exist in the first place, namely the high temperature of exhaust gasses.

Compared to a regular exhaust, the exhaust gasses arrive at the exit of the insulated composite exhaust with a significantly higher temperature. Especially in situations with long periods of high engine load, for instance while ascending a mountain pass, the exhaust gasses could exit with temperatures of several hundred degrees Celsius. After such a period, the exhaust gas flow could potentially be harmful for people or animals passing behind the vehicle and it could set fire to surfaces behind the vehicle such as dry grass.

One option to avoid such potential consequence of a high-load period, could be improved mixing of the exhaust gas stream with surrounding air. In terms of efficiency, passive mixing is probably preferred over active mixing. Mixing ambient air into the exhaust gas stream towards the upstream end is prevented by the acoustic requirements, but it might be possible downstream of the silencers. Finding a suitable mixer configuration and location could require substantial amounts of

further research.

The mounting of steel exhaust systems to the car underbody involves connections with rubbers that act as vibration dampers and accommodate the thermal expansion. It is complicated to estimate whether such rubbers are also needed for the composite exhaust system, but there are several factors that could be favourable. First, the composite shell could transmit vibrations to a lesser extent, because it has a lower stiffness and in the case of thermoplastics a higher attenuation than steel, especially at elevated temperatures. Second, sound is dampened along the complete length of the exhaust system, although not equally for all frequencies. Third, temperature and coefficient of thermal expansion of the shell are lower than those of a steel exhaust and the thermal expansion is therefore smaller.

For the lower dominant engine frequencies, silencers will still be needed in the composite exhaust system. Those larger volumes along the exhaust system can in principle also be made according to the concept. The interior of such silencers and their manufacturing will have to be completely re-engineered though.

5.1.9. Repair and recycling

Once the exhaust system has a mature configuration, the possibility for repair and maintenance has to be considered. For regular exhausts repairs are relatively easy as exhaust can be cut and welded with relative ease. Common causes for repair in regular exhausts are fatigue, vehicle damage (accidents), and to a lesser extent corrosion. Although fatigue and corrosion are probably less relevant for the system under consideration, there will be a need for repair because of accidents and potentially also other critical factors, such as loss of insulation integrity with shell damage as a result.

The current EU-regulation for end-of-life (passenger) vehicles aims to promote taking reuse and recycling into account during vehicle design and production [33], but it does so without minimum requirements or a financial incentive. Given the their different nature, the insulation system and shell have to be considered and processed separately.

The fibrous insulation can technically be recycled to other glass products through melting and forming. The most suitable new product form will depend on the financial incentive, influenced amongst others by the demand and the cost of competing virgin materials. Glass has to be removed from end-of-life vehicles and the insulation of the alternative exhaust system can in principle be handled similar to the glass wool that is regularly used in silencers of steel exhaust systems. If the fibrous insulation is not recycled for whatever reason, then the insulation can be landfilled. Silica is one of the most abundant material forms in the earth and generally non-reactive. To prevent release of silica dust into the atmosphere and avoid the potential health risk related to inhalation, it should not be left exposed though, but be covered or buried.

Recycling of fibre-reinforced plastics is an engineering field (and industry) that is very much under development. Despite the fact that the potential of such recycling is increasing with the increased use of fibre-reinforced plastics[6], it currently still

[6]For instance due to the growth of the wind turbine industry.

lacks large-scale results. The most challenging aspect is preserving the mechanical properties and most initiatives are therefore forms of downcycling.

In general, the type of matrix material is a major factor for the method of recycling due to the different characteristics of thermosetting and thermoplastic polymers. The challenge for thermosets is to get rid of the matrix to recover the fibres while preserving the fibre quality. Recently, the first thermoset recycling developments of larger scale have appeared [34, 35]. The matrix of fibre-reinforced thermoplastics can in principle be reshaped with sufficient heat and pressure, the fibres however limit the dimensional freedom substantially. To overcome this limitation, thermoplastic composites are often chopped into small pieces and then shaped into a new product, with lower mechanical properties.

The EU regulation does not distinguish between plastics and fibre-reinforced plastics and shredding composites therefore meets the minimum requirements for the treatment of end-of-life vehicles [33]. As a result, fibre-reinforced plastics used in the passenger vehicles are not necessarily recycled. Although quality recycling of composites is technically challenging and generally not established, the EU-legislation allows its use and perhaps even stimulates it, given the emphasis on emission reduction. Formally, recycling is therefore not a challenge for realization of the concept. If, however, greenhouse gas emission reduction over the complete life cycle is the goal, then it should certainly be considered a challenge.

Fortunately, the shell can potentially be produced using production-scrap or recovered/recycled fibres or thermoplastic composites from other products without affecting the performance. This is a possibility because the load-levels in the exhaust shell are generally low and the mechanical requirements on shell thickness and fibre type and quality and not necessarily those that dictate the design.

5.1.10. System design

The dimensioning of the cross-section of an exhaust in line with this concept is a trade-off between price and mass. The higher the limit temperature of the outer shell, the less insulation is needed and the lower the mass. However, the material and shaping cost of polymers and composites increase more than proportional with increasing thermal stability. So generally, larger mass saving with respect to steel means higher cost. The compromise will depend on the business case and thus on the type of car model and it could benefit from methods of design optimization.

Given all mentioned factors of influence, the design is more than the dimensioning of the cross-section. Not only does it include material forms, material densities and component boundaries, but it also includes detail designs of the insulation support, junctions, mounting brackets and silencers. Furthermore, those designs have to take into account the assembly and manufacturing order and processes. Ending up with a design that satisfies all criteria can be considered the final challenge and will require some form of systems engineering.

5.2. Concept mass, CO_2 emission and material cost

The potential for mass reduction and for the corresponding CO_2 reduction are estimated for the current state of the concept. This estimate is rather preliminary, given the uncertainty over the durability of the insulation system and the manufacturing of the complete system including silencers. Next, the monetary cost of the material and its primary processing is compared for exhaust systems made of different candidate materials to get an idea of their cost-competitiveness.

5.2.1. Mass

The potential for mass reduction that can be achieved with the current system has become smaller since the first work on this concept in 2009. Steel exhausts systems have evolved under the focus on emission reduction and as a result their wall thickness and thus system mass have reduced over the years. A wall thickness of less than 1 mm is becoming more common. This incentive has only increased with the transition from the NEDC emission certification test to WLTP (Worldwide harmonized Light vehicles Test Procedure), because vehicle mass plays a larger role in the latter [36, 37].

The mass of the straight section of the heat transfer samples used for the tests in this thesis is roughly comparable to that of a steel exhaust pipe, so in that respect no mass reduction is achieved yet. However, given the conservatism in the design and the fact that exhaust systems are more than straight pipes, there is still potential for a mass advantage for the composite exhaust system. If the shell and insulation thickness can be reduced with further development, then the composite exhaust system could still offer a lower mass. More so, if mass can also be saved on the heavier or more complex system components such as the silencers and mounting brackets.

5.2.2. CO_2

For performance vehicles, mass saving can be a goal of its self, but for general passenger vehicles it is a means to an end, namely to benefit from or meet current vehicle greenhouse gas emission regulation. Although the concept is currently no lighter than a conventional exhaust system, it is worth analysing the potential influence of the composite exhaust system on the CO_2 emission of a passenger vehicle.

First only the emission during use is considered, because it is relevant to the certified CO_2 emission of vehicles and thus to manufacturers. To put that into perspective, after that the production phase CO_2 emission is also provided.

Use phase

It would be ideal to be able to provide the effect of the composite exhaust system on both the real world and certified CO_2 emission. The latter would require analysis of the mass difference on the WLTP emission outcome and although there is some relevant literature [37], an in-depth analyses of the test protocol is deemed beyond the scope of this thesis. There is some correlation between the certified CO_2 emission and the real-world emission [38], so the latter can also provide an indication

for it. Additionally, a recent study showed that the projected WLTP-based emissions of vehicles registered in 2022 with masses of 1000 and 1300 kg and petrol engines differed by 9 gCO_2/km, indicating a mass influence of 0.03 gCO_2/km/kg[7] [39].

A lower mass generally results in less required (engine) work per travelled distance. Firstly, a lower mass results in a lower rolling resistance force and secondly, for the same acceleration, less force is needed. The former can be approximated quite easily, but the latter will vary strongly with the use of the vehicle.

Fortunately, there has been some research on the general effect of mass on the real-world fuel consumption and thus CO_2 emission of vehicles [40, 41]. By using the outcomes of those studies, both effects can be taken into account. For vehicles with a petrol engine both studies report for each kg less a reduction of 0.03 gCO_2/km[8].

If the mass of whole composite exhaust system could be 10 kg less than that of the steel alternative, then the reduction in CO_2 emission would be 0.3 g/km. Assuming an exhaust system design life of 300,000 km, a 10 kg mass saving would nevertheless save 90 kg of CO_2. Putting the reduction in perspective: by assuming an average vehicle mass of 1300 kg and average CO_2 emission of 122 g/km, a mass reduction of 0.8% thus results in 0.3% less CO_2 emission.

5

Production phase

It is interesting to determine the amount of CO_2 needed for production of the steel and composite exhaust system, to put the potential CO_2 reduction from the use phase into perspective and also to study the difference between steel and composite production.

The amount of CO_2 emission related to exhaust system production was estimated for both existing and candidate materials using the GRANTA EduPack material and processing database [4]. For each material the same contributions were included, namely the emissions for the primary production of the material, its primary processing and coarse machining.

The number of insulation materials in the databased was limited and thus, silica fibre without a forming process was used to represent the insulation. Also, of the candidate matrix materials only those with mature automated forming processes were included. In some cases, high-thermal stability also means difficult processing and as a consequence the thermosets polyimide and vinyl ester and the thermoplastics PARA, PEEK, PEI and PPS were excluded.

The primary forming process differed between materials: roll forming for the metals and compression or injection moulding for the fibre-reinforced plastics. Also, for stainless steel and titanium, the primary production emission was corrected for the reduced emission of the fraction of recycled material. For the composite materials, the fraction of recycled materials was negligible.

[7] The vehicle mass category of 1700 kg was ignored by the author, as vehicles in that category tend to be Sports Utility Vehicles which have larger configurational differences with smaller vehicles and the difference is therefore less representative for the influence of mass.

[8] The reported value of 2.0 g/km for 100 kg mass difference on page 4 of Weiss et al. [41] seems inconsistent with the mentioned 0.13 l_{fuel}/100km/100kg and the factor of 2.33 kg CO_2/l_{fuel}. A recalculation based on 0.13 l_{fuel}/100km/100kg results in 0.03 gCO_2/kg/km.

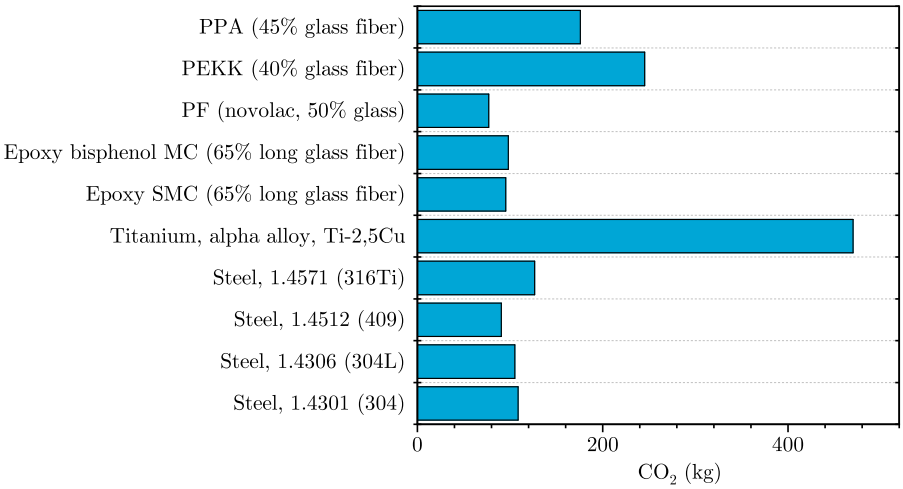

Figure 5.11: CO_2 emission associated with material production and processing for different candidate exhaust systems.

Since the emission contributions are per kilogram, an estimate of the material mass was needed. The following masses were assumed for an average exhaust system: 30 kg for steel; 15 composite shell and 15 kg insulation material for the composite system; and 17 kg for titanium (density normalized with respect to steel).

The results are shown in Figure 5.11 for several metals used for exhaust systems and for several candidate materials for the shell of the composite exhaust system including the contribution of the silica insulation (45 kg of CO_2).

At least two aspects are worth mentioning. First, the CO_2-emission of the production of the composite exhaust system can be competitive with steel if thermosetting resins are used. Given the multi-material nature, the more complex forming of the composite materials and the lack of recycled fraction, this is considered surprising. Second, the CO_2-emission that could potentially be saved in the use phase is roughly equivalent to the production emission. If one thus wants to achieve CO_2 reduction over the full life cycle rather than only during the use phase, then the contribution of production has to be taken into account. In that light, titanium and even more so fibres rich in alumina (not shown) should be avoided because of the factors higher production CO_2-emission.

5.2.3. Monetary cost of materials and processing

The concept is not mature enough yet for an elaborate monetary cost comparison, but comparing just the material and processing cost can offer insights into the competitiveness of different candidate exhaust systems. Using the same database as for the production CO_2-emission estimate, the combined material and proces-

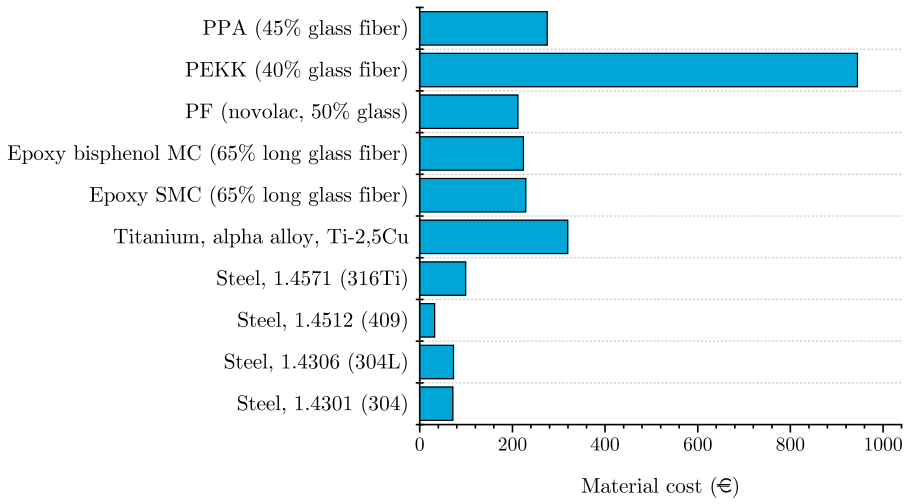

Figure 5.12: Combined material and material processing cost for different candidate exhaust system.

sing cost was estimated for exhaust systems made with the previously considered materials and masses, see Figure 5.12.

Before comparing the values, two aspects are worth mentioning. First and parallel to the estimation of CO_2 emission, the cost of the composite systems includes a contribution from the insulation in the form of 15 kg of silica. This contribution is for the silica material only, not its processing. Second, the listed material and processing cost does not necessarily reflect the cost for an actual exhaust system made in series of several hundred thousand units. However, given the fact that the costs all come from the same source, the values are considered useful for relative comparison.

Several aspects stand out from the material and processing cost comparison. Firstly, the €187 related to the silica insulation dominates the cost of the composite exhaust systems except for PEKK. The AES insulation used in the tests described in this thesis could probably halve that cost, even with a silica liner. Secondly, all steel variants are at least a factor two less costly than the other alternatives. The exhaust steel with the lowest maximum service temperature, EN 1.4512, stands out with a cost of only €32. Thirdly, there is a large difference between the alternatives. The glass-filled phenol formaldehyde (PF) is highly competitive with a material and processing cost (excluding insulation) of €25. Whereas, the cost of a PEKK exhaust system surpasses even titanium. Note that Nextel alumina fibres, although not shown, are in a league of their own with a material price well exceeding €1000/kg, which is consistent with the price index of Table 5.1.

5.3. Conclusions

Remaining challenges and solution options were identified for the composite exhaust system using a structured approach. The challenges range from further research on durability, manufacturing automation and recycling to the final design, assembly and integration of the insulation system.

The insulation system durability has the highest priority for further attention. The configurations tested were not durable enough, but there are a few remaining alternatives. In the end, none of the technical obstacles was labelled as definitively impossible to overcome. Once a sufficiently durable insulation configuration has been found, there will probably be at least several technically feasible configurations for this concept.

The current realization of the concept has a straight pipe mass roughly equal to that of steel and therefore does form a mass reduction solution. As the design is not yet mature, further development could still result in a lower mass. The CO_2 emission during production is about as large as that of steel if the shell is a thermosetting polymer, moreover, this amount is roughly equal to what could be saved during use if the exhaust were 10 kg lighter. Thermoplastics have a higher associated emission and material cost. The material and forming cost of the thermosetting shell is comparable to that of steel and in some cases even less. However, the material cost of the the insulation is several times more, making the concept more costly in terms of materials and processing.

References

[1] Frenzelit GmbH, *Solutions for acoustic and heat insulation,* www.frenzelit.com, aT/2/09.10/02/WY.

[2] P. M. Sawko and H. E. Goldstein, *Performance of Uncoated AFRSI Blankets during Multiple Space Shuttle Flights*, NASA Technical Memorandum 103892 (National Aeronautics and Space Administration, 1992).

[3] B. M. Trujillo, R. R. Meyer Jr., and P. M. Sawko, *In-Flight Load Testing of Advanced Shuttle Thermal Protection Systems*, NASA Technical Memorandum 86024 (National Aeronautics and Space Administration, 1983).

[4] Granta Design Limited, *CES EduPack 2019,* Material database software (2019), version 19.2.0.

[5] E. Le Bourhis, *Glass: Mechanics and Technology*, 2nd ed. (Wiley-VCH Verlag GmbH & Co. KGaA, 2014).

[6] K. Daryabeigi, *Heat transfer in high-temperature fibrous insulation,* Journal of Thermophysics and Heat Transfer **17**, 10 (2003).

[7] K. Daryabeigi, G. R. Cunnington, and J. R. Knutson, *Combined heat transfer in high-porosity high-temperature fibrous insulation: Theory and experimental validation,* Journal of Thermophysics and Heat Transfer **25**, 536 (2011).

[8] S. Zhao, B. Zhang, and X. He, *Temperature and pressure dependent effective thermal conductivity of fibrous insulation,* International Journal of Thermal Sciences **48**, 440 (2009), int J Therm Sci.

[9] F. T. Wallenberger and P. A. Bingham, eds., *Fiberglass and Glass Technology*, Energy-Friendly Compositions and Applications (Springer, 2010).

[10] R. H. Doremus, *Glass Science* (Wiley, 1994).

[11] P. Comodi, F. Cera, G. D. Gatta, N. Rotiroti, and P. Garofani, *The devitrification of artificial fibers: A multimethodic approach to quantify the temperature–time onset of cancerogenic crystalline phases,* The Annals of Occupational Hygiene **54**, 893 (2010).

[12] C. Ziemann, P. T. C. Harrison, B. Bellmann, R. C. Brown, B. K. Zoitos, and P. Class, *Lack of marked cyto- and genotoxicity of cristobalite in devitrified (heated) alkaline earth silicate wools in short-term assays with cultured primary rat alveolar macrophages,* Inhalation Toxicology **26**, 113 (2014).

[13] P. J. Lezzi, E. E. Evke, E. M. Aaldenberg, and M. Tomozawa, *Surface crystallization and water diffusion of silica glass fibers: Causes of mechanical strength degradation,* J. Am. Ceram. Soc. **98**, 2411 (2015).

[14] G. N. Greaves and S. Sen, *Inorganic glasses, glass-forming liquids and amorphing solids,* Advances in Physics **56**, 1 (2007).

[15] Q. Zheng, Y. Zhang, M. Montazerian, O. Gulbiten, J. C. Mauro, E. D. Zanotto, and Y. Yue, *Understanding glass through differential scanning calorimetry,* Chemical Reviews **119**, 7848 (2019).

[16] V. M. Fokin, A. S. Abyzov, N. S. Yuritsyn, J. W. P. Schmelzer, and E. D. Zanotto, *Effect of structural relaxation on crystal nucleation in glasses,* Acta Materialia **203**, 116472 (2021).

[17] I. Zaplatynsky, *Shrinkage of amorphous silica fibers,* in *Proceedings of the 7th Annual Conference on Composites and Advanced Ceramic Materials*, Ceramic Engineering and Science Proceedings Series, Vol. 44, edited by W. Smothers (John Wiley & Sons, 1983) pp. 492–501.

[18] C. T. Moynihan, *Structural relaxation and the glass transition,* in *Structure, dynamics, and properties of silicate melts*, Reviews in Mineralogy, Vol. 32, edited by J. F. Stebbins, P. F. McMillan, and D. B. Dingwell (Mineralogical Society of America, 1995) Chap. 1, pp. 1–20.

[19] National Institute for Occupational Safety and Health, *Asbestos fibres and other elongated mineral particles: State of the science and roadmap for research,* DHHS Publication No. 2011-159 (2011).

[20] A. Campopiano, A. Cannizzaro, F. Angelosanto, M. L. Astolfi, D. Ramires, A. Olori, S. Canepari, and S. Iavicoli, *Dissolution of glass wool, rock wool and alkaline earth silicate wool: Morphological and chemical changes in fibers,* Regulatory Toxicology and Pharmacology **70**, 393 (2014).

[21] T. P. Brown and P. T. C. Harrison, *Crystalline silica in heated man-made vitreous fibres: A review,* Regulatory Toxicology and Pharmacology **68**, 152 (2014).

[22] T. Tonnesen, P. Dietrichs, and R. Telle, *Linear shrinkage, resilience and microstructural changes in high temperature insulating wools in maximum use temperature range,* Advances in Applied Ceramics **104**, 249 (2005).

[23] Morgan Thermal Ceramics, *Superwool Plus Insulating fibre - Technical Manual* (2011).

[24] W. E. Black and W. S. Betts, *Vibration damage testing of thermal barrier fibrous blanket insulation,* Nuclear Engineering and Design **80**, 375 (1984).

[25] A. Filounek, S. Otto, and G. Walter, *Schutz poröser wande von industrieöfen vor schadigung durch kondensate,* GASWÄRME International **53**, 279 (2004).

[26] F. T. Wallenberger, *Structural silicate and silica glass fibers,* in *Advanced inorganic fibers: processes - structures - properties - applications*, edited by F. T. Wallenberger (Kluwer Academic Publishers, 2000) Chap. 6, pp. 129–168.

[27] ASTM International, *Standard Test Method for Thermal Conductivity of Refractories*, C201, 2013.

[28] ASTM International, *Standard Test Method for Steady-State Heat Flux Measurements and Thermal Transmission Properties by Means of the Guarded-Hot-Plate Apparatus*, C177, 2013.

[29] O. K. Bergsma, *Three Dimensional Simulation of Fabric Draping*, Ph.D. thesis, Delft University of Technology (1995).

[30] G. Ridolfi, *Composite exhaust system for lighter weight cars*, Master's thesis, Delft University of Technology, Delft (2012).

[31] C. A. Mahieux, *Environmental Degradation in Industrial Composites* (Elsevier Ltd, Kidlington, UK, 2006).

[32] K. V. Pochiraju, G. P. Tandon, and G. A. Schoeppner, eds., *Long-term Durability of Polymeric Matrix Composites* (Springer, 2012).

[33] European Parliament and the Council, *Directive 2000/53/EC of the European Parliament and the Council of 18 september 2000 on end-of-life vehicles,* Official Journal of the European Union (2000), L269.

[34] SIEMENS Gamesa, *Siemens gamesa pioneers wind circularity: launch of world's first recyclable wind turbine blade for commercial use offshore,* (2021), press release.

[35] European Commission, *Low energy chemo-thermal recycling of carbon fibre composites, a central step to a circular economy for cfrp products,* LIFE funding programme (2022).

[36] European Commission, *Commission regulation (EU) 2017/1151 of 1 june 2017 supplementing Regulation (EC) no 715/2007 of the European Parliament and of the Council on type-approval of motor vehicles with respect to emissions from light passenger and commercial vehicles (euro 5 and euro 6) and on access to vehicle repair and maintenance information, amending Directive 2007/46/ec of the European Parliament and of the Council, Commission Regulation (EC) no 692/2008 and Commission Regulation (EU) no 1230/2012 and repealing Commission Regulation (EC) no 692/2008,* Official Journal of the European Union (2017), L175.

[37] N. E. Ligterink, P. van Mensch, and R. F. A. Cuelenaere, *NEDC - WLTP comparative testing*, Tech. Rep. R11285 (TNO, 2016).

[38] R. Van Gijlswijk, M. Paalvast, N. E. Ligterink, and R. Smokers, *Real-world fuel consumption of passenger cars and light commercial vehicles*, Tech. Rep. R11664 (TNO, 2020).

[39] N. E. Ligterink, A. Bhoraskar, and G. C. Holmes, *Trends in energy efficiency of conventional petrol and diesel passenger cars*, Tech. Rep. R11642 (TNO, 2021).

[40] L. Ntziachristos, G. Mellios, D. Tsokolis, M. Keller, S. Hausberger, N. Ligterink, and P. Dilara, *In-use vs.type-approval fuel consumption of current passenger cars in europe,* Energy Policy **67**, 403 (2014).

[41] M. Weiss, L. Irrgang, A. T. Kiefer, J. R. Roth, and E. Helmers, *Mass- and power-related efficiency trade-offs and* co_2 *emissions of compact passenger cars,* Journal of Cleaner Production **243**, 118326 (2020).

6

Discussion & Conclusions

More insight into the feasibility of the lined composites exhaust concept is welcome in order to bring it closer to potential realization. With that, an additional solution to reduce the environmental impact of road transportation can potentially be realized.

The main aim of this thesis is to quantify the three most influential and yet uncertain factors that define the performance of a fibre-reinforced exhaust system, namely the flow resistance, heat transfer and durability. This has been done experimentally using newly developed setups with as representative conditions as possible.

6.1. Literature and research questions

The main aim translated into the following main research question:

> How can the friction, heat transfer and wear of an internally lined exhaust system be quantified, and what do the eventual results mean for the associated mechanisms and the feasibility of the concept?

An idea of the most important influences on the flow state of the concept exhaust is needed to be able to understand the performance of the alternative wall configuration and to estimate the effect of changes in this configuration. With that, directions for potential improvement can be determined.

The interaction between the flow and the flow boundary is generally understood for smooth and solid boundaries and also for more complicated boundaries. However, the concept under consideration combines features from several special boundaries and the combined effect is yet unknown. On top of that, the exhaust gas flow is not only turbulent but also pulsating. As modelling was considered more challenging because of the complexity of the configuration and material properties, an experimental approach was chosen. Starting with constant insulation properties, i.e. ignoring insulation wear, the first research questions related to friction and heat transfer are:

1. How can the friction and heat transfer rates of exhausts systems that are internally lined with fibrous insulation be quantified?
2. What can be concluded on the friction and heat transfer mechanisms based on their quantification experiments?

Besides the flow state, understanding of the degradation of the insulation as a result of the exposure to the flow is also essential for sufficient performance of the concept.

3. How can the wear rate of an exhaust system that is internally lined with fibrous insulation be quantified?
4. What can be concluded on the wear mechanism based on the performed experiments?

Finally, its is worth examining the concept itself again. Mainly, because the potential of a composite exhaust system as an alternative for the conventional steel ones depends on more than friction, heat transfer and wear. In terms of concept feasibility it is worth looking at its mass, cost and CO_2 emission. Also, the realization up to this point can be revisited with the improved understanding of the conditions and performance to see whether there are alternative configurations that seem more promising. With that it is also necessary to look at remaining realization challenges such as those related to manufacturing.

5. What challenges and uncertainties remain for the realization of the concept?
6. What is the general performance (potential) of the concept in terms of mass, cost and CO_2 emission?
7. What configuration and application of the concept could have the largest potential, based on the performed work?

6.2. Test for friction and heat transfer

A test method was developed to determine the friction and thermal resistance of pipe-shaped samples that can have a variety of wall configurations. The setup can be combined with different flow sources, but in this study mostly combustion engines were used. Samples were tested over ranges of Reynolds numbers and non-dimensional frequencies relevant to combustion engine exhaust gas flow. The flow was turbulent and pulsating.

The streamwise pressure drop and mass flow rate were measured and after subtraction of the contribution of the interface components, the friction factor of the tested wall configuration was determined. This proved accurate enough to distinguish between wall configurations and to generally compare with results from other studies.

The heat flux derived from the streamwise temperature drop alone proved not accurate enough at higher mass flow rate, in part because of the small magnitude of the temperature drop itself. It was therefore used to calibrate a model of the

external thermal resistance that used sample shell temperature measurements as input. From this model the heat transfer rate was obtained.

The tested alternative wall configurations consisted of an outer shell, lined with a fibrous insulation layer that was kept in place using silica fabric and a steel wire-mesh. The insulation density, the amount of insulation compression and wire-mesh pitch were varied.

The sample flow boundaries had a combination of properties not covered by existing literature: the bulk could be considered flexible, yet the mesh made the roughness non-homogeneous and the lining fabric made the insulation effectively impermeable.

Measurement of the temperature of the interface between the insulation system and the exhaust gas flow proved inaccurate. As a result, no distinction could be made between the thermal resistance of the boundary layer and the fibrous insulation layer. However, the reference sample with known properties showed that the insulation resistance dominates that of the boundary layer. The total thermal resistance can thus serve as a first indication of the relative difference between insulation configurations.

The friction factor proved constant over the tested range of Reynolds numbers and pulsation frequencies for the lined samples. The friction factors are in line with those found in literature for configurations with solid walls, steady flow and similar wire pitches. The insulation variation did not have a significant influence. This indicates that the non-sinusoidally pulsating flow and compliant wall have no substantial contribution or interaction compared to the influence of the discrete roughness.

The influence of the interface on the heat transfer was similar as observed for friction, but the thermal resistance was also affected by the insulation. The thermal radiation resistance not only increased substantially with increasing insulation density, but also with compression of the fibrous insulation[1].

6.3. Test for wear

To assess the wear of insulation systems under influence of high temperature turbulent flows, such as those from combustion engines, a test rig was designed and built. Although the rig uses flat rather than cylindrical samples, it provides similar thermal and fluid-dynamic loading with generally similar mechanical support. Besides the test rig itself, a test campaign was described including the complete test setup and procedure.

The sample rig can be removed from the flow source and opened to visually inspect the sample surface and measure its mass without having to remove the sample from the rig. This allows mass measurement in between exposure cycles. The uncertainty in the mass change was estimated at less than 0.2 gr or about 0.1%. Other inspection techniques could also be applied in between these cycles.

The tested insulation systems had a similar configuration as the samples used for the friction and heat transfer testing: fibrous insulation with a liner and metal

[1] compared to non-compressed insulation of the same effective density

mesh on top. Several aspects were varied, such as the duration of thermal ageing before testing and the thickness of the mesh wires.

Several failure mechanisms were observed. In some cases the mechanical support proved too weak for the samples. In most samples, the insulation damage seemed related to the presence of *shot* in the insulation material employed. The observed insulation system durability proved insufficient for application in exhaust systems, but given the material specific influence, this cannot be generalized.

6.4. Realization challenges

The challenges that remain before the lined exhaust system could be realized were identified and alternatives analysed. The main findings are repeated here.

If the concept is to be suitable for all combustion engine types, then the maximum gas temperature limits the range of candidate materials for the insulation to thermally-stable metals and ceramics. Given their lower density, ceramics offer the largest potential for a low-mass system. However, they come with substantial uncertainty regarding their performance and durability under these conditions. Irrespective of the type of ceramic, the fibrous form is the first choice because of its higher thermal shock resistance and strength compared to the bulk form.

At the temperatures under consideration, the internal structure of almost all ceramic fibres alters compared to the as-produced state. This change generally negatively affects the mechanical performance, decreasing strength and compliance. In short, the higher the thermal stability of a fibre material, the higher the energy consumption during manufacturing and thus the higher the material cost. No single performance parameter was found that indicates whether a ceramic material would be suitable as insulation material for this application. The maximum continuous use temperature can serve as a first indication, but was often too optimistic for this application.

Alkaline Earth Silicate fibrous insulation was used in all samples so far. It was chosen because of its sufficiently high maximum use temperature, its relatively low cost and because it is not considered carcinogenic. Besides fibres, this insulation contains *shot*: relatively large frozen drops of ceramic that result from its manufacturing process. During wear testing the insulation performance often proved to be the limiting factor. In some cases the fibrous network around a single large shot element was damaged, more often the damage of the insulation was distributed along the longitudinal axis of the sample with the shot left on the bottom of the sample container. It is expected that insulation without shot could perform substantially better under these conditions.

Besides the thermal and mechanical loading, other influences can also affect the durability. Some of the combustion products for instance, either during engine operation or afterwards, or the dynamic loading due to the vehicle motion.

Shaping and assembling the insulation system also brings challenges. The design and manufacturing of junctions in the insulation system is one problem that requires further investigation. Three concepts for mechanical support were identified and two of those were tested. Although generally feasible, the double curvature in the bends is one of the aspects that requires investigation for all these concepts.

Fibre-reinforced plastics are applied in high-temperature applications, so the challenge lies more in the design than in further development. For instance, by taking into account road debris impact and by determining the subdivision of the shell. Shell manufacturing is considered spossible with both thermoplastic and thermosetting resins and with long and short fibres.

Combining the insulation and shell during manufacturing is another challenge. Due to the aspect ratio of the shell, adding insulation after its production is not straightforward. The primary way to tackle this is to divide the shell into multiple parts and insert the insulation before joining those parts. A second way could be to manufacture the shell with the insulation already inside. Using a straight exhaust design would simplify manufacturing greatly, but modifying the vehicle underbody design is not considered feasible.

Just like a regular exhaust system, the alternative exhaust concept has interfaces. The upstream interface with the engine (manifold) or catalytic convertor had to be tackled for the tests of Chapter 3, where the main remaining challenge was the durability of the adhesive connection with the shell. The downstream end requires no mechanical connection, but the higher exhaust gas temperature at the exit could be unwanted in some cases. Mixing the exhaust gas flow with ambient air could theoretically solve this, but this requires further investigation. The mounting of the exhaust system is considered a minor challenge, as the solution used for regular exhausts could be used. However, more simple solutions are potentially possible.

6.5. Feasibility

The feasibility of the concept was analysed based on the current state. First the concept mass, carbon dioxide emission and material cost were estimated and then, putting those together, the general feasibility was assessed.

The mass of the straight sections used for the tests in this thesis is roughly comparable to that of a steel exhaust pipe. So, with this preliminary configuration no mass reduction has been achieved yet. There is still some potential, for instance if the shell or insulation thickness could be reduced or if the silencers and mounting brackets could be simplified.

Two phases were distinguished in terms of CO_2 emission: production and use. Reduction of the latter is stimulated through legislation; during use a 10 kg mass reduction theoretically saves 90 kg of CO_2 over 300,000 km. The CO_2 emission related to material manufacturing and processing proves quite similar for steel and the concept with a thermosetting polymer shell, but not with thermoplastics. Also the CO_2 emission related to manufacturing is comparable to what could be saved during use and thus has to be taken into account if a life cycle CO_2 reduction is the goal.

Without the final configuration, no elaborate cost comparison is possible, but the cost of materials and processing will form a large part; this was estimated for several candidate configurations. Parallel to the CO_2 emission, the cost of thermoset polymer shells is comparable to steel. That however excludes the material cost of the insulation, which is several times higher.

6.6. Potential

The combination of the requirements and the extreme conditions found in combustion engine exhausts is a challenging one. The current work shows that the concept does not necessarily perform satisfactory or save mass for general use with all engine types. That goal is theoretically still possible, but it certainly requires additional research and development and perhaps even several innovations. Given the results presented here, future efforts would probably better be focussed on more specialized or other applications of the concept.

The potential of the concept in combination with port-injected engines, with their high gas temperature, is probably smallest. The employed AES insulation material, with its shot content, most likely cannot provide sufficient durability. If it somehow could, then the concept does not offer a mass benefit yet and without that, its probably lower production CO_2 emission will not justify the higher cost.

Compared to AES, there are several alternative current-day (shot-free) engineering materials available that most likely perform better in terms of durability. However, the higher silica and alumina content of those more thermally stable materials makes most of them unacceptable due to the health risks associated with their dust form and, furthermore, the production CO_2 emission and material cost of the system would be substantially higher than with AES.

If high-performance insulation material is used that has no associated health risks, then further development together with a high-performance, high-cost shell material could provide an alternative with some mass reduction for high performance vehicles, but compared to the existing titanium alternative the benefit would be limited. Altogether, the potential for port-injected engines seems rather limited.

It could be that the concept (with AES or another relatively affordable insulation) does perform satisfactory in the exhaust environment of lean-burning engines. Many of the durability decreasing effects are temperature dependent and would be less severe due to the lower exhaust gas temperatures. Furthermore, lower gas temperatures could enable some mass reduction, because the smaller required temperature drop means less insulation and a smaller shell radius. This makes further development for lean-burning engines more attractive than for port-injected engines, but the material cost would still be about twice that of steel.

Summarizing, the potential for the concept as a competitive alternative that offers mass reduction is limited for passenger vehicles. However, if the retained exhaust gas heat could serve another useful purpose for the vehicle, then the potential of the concept would be worth reassessing. Lastly, there could also be other systems that could benefit from a lower-mass exhaust system for which a specific feasibility analysis might be worthwhile. Trucks or turboprop helicopters, for instance, could have very different boundary conditions.

A

Appendix to Chapter 3

This chapter contains the material from the appendix of the article [1] that forms the basis for Chapter 3.

A.1. Uncertainty analysis of temperature drop and heat loss rate

Measurement uncertainty analysis, for instance using the method outlined by Dunn [2], allows differentiation between the contributions of different sources of error. More specifically it provides a framework to estimate the effect of different random and bias errors on the uncertainty of a result. Given the simplicity of the measurement chain for the temperature drop specifically, the uncertainty analysis of the mean using the mentioned method is not too complicated.

The principle of the method is to estimate the true variance of the normal distribution that corresponds to the measurement. As such, it requires an estimate of the variance of the different contributions, even the inherent non-probabilistic ones. The measurement of the temperature drop for a single test stage classifies as a so-called multiple-measurement measurand experiment. Because of the multiple measurements, the standard deviation of the random error is readily available from the data points used for the average temperature drop. The bias (or systematic) error was estimated from comparison with extra tests with the gas temperature drop thermocouples having swapped position. Several tests besides those published in Chapter 3, were ran to obtain sufficient information regarding the bias error.

Using the method of Dunn [2] and assuming sufficiently large degrees of freedom to apply the Gaussian distribution, results in the following expression for the 95% confidence uncertainty in the temperature difference

$$U_{T,95} \simeq 2\sqrt{S_{\bar{B}_{\mathrm{da}}}^2 + S_{\bar{B}_{\mathrm{tc}}}^2 + S_{\bar{P}_{\mathrm{tc}}}^2} \tag{A.1}$$

where $S_{\bar{P}_{\mathrm{tc}}}$ is the standard deviation of the random error in the mean of the thermocouple measurement and $S_{B_{\mathrm{da}}}$ and $S_{B_{\mathrm{tc}}}$ are the standard deviations of the systematic errors corresponding to the data acquisition and thermocouple, respectively.

Quantifying the random and systematic standard deviations is all that remains to establish the uncertainty. The random uncertainty of the mean value can be obtained from the standard deviation of the set of temperature drops used for the average as follows:

$$S_{\bar{P}_{\mathrm{tc}}} = \frac{S_{P_{\mathrm{tc}}}}{\sqrt{N}} \tag{A.2}$$

where N is the number of measurements in the set, resulting in $S_{\bar{P}_{\mathrm{tc}}} = 0.1$ °C. Next to that, the standard deviation of the bias error of the differential temperature measurement was estimated by comparing the difference in the results of a regular measurement of a sample and one with the differential thermocouples swapped. The difference varied between 0.1 and 2.2 °C for the different stages, leading to a standard deviation of $S_{B_{\mathrm{tc}}} = 1.0$ °C. Finally, by assuming that the manufacturer-specified accuracy represents the 95% confidence bias limit, means that its standard deviation is half the limit: $S_{B_{\mathrm{da}}} = 0.1$ °C.

Having also established the uncertainty of the specific heat and the mass flow rate through the uncertainty in the correlations and equipment, allows the calculation of the uncertainty of the heat loss rate through the propagation of the relative errors. The resulting 95% overall uncertainty of the heat loss estimate based on the gas temperature drop is indicated in Figure A.1.

A.2. Thermocouple heat balance model

The thermal interaction of a gas thermocouple with the surrounding sample in the case of the experiment described in this section was modelled to estimate the temperature difference between the gas and that of the different hot junctions along its length[1]. This was done for both the steel mesh and the solid steel liner (HS) configuration because of the difference in wall roughness and corresponding wall surface temperature.

In general, the equilibrium temperature of a sheathed thermocouple in a gas flow is the result of the balance between different heat transfer mechanisms [3]:

$$q_{\mathrm{cond}} = q_{\mathrm{rad}} + q_{\mathrm{conv}} \tag{A.3}$$

where q_{cond} represents the heat transfer rate through conduction, q_{rad} is the heat transfer rate through radiation and q_{conv} is the heat transfer rate through forced convection.

The equilibrium temperature was obtained by solving Equation A.3 numerically for the one-dimensional case of a thermocouple discretized into eight isothermal elements of equal length. The contributions of radiation, convection and conduction were based on the temperature difference between the node in the centre of each element and the object of interaction. The set of elements covered the section of

[1] See section 3.2.3.

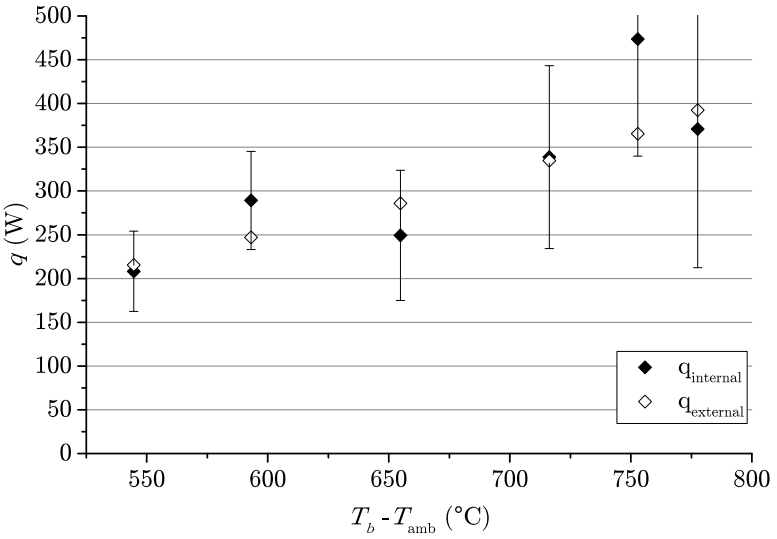

Figure A.1: The heat loss rate over the instrumented length of the lined section of sample 128-18-H-2 as a function of the temperature difference between the exhaust gas and ambient, based on either the gas flow temperature drop ('internal', solid diamonds), or on the external thermal resistance model ('external', open diamonds) with its forced convection velocity obtained through a least-squares fit of these two rates. Also indicated is the 95% uncertainty of the heat loss rate based on the gas temperature drop.

the thermocouple that was exposed to the gas, so the last element ended at the wall.

The conductive heat transfer was estimated as simple one-dimensional conduction, using the average temperature between the two elements as the input for the calculation of the thermal conductivity of Inconel. The contribution of the magnesium oxide and the thermocouple wires inside the individual thermocouples was deemed negligible and thus the elements were given the area and conductivity corresponding to the sheaths. The highly temperature-dependent thermal conductivity of Inconel was taken into account using the following linear approximation as a function of the temperature in Celsius: $\lambda = 14.221 + 0.0162T$. For the last element, the conductive heat exchange with the segment of the thermocouple beyond the flow had to be approximated. This was done by assuming that the length through the insulation was adiabatic and that the thermocouple temperature at the shell, so in the mount, equalled that of the shell.

The nett radiation energy transfer between the two grey bodies of the thermocouple and the duct inner wall, was approximated by that between two concentric pipes with the one having a much larger area than the other: $q_{\mathrm{rad}12} = \epsilon_1 \sigma (T_1^4 - T_2^4)$. The required hemispherical emissivity of the oxidized Inconel sheath of the thermocouple was estimated at 0.83. Next to this, the emissivity of the exhaust gas was calculated according to the method presented in [4] because of the presence of the selective radiators H_2O and CO_2. Its emissivity, over a distance relevant to

this model, was less than 0.1 and thus ignored.

The wall temperature of the sample (required for the radiation estimate) was approximated by solving the combined heat transfer from gas to the wall for the temperature difference needed to have the heat transfer rate found earlier. The convective heat transfer rate for the wire-mesh lined wall was based on the approximation for the Nusselt number from Norris[2] [5]. Similarly, the Nusselt number for the solid-walled sample was obtained from the expression of Gnielinski found in Table 8.3 of Karwa [6]. The gas radiation in both cases was determined according to [4].

For the thermocouple, the Nusselt number for forced convection over a cylinder in cross-flow was calculated using equations (3-5) of Gnielinski [7], approximating the cross-sectional variation in velocity using the velocity defect law [8] and the friction velocity. As a first approximation, the temperature profile was assumed equal to the velocity profile, because the Prandtl number of the flue gas is not too far from unity (0.74) and the thermal boundary layer thus has a thickness similar to that of the momentum one [6]. The temperatures at the extremes of this profile were the wall temperature as estimated for the radiation and the measured gas temperature. The thermal conductivity of the fluid was that according to the bulk fluid temperature.

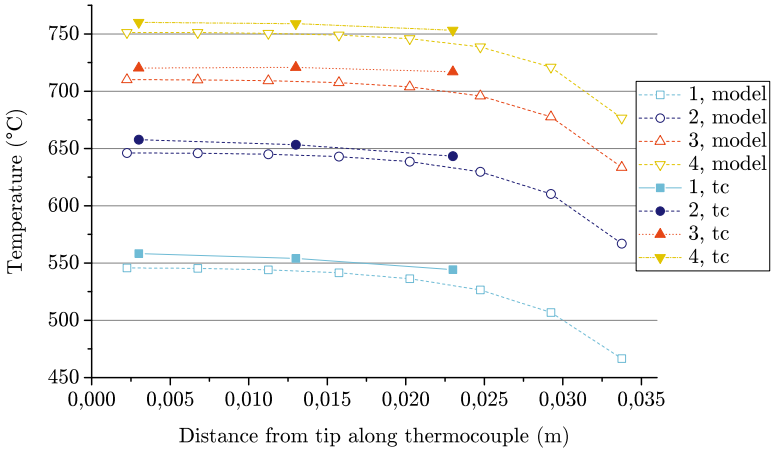

Figure A.2: Gas temperature as a function of distance along the thermocouple from the tip, for both model and thermocouple reading ('tc') for four different stages of the test sequence of 128-16-HS-1. The model uses the measured temperature as input gas temperature.

Using the above estimations for the contributions of conduction, convection and radiation, the temperature distribution along the thermocouple could be estimated for the two main wall configurations. In order to validate the model, its thermocouple temperature distribution was calculated for four different stages of the performed experiment and compared to the temperatures of the three hot junc-

[2]Using a coefficient of 0.5 because it matches the wire sources better than the general coefficient of 0.63.

tions of the middle gas thermocouple during those stages. Figure A.2 shows both temperature distributions for sample 128-16-HS-1.

The temperature trends along the thermocouple of the model and measurements are similar and the model thus seems to capture the behaviour sufficiently. The model can thus be used to estimate the error resulting from the assumption that the thermocouple temperature equals the gas temperature. For the thermocouple tip, the first element of the model, the difference is shown in Figure A.3. Besides the smooth-walled sample, the temperature difference of the wire mesh sample 128-16-H-4 is also shown.

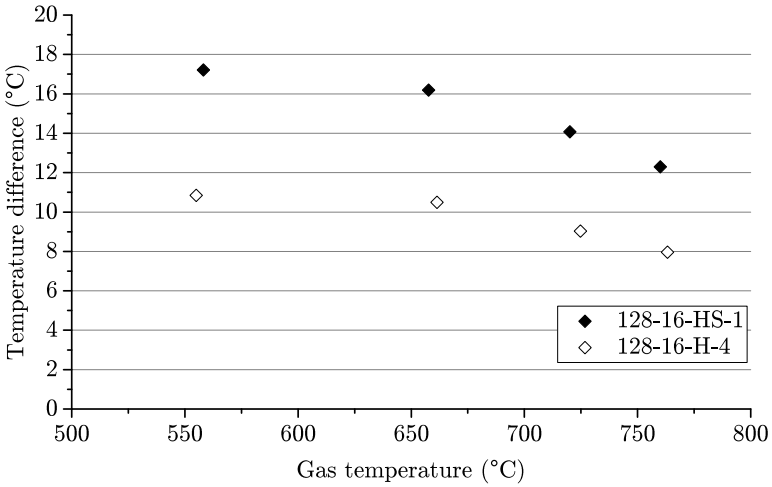

Figure A.3: Temperature difference between the gas temperature and the sheath temperature according to the proposed model for samples 128-16-HS-1 and 128-16-H-4.

The sample 128-16-H-4 has the wire-mesh for support of the lining and the inaccuracy of the Nusselt number, and thus the wall temperature itself, is larger than for HS-1. The increased roughness is nevertheless coupled to increased heat transfer, resulting in a higher wall temperature and consequently a smaller temperature difference with the gas. This is reflected in the smaller temperature difference found by the model when compared to the solid smooth wall.

A.3. Viscous dissipation

The heat balance between gas temperature and heat flux to the boundary in the form of Equation 3.4 is only valid if viscous dissipation is negligible. The validity of this assumption is worth investigating because of the uncommon combination of a wall with a relative large friction factor, peak fluid velocities of over 50 m s^{-1} and a much larger fluid viscosity than at room temperature.

To estimate the magnitude of viscous dissipation we start from the same principal equation as for the heat balance, namely the general expression for the thermal

energy balance of a differential fluid element [9]:

$$\rho c_{\mathrm{p}} \frac{\mathrm{D}T}{\mathrm{D}t} = -\nabla \cdot \mathbf{q} + \beta T \frac{\mathrm{D}p}{\mathrm{D}t} + \mu \left[-\frac{2}{3} \left(\chi \frac{\mathrm{D}p}{\mathrm{D}t} - \beta \frac{\mathrm{D}T}{\mathrm{D}t} \right)^2 + \Phi_{\mathrm{inc}} \right] \tag{A.4}$$

where $\mathbf{q}$ is the heat flux vector, β the coefficient of thermal expansion, μ the dynamic viscosity, χ the volume compressibility and Φ_{inc} the rate of viscous dissipation for an incompressible fluid. This general expression simplifies with further assumptions for the specific case at hand.

Focussing on the time-mean solution and assuming an ideal gas, negligible pressure variations and small enough temperature differences to ignore density variations, but keeping the viscous dissipation term for incompressible fluids, reduces Equation A.4 to:

$$\rho c_{\mathrm{p}} \overline{\mathbf{u}} \cdot \nabla \overline{T} = -\nabla \cdot \mathbf{q} + \mu \Phi_{\mathrm{inc}} \tag{A.5}$$

where the overscore indicates the time-mean value of the variable.

If we subsequently assume that the total temperature change is a linear combination of that due to viscous dissipation and that resulting from the equilibrium described using equation 3.4, then we can focus on the viscous dissipation only.

Because of the large thermal resistance in the wall and the relatively low conductivity of the gas, it is also assumed that the heat generated through viscous dissipation results predominantly in fluid temperature increase. This means that we can ignore the heat flux term.

The equation still includes the product of the velocity vector and the temperature gradient but there can only be a non-zero time-mean velocity in the streamwise (x-)direction. Consequently, the equation further reduces to:

$$\rho c_{\mathrm{p}} \overline{u} \frac{\partial \overline{T}}{\partial x} = \mu \Phi_{\mathrm{inc}} \tag{A.6}$$

which still applies to a differential fluid element.

Now integrate the expression over the fluid cross-section to obtain the temperature difference over a differential length of the pipe:

$$\int \rho c_{\mathrm{p}} \overline{u} \frac{\partial \overline{T}}{\partial x} dA = \int \mu \Phi_{\mathrm{inc}} dA \tag{A.7}$$

which still includes quantities that cannot be compared to those measured during the experiment.

So, we introduce the velocity-weighted bulk temperature T_b to be able to express the radially varying temperature in a single number:

$$T_b = \frac{\frac{1}{\pi R^2} \int \overline{u} \overline{T} dA}{\frac{1}{\pi R^2} \int \overline{u} dA} \tag{A.8}$$

where the denominator is equal to the bulk velocity u_b, which varies hardly along the x-direction.

The term for viscous dissipation on the right hand side of Equation A.7 also has to be related to measured quantities. In essence, viscous dissipation is the conversion of mechanical energy to heat through viscous heating. In steady-state pipe flow, the loss in mechanical energy can directly be related to the pumping power as follows:

$$\int \mu \Phi_{\text{inc}} dA = \int \rho \epsilon dA = \int -\overline{u} \frac{\mathrm{d}\overline{p}}{\mathrm{d}x} dA \tag{A.9}$$

where $\rho\epsilon$ is the dissipated power per unit volume.

Equating equations A.9 and A.7, introducing the bulk temperature and performing the integration over the circular cross-section of the sample interior (up to radius R) yields:

$$\rho c_{\text{p}} \pi R^2 u_b \frac{\mathrm{d}T_b}{\mathrm{d}x} = \pi R^2 u_b \left(-\frac{\mathrm{d}\overline{p}}{\mathrm{d}x} \right) \tag{A.10}$$

which is valid for a differential length dx. Using the discrete difference over the measurement section rather than the gradient yields:

$$\Delta T_b = \frac{\Delta p}{\rho c_{\text{p}}} \tag{A.11}$$

where Δp is static pressure drop. The outcome of equation A.11 for sample 12-16-H-4 is shown in Figure A.4. The temperature difference is a good measure for the engine load, note however that not only the gas temperature increases with increasing engine load, but so does the mass flow rate.

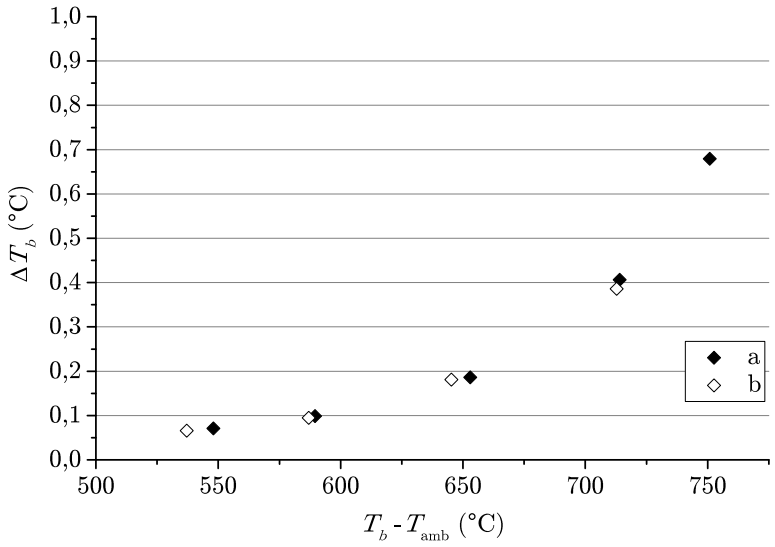

Figure A.4: Estimate of the temperature increase due to viscous dissipation over the instrumented length versus the temperature difference between the exhaust gas and ambient for two different test sequences of sample 128-16-H-4.

A

The observed temperature differences due to viscous dissipation are negligible compared to the absolute gas temperature, but at the higher engine loads the magnitude is sufficient to require incorporation in Equation 3.4 because the measured temperature drop over the sample is of the order of 10 °C. However, this estimated fluid temperature increase due to viscous dissipation could be conservative since part of the pumping power that is now assigned to heating the fluid, in reality went into deforming the fabric and fibres in the wall.

References

[1] C. Reurings, S. Koussios, O. K. Bergsma, W.-P. Breugem, K. Vergote, L. Paeshuyse, and R. Benedictus, *The influence of a porous, compliant layer with overlying discrete roughness elements as exhaust pipe wall on friction and heat transfer,* Heat and Mass Transfer **56**, 2367 (2020).

[2] P. F. Dunn, *Measurement and data analysis for engineering and science*, 2nd ed. (CRC Press, Boca Raton, FL, USA, 2010).

[3] R. M. Park, R. M. Carroll, P. Bliss, G. W. Burns, R. R. Desmaris, F. B. Hall, M. B. Herzkovitz, D. MacKenzie, E. F. McGuire, R. P. Reed, L. L. Sparks, and T. P. Wang, eds., *Manual on The Use of Thermocouples in Temperature Measurement*, 4th ed. (ASTM International, 1993) MNL12-4TH.

[4] D. Vortmeyer and S. Kabelac, *K3 gas radiation: Radiation from gas mixtures,* in *VDI Heat Atlas*, edited by VDI e. V. (Springer-Verlag, Berlin Heidelberg, 2010) 2nd ed.

[5] R. H. Norris, *Some simple approximate heat-transfer correlations for turbulent flow in ducts with rough surfaces,* in *Augmentation of Convective Heat and Mass Transfer*, edited by A. Bergles and R. Webb (The American Society of Mechanical Engineers, New York, 1970) pp. 16–26.

[6] R. Karwa, *Heat and Mass Transfer* (Springer, Singapore, 2017).

[7] V. Gnielinski, *G6 heat transfer in cross-flow around single tubes, wires, and profiled cylinders,* in *VDI Heat Atlas*, edited by VDI e. V. (Springer-Verlag, Heidelberg Berlin, 2010) 2nd ed.

[8] J. O. Hinze, *Turbulence* (McGraw-Hill, New York, 1975).

[9] G. L. Morini, *Viscous dissipation,* in *Encyclopedia of Microfluidics and Nanofluidics*, edited by D. Li (Springer, 2015) 2nd ed., pp. 3442–3453.

B

Appendix to Chapter 4

This chapter contains the uncertainty analysis from the appendix of the article [1] that forms the basis for Chapter 4.

The uncertainty in the mass change as obtained in the here presented measurement procedure was estimated using the method outlined by Dunn [2]. Differentiation between the contributions of different sources of error allows an estimate of the uncertainty in the final result. The method is based on probabilistic considerations, which means that the random and systematic errors are all described in terms of Gaussian distributions. In this case, three sources of error were included, two random ones and one systematic.

Because the mass can be measured directly and the mass difference is simply the subtraction of two consecutively measured masses, the uncertainty of the scale has a large influence. It has both a random variation (influence on the average) and a bias (systematic error). The former, the random uncertainty of the average value, was obtained from the standard deviation of the set of mass measurements $S_{P_{\mathrm{sc}}}$ as used to compute the average:

$$S_{\bar{P}_{\mathrm{sc}}} = \frac{S_{P_{\mathrm{sc}}}}{\sqrt{N}} \tag{B.1}$$

where N is the number of measurements in the set, resulting in $S_{\bar{P}_{\mathrm{sc}}} = 0.01\mathrm{g}$. The latter, the standard deviation of the bias error of the mass measurement using the mentioned scale, was estimated by assuming that the manufacturer-specified accuracy (0.5g) represents the 95% confidence level bias limit. This means that the standard deviation is roughly half the limit: $S_{B_{\mathrm{sc}}}$ = 0.25g.

The last source of error, which is also random, is the variation in conditions for the different mass measurement series. Its contribution was estimated based on repeated test rig mass measurements at different occasions. The resulting standard deviation, $S_{\bar{P}_{\mathrm{co}}}$, while taking into account the Student's t distribution, was 0.04 g.

The expression for the combined standard uncertainty for the mass change, u_r, requires the determination of the absolute sensitivity coefficients θ_i for the different

average masses. In this case, these are the derivatives of the expression for the mass change $r = x_1 - x_2$ with respect to the two different measurands x_1 and x_2, where the measurands represent the sample mass before and after the (continued) exposure, respectively, leading to $\theta_1 = \partial r/\partial x_1 = 1$ and $\theta_2 = \partial r/\partial x_2 = -1$.

A look at the resulting expression for the combined standard uncertainty, reveals that the bias error will cancel out since it is common to both measurements. This leaves only the two random contributions. Since these are not common to both mass measurements, their covariances are zero. The remaining expression for the total uncertainty in the mass change at a 95% confidence level is then:

$$U_{mass,95} = t_{\nu_r,95} u_r \tag{B.2}$$

with

$$u_r^2 = \theta_1^2 S_{\bar{P}_{sc}}^2 + \theta_2^2 S_{\bar{P}_{sc}}^2 + \theta_1^2 S_{\bar{P}_{co}}^2 + \theta_2^2 S_{\bar{P}_{co}}^2 \tag{B.3}$$

and $t_{\nu_r,95}$ being the Student's t distribution. Substitution of the values and the number of degrees of freedom results in a total uncertainty in the mass change at a 95% confidence level of $U_{mass,95}$ = 0.16 g.

References

[1] C. Reurings, S. Koussios, O. K. Bergsma, K. Vergote, L. Paeshuyse, and R. Benedictus, *Experimental method for investigating wear of porous thermal insulation systems exposed to realistic, hot, turbulent gas flow.* Wear **466–467**, 203536 (2021).

[2] P. F. Dunn, *Measurement and data analysis for engineering and science*, 2nd ed. (CRC Press, Boca Raton, FL, USA, 2010).

Acknowledgements

Although this dissertation bears my name, the work that is described within would not have been possible without contributions by many others. Some people have made large contributions, some small. Some have aided the research itself, whereas others have supported me socially or in other ways. Here I attempt to acknowledge some of those contributions. I realize I cannot be complete and I therefore already thank those readers that I have not mentioned, but who have supported me during the past years.

First, I want to thank Sotiris Koussios, my daily supervisor at TU Delft. It was your introduction to this project, that started this journey. Your critical feedback helped to bring the work and writing to a higher level. I also enjoyed our many conversations on our shared passion: automobiles.

Next, I want to express my gratitude to Karel Vergote, my daily supervisor at Bosal. Thank you for always making time to help advance this project, both in Lummen and in Delft, despite all your other obligations. Many times you formed the bridge between my, sometimes unusual, requests and the R&D-possibilities at Bosal. Special thanks for the feedback during the final stages of the project.

My thanks also go out to Otto Bergsma for stepping in so many times. Whether it was to come to Lummen for a project meeting on behalf of Sotiris, or to act as interim co-promotor during the final stages of this project, you always did so and brought your positive, constructive attitude.

Luc Paeshuyse, thank you for your confidence and for keeping the project work also aligned with the interest of Bosal, even when it went into a different direction than initially anticipated.

I furthermore want to thank my promotor Rinze Benedictus, for giving me the opportunity to start on this project as a PhD candidate and for the support to see it through to the end.

The many experiments performed for this thesis would not have been possible without the lessons, experience, helping hands and craftsmanship from people from both Delft and Lummen. The colleagues of the Delft Aerospace Materials Laboratory (DASML) and *Dienst Elektronische en Mechanische Ontwikkeling* (DEMO) have contributed greatly to, amongst many things, the design and manufacturing of the heat transfer samples. In particular, I want to thank Bart, Berjan, Berthil, Bob, Cees, Ed, Frans, Fred, Gertjan, Johan, Marianne, Misja, Rob and Victor.

The same holds for the contribution of many employees of the Bosal R&D department, for I could not have done without their support with, for instance, exhaust gas flow measurement, acoustic testing and test setup adjustments. Bernard Lehaen, Dave Mariën, David Theunis, Dirk Vanderheyden, Filip Dörge, Luk Dedene, Tom Laureys, Vik Haesen and Wim Mertens deserve specific mention for their contributions.

Wim-Paul Breugem of the faculty of 3mE also deserves my thanks, as he was kind enough to answer my call for support regarding the peculiarities of flow over permeable boundaries.

Of all the other Structural Integrity & Composites colleagues, I want to separately thank Gemma van der Windt for her support with all the paperwork and meeting scheduling, and also for her dedication to the research group.

SI&C is not just a group where quality scientific work is performed, but during my years as a member I also thoroughly enjoyed its social environment. Whether at the lab coffee table, a conference, the potluck dinners or just the office corridor, often it was possible to exchange personal, social, cultural or even philosophical experiences with a diverse group of colleagues. In Atmosfeer the group often got even more diverse with colleagues from other groups joining in. Of all the fellow PhD candidates, office mates, post-docs, professors, internship and MSc students, I want to specifically thank: Adrian (2x), Andrei, Arijana, Borrdephong, Bram, Bruce, Calvin, Casper, Chirag, Christian, Christos, Clemens, Cornelis, Daniel, Daniël, Daniella, Derek, Dimitrios, Eirini, Fabrício, Freddy, Freek, Giacomo, Gillian, Hongwei, Huajie, Hugo, Ilias, Ilhan, Irene, Jesse, John-Alan, Javier, Jos, Julian, Julie, Julien, Jurij, Kiki, Konstantin, Laura, Lei, Leila, Liaojun, Liesbeth, Lucas, Marcias, Marcelo, Maria, Maro, Martino, Mayank, Megan, Meysam, Michael, Michiel (2x), Mohamed, Morteza, Nicolas, Nikos (2x), Ozan, Paul, Pedro, Ping, René, Renee, Roger, Romina, Satya, Silvia, Sofia, Taylor, Tian, Vincent, Vincentius, Vincenzo, Wouter (2x), Wandong, Yannos, Zahid.

I also want to thank two groups of friends for providing great distractions from the scientific work. Fellow aerospace engineers: Arne, Auke, Erik, Jeremy, Mark, Noud, Robin, Sjoerd, Sjors, Siebe and Thijs, and high-school peers: Alwin, Bob, Mark, Ronald, Sjors and Stefan.

Lastly, I want to thank Juliette and my family. Juliette, thank you for the joy you bring me and for your understanding of all the (weekend) hours of my time that I have spent finishing this dissertation. Mum, Dad, sister Lisanne and brother-in-law Sjaak, thank you for your constant support, patience and interest in the progress of this work.

Niels

Curriculum Vitæ

Cornelis (Niels) REURINGS

The author was born in Amsterdam, the Netherlands, on the 25th of April of 1988. In 2006 he graduated from the Veenlanden College in Mijdrecht. After that, he then enrolled in the Aerospace Engineering program of the Delft University of Technology and received the degree Bachelor of Science *cum laude* in 2009.

The author then pursued a master's degree within the the Aerospace Structures and Materials department of the same faculty. He started in the Design and Production of Composite Structures chair of Prof. Ir. A. Beukers, which then became part of the Structural Integrity & Composites section of Prof. Dr. Ir. R. Benedictus. During this program he performed a three-month internship at the Japan Aerospace Exploration Agency (JAXA) in Chofu, Japan, under supervision of Dr. Y. Hirano. Back in the Netherlands, he become supervisor for four students of a vocational education program (MBO) on metallic and composite aircraft repair at the ultralight aircraft manufacturing company ACLA in Oegstgeest for the last two months of their internship. The author then worked on his master's thesis, entitled: 'Analysis and verification of fibre-reinforced, flexible and high pressure inflatable tubes' under supervision of Prof. Dr. Ir. R. Marissen (part-time professor employed by the company DSM). In December 2012, the author obtained the Master of Science *cum laude* degree in Aerospace Engineering.

In 2013 the author was hired as PhD candidate for the research project between with the Delft University of Technology and Bosal Emission Control Systems from Lummen, Belgium, that led to this thesis. He started this four-year project in September 2013, under supervision of Dr. Ir. S. Koussios and Dr. Ir. O.K. Bergsma from DUT and Dr. Ir. K. Vergote and Mr. L. Paeshuyse from Bosal. Prof. Dr. Ir. R. Benedictus acted as promotor and Dr. Ir. S. Koussios as co-promotor. When his contract as a PhD candidate ended, he continued working on completion of this thesis in his own time.

In 2018, the author was employed as course manager at DUT to develop the new MSc-course Industrial Composite Manufacturing together with a part-time associate professor from DLR, Germany.

In January 2019 he joined the Dutch Safety Board (Onderzoeksraad voor Veiligheid) as technical investigator, working mostly on the technical aspects of industrial, construction and railroad safety.

List of Publications

Journal papers

2. **C. Reurings**, S. Koussios, O. K. Bergsma, K. Vergote, L. Paeshuyse, and R. Benedictus, *Experimental method for investigating wear of porous thermal insulation systems exposed to realistic, hot, turbulent gas flow*, Wear **466–467**, 203536 (2021).

1. **C. Reurings**, S. Koussios, O. K. Bergsma, W.-P. Breugem, K. Vergote, L. Paeshuyse and R. Benedictus, *The influence of a porous, compliant layer with overlying discrete roughness elements as exhaust pipe wall on friction and heat transfer*, Heat Mass Transfer **56**, 2367 (2020).

Conference papers

3. **N. Reurings**, S. Koussios, O. K. Bergsma and K. Vergote, *Evaluation of conjugate, radial heat transfer in an internally insulated composite pipe*, 20th International Conference on Composite Materials, July 19-24, 2015.

2. Y. Hirano, **C. Reurings**, Y. Iwahori, *Damage behavior of CFRP laminate with a fastener subjected to simulated lightning current*, 15th European Conference on Composite Materials, 24-28 June, 2012.

1. Y. Hirano, **C. Reurings**, Y. Iwahori, *Damage resistance of graphite/epoxy laminates with a fastener subjected to artificial lightning*, 18th International Conference on Composite Materials, August 21-26, 2011.